The Hong Kong Polytechnic University

Department of Electronic and Information Engineering

Modeling and Design of Current Driving Circuits for Light-emitting Diodes

By

MOK Kwan Tat

A thesis submitted in partial fulfillment of the requirements for the degree of

Master of Philosophy

August 2012

Certificate of Originality

I hereby declare that this thesis is my own work and that, to the best of my knowledge and belief, it reproduces no material previously published or written, nor material that has been accepted for the awards of any degree or diploma, except where due acknowledgement has been made in the text.

______________________________(Signed)

MOK Kwan Tat (Name of Student)

To Anne

Abstract

The development progress of light-emitting diodes (LEDs) and their related technologies have skyrocketed in recent years. The rapid growth of the LED related technologies can be attributed to the breakthrough in the LED's luminance efficacy improvement and the development of new materials for making white color LED phosphor.

Along with the development of new LED technologies, different LED driving circuits and driving methods have been studied for optimizing the system's performance in terms of power efficiency, luminance efficacy, thermal design, color and light quality, power factor and cost. Recent research has shown that the above mentioned performance aspects can be affected by the choice of the LED driving method. The benefits and drawbacks of different LED driving methods, including amplitude mode (AM), pulse-width modulation (PWM) and bi-level have been extensively studied and analyzed. Notwithstanding the abundant performance studies and analyses of the LED driving methods, there is insufficient fundamental research on the characterization of LED driving systems. Thus, the objective of this thesis is to undergo an in-depth investigation of the circuit design and properties of various LED driving methods.

This thesis consists of four parts. In the first part, we examine the

problems of the existing LED models, specifically, the effect of junction temperature on the AC and DC resistance of the LED are difficult to predict and the semiconductor parameters required in the model are not readily measurable. Consequently, a numerical model of the LED using laboratory measured data is developed and proposed. The model characterizes the relationship of the forward voltage, the forward current and the case temperature of the LED and the evaluation on the values of DC and AC resistances under various conditions is made possible.

In the second part of this thesis, an in-depth survey on the implementation methods, namely AM, PWM and Bi-level current driving methods, are conducted. The LED current waveform and the dimming factor are defined on each of the driving methods.

In the third part of this thesis, the large-signal and the small-signal models for LED current driving systems are derived. It can be used to evaluate the steady-state operation point of the system and predict the system loop gain as well as the system stability.

In the last part of this thesis, a systematic synthesis procedure for deriving new topologies for DC-DC power converters is proposed. The proposed method applies the fundamental duality principle of electrical circuits to generate new DC-DC power converters. The method can identify the uncovered basic power converter structures including voltage-to-current power converters which are potentially suitable for use in LED driving systems.

Achievements

Journal Papers (Related to this thesis)

1. S. K. Ng, K. H. Loo, Y. M. Lai, C. K. Tse and K. T. Mok, "Sequential variable bi-level driving approach suitable for use in high color precision LED display panels," *IEEE Transactions on Industrial Electronics*, No. 99, 2012.

Conference Papers (Related to this thesis)

1. K. T. Mok, Y. M. Lai, and K. H. Loo, "Synthesis of two-state ladder-structured DC-DC power converters by duality principle," *Annual Conference of the IEEE Industrial Electronics Society, (IECON 2012)*, Montreal, Canada, October 2012.(Accepted)
2. S. K. Ng, K. H. Loo, Y. M. Lai, K. T. Mok and C. K. Tse, "Variable bi-level phase-shifted driving method for high-power RGB LED lamps," *IEEE International Conference on Power Electronics and ECCE Asia (ICPE & ECCE)*, Jeju, Korea, pp.782-787, May 2011.

Other Publications

1. K. T. Mok, Y. M. Lai, K. H. Loo, W. C. Chan, C. F. Lee and W. Y. Lai, "A high-output-current and low-power-loss thin-film transistor liquid-crystal display (TFT-LCD) driver for portable

devices," *International Journal of Power Electronics*, Vol. 4, No. 3, pp. 240 - 257, 2012.

2. K. T. Mok, Y. M. Lai and K. H. Loo, "A single-stage bridgeless power-factor-correction rectifier based on flyback topology," *IEEE International Telecommunications Energy Conference (INTELEC)*, Amsterdam, the Netherlands, Oct. 2011.
3. K. T. Mok, "A high performance power system for mobile thin-film transistor liquid-crystal display driver IC," *IEEE Student Paper Contest*, Hong Kong, 2009.(First Prize)
4. K. T. Mok, Y. M. Lai, W. C. Chan and C. F. Lee, "High-output-current and low power-loss mobile thin-film transistor liquid-crystal display driver," *IEEE International Conference on Power Electronics and Drive Systems*, Taipei, Taiwan, pp.1030-1034, Nov. 2009.

Industrial Project

1. Implementation of bi-level driving technique on LED back-light for LCD panels. The technology was adopted by Beijing BOE Optoelectronics Technology Co. Ltd.

Acknowledgements

Many people have contributed to this research work. I am deeply indebted to my supervisors, colleagues and friends for their inestimable support over the past years.

First and foremost, I am indebted to Dr Yuk Ming Lai for providing a chance for my research study. Thanks are also due to Prof. Michael Tse for his encouragement.

I want to express my deepest gratitude to the members in the Board of Examiners who devote time to reviewing my thesis.

I also wish to express my sincere thanks to the members in Applied Nonlinear Circuits and Systems Research Group for the great time we have engaged in discussions about the research and shared the ups and downs of life.

Particular mention should be made to Miss Salina Chan (SAO) and Dr Ho Cheong Wong (UHS), who helped me overcome the difficulties during the period of my study.

In particular, I am grateful to two of my friends, Mr. Nathan Li, a cadet pilot at Dragonair, and Miss Human Chui, a translator, for their help to refine the thesis.

I am indebted to Mr. Andrew Ip, my supervisor in my current job, for providing me a flexible time arrangement to complete my research study.

I would also like to thank my friends, Mr. Daniel Po, Miss Rita Kwan, Miss Peggy Yu, Miss Jasmine Chung, Miss Cherry Chu and many others. Their spiritual support to me is invaluable.

Contents

List of Figures

List of Tables

Nomenclature

i_{d}	Instantaneous LED forward current
v_{d}	Instantaneous LED forward voltage
T_{j}	Instantaneous LED junction temperature
V_{th}	Constant voltage sink in piecewise linear model
I_{S}	Saturation current in Shockley diode model equation
V_{T}	Thermal voltage
k'	Boltzmann constant
q	electrical charge of an electron
V_{d}	LED forward voltage at a sepecific operating point
I_{d}	LED forward current at a sepecific operating point
T_{jo}	LED junction temperature at a sepecific operating point
R_{d}	DC resistance of an LED
$\hat{r_{\mathrm{d}}}$	AC resistance of an LED
$f_i()$	LED characteristic function
$v_{\mathrm{d},jk}$	Instantaneous LED network voltage
$i_{\mathrm{d},jk}$	Instantaneous LED network current
$V_{\mathrm{d},jk}$	Voltage across LED network at a sepecific operating point
$I_{\mathrm{d},jk}$	Current across LED network at a sepecific operating point
$f_{i,jk}()$	Characteristic function of LED network with j rows and k column

I_{O},i_{O}	Output current of power converter
V_{O},v_{O}	Output voltage of power converter
R_{Sen},r_{Sen}	Current sensing resistance
V_{ref},v_{ref}	reference voltage of power converter
$u(t)$	Unit step function
D,d	Switching duty cycle of power converter
T_{S}	Switching period of power converter
f_{S}	Switching frequency of power converter
D_{d}	Dimming duty cycle of LED
T_{d}	Dimming period of LED
k_{d}	Dimming factor

Chapter 1

Introduction

1.1 Motivation

Lighting accounts for more than 20% of the total energy consumption in the US and it is expected that the figures in developing countries are even higher [1, 2]. Such a large amount of energy consumption has prompted researchers and engineers to develop new technologies to improve the performance of lighting systems. In the beginning of the last century, incandescent light bulbs were the major lighting equipment all over the world. The efficacy of incandescent light is about 14 lm/W, which would only provide a lifetime of several hundred to 2,000 hours [3]. Since then, the lighting technology did not have any breakthrough improvement until the invention of the fluorescent lamp in 1976 by Edward E. Hammer, an engineer with General Electric [4]. Due to the continuous improvement of the fluorescent lamp, its efficacy can reach to 100 lm/W with the life time between 6,000 and 15,000 hours [5].

In recent years, light emitting diodes (LEDs) used in general lighting has become more and more popular because of the technological advancement of white LEDs. The performance of the commercial high-power phosphor-converted white LEDs could reach over 80 lm/W in 2007 while the laboratory test have shown more than 100 lm/W [6]. Besides, the long life time is a key advantage of LEDs, which is around 25,000 to 100,000 hours [7]. The long-lifetime high-efficacy LEDs are highly suitable for general lighting. However, there are still several challenges are yet to solve. First, the heat generated by LEDs is a major factor that shortens the lifetime [8]. The luminous efficacy is reduced when operating at high temperature [9]. Hence, a high-performance and low-cost thermal design of LED fixtures are required. Second, even though the lifetime of LEDs can reach up to 100,000 hours, the electrolytic capacitors inside the power converter systems can only provide several thousand hours of operation. The lifetime of LED power systems should be improved. Third, as most of the general lighting equipment is powered by an AC mains power system, efficient and robust power converters are required for converting a line AC power source to low-voltage current source and performing power factor correction function.

In view of the above issues, different converter topologies, feedback sensing methods, LED driving methods and related techniques are proposed in order to improve the overall LED lighting systems in terms of power efficiency, luminous efficacy, thermal improvement and lifetime of the systems [10]–[12]. Recently, a bi-level LED driving method was proposed in which the luminous efficacy of the lighting system can be improved in dimmed control comparing the pulse-width modulation (PWM) driving method. The method optimized both current control flexibility and the efficacy over the traditional amplitude tuning method and the PWM method [13, 14].

Despite of the fact that the general validity of the bi-level LED driving method has been verified, there are other uncertainties. First, the LED driving systems using amplitude tuning, pulse-width modulation and bi-level methods, are not yet studied thoroughly. The large-signal system performance analysis, the small-signal AC stability analysis and the non-linear property of the voltage-current relationship of LEDs are also understated. Second, the effects of the thermal condition of the LED lighting system on the various system's parameters under those three driving methods are unknown. Third, the feasibility of implementing the bi-level driving method into the commercial market is an unknown. Therefore, the objective of the research is to address the area mentioned above. Also, a systematic and fundamental study on the development of suitable LED lighting systems based on different LED driving methods are proposed.

1.2 Literature Review

This section provides a literature review on existing power converter systems for general light-emitting diode drivers (LED drivers). Fig. 1.1 shows a generic illustration diagram of a general LED driver, which consists of a power source, a power converter, the LED networks, a feedback sensing circuit and a control circuit. The power source is either a DC voltage source, AC voltage source or a power source of any kind depending on the applications. There are many power converter topologies that are suitable for LED power systems. The details of those topologies, LED connection arrangement, feedback sensing methods and other potential problems related to LED drivers will be briefly reviewed. The LED driving systems are analyzed in this section in terms of (i) converter topologies, (ii) connections of LED networks, (iii) feedback sensing methods, (iv) LED driving methods and (v) other related issues.

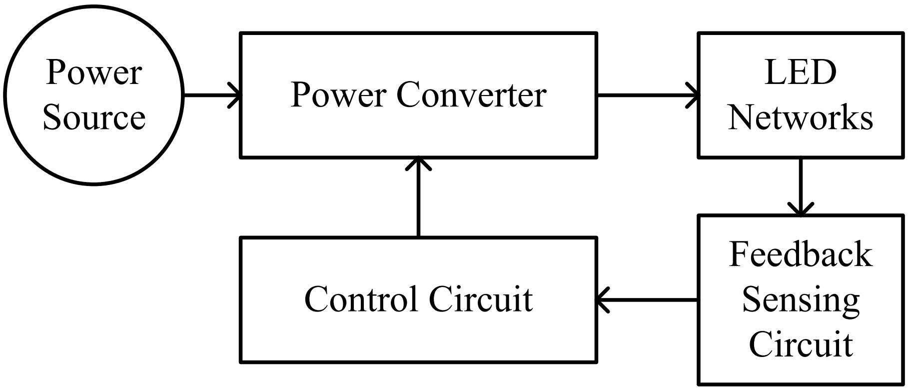

Figure 1.1: Generic illustration diagram of a general LED driver.

1.2.1 Converter Topologies

Different topologies for LED drivers are reviewed in this section. The classification of converter topologies of LED drivers are divided into four types including DC-DC, AC-DC, direct AC driven and other special topologies. The details of each type of topologies are mentioned as follows.

1.2.1.1 DC-DC Topologies

All traditional DC-DC power converters can be used in constructing LED drivers, as reported in the literature. A digital control boost and synchronous buck power converters are adopted as LED drivers in [15] and [16] respectively. Ćuk converter was analyzed in [17]. The Ćuk converter can achieve non-pulsating input and output current which delivers stable output current to drive LEDs. The boost-buck^2 power converter is presented in [18] to achieve a wide-range voltage-conversion LED driver. The tapped-inductor converters used as LED drivers are discussed in [19].

1.2.1.2 AC-DC Topologies

AC-DC conversion is an important issue in LED general lighting systems since most of the power sources of the existing lighting systems are coming from the AC mains. A proper and effective design of such LED drivers can improve the efficiency of the 20% of the total global electricity consumption in the world [1]. There are a number of AC-DC converter topologies for LED drivers [20]– [31]. Most of them are required to deliver a constant output current to LEDs while they are able to maintain a high power factor. The differences between those topologies are discussed as follows.

Flyback Converter The flyback converter is the most cost effective isolated AC-DC step down topology that is widely used in many electronic appliances. In LED drivers, the flyback converter is also adopted for AC-DC conversion. H. M. Pang et al. addressed the stability issue when using flyback converters for LED drivers [20]. Tzuen-Lih Chern et al. demonstrated the feasibility of using the flyback converter as a single-stage power factor correction LED driver [21].

Boost Pre-Regulator with Flyback Converter Another possibility for AC-DC LED drivers is o use a boost-type pre-regulator as a first stage for power factor correction and cascade a flyback converter as a second stage for output current regulation. The implementation of this kind of configuration can be found in the literature [22, 23].

Boost-Flyback Converter The boost-flyback converter is a single-stage power factor correction converter that combines the boost pre-regulator and the flyback converter as one single converter using one active switch. The implementation of such as converter for LED drivers can be found in the literature [24, 25].

SEPIC Converter Apart from those isolated AC-DC power converters mentioned above, the SEPIC converter is a possible solution for single-stage non-isolated power factor correction converters. The related literature can be found in [26, 27].

Other AC-DC Topologies The aforementioned converters, including boost and flyback converters are PFC power converters commonly found in a wide range of applications. There are other specific topologies implemented as AC-DC PFC LED drivers. Xiaohui Qu et al. proposed a resonant PFC pre-regulator for use as an LED driver [28], in which there is no electrolytic capacitor on the primary side of the transformer and hence no high voltage rating electrolytic capacitor is needed in the design. Y. X. Qin et al. proposed using a resonant dual buck converter cascaded with a forward-type converter as an LED drivers [29]. Such a driver can deliver DC output current and achieve power factor correction without the need of electrolytic capacitors. The problem of this design is that it requires a large inductor to make sure the resonant dual buck converter can deliver a stable current to forward-type converter. Kening Zhou et al. presented a two-stage power converter for use as LED drivers [30]. The first stage is a self resonant passive power factor correction circuit and the second stage is a floating buck converter. Mineiro Sa et al. proposed a self-oscillating zero-voltage switching clamped-voltage LED driver [31]. The advantage of this design is that no controller IC is needed and hence the cost is reduced. However, the design does not contain any PFC circuit.

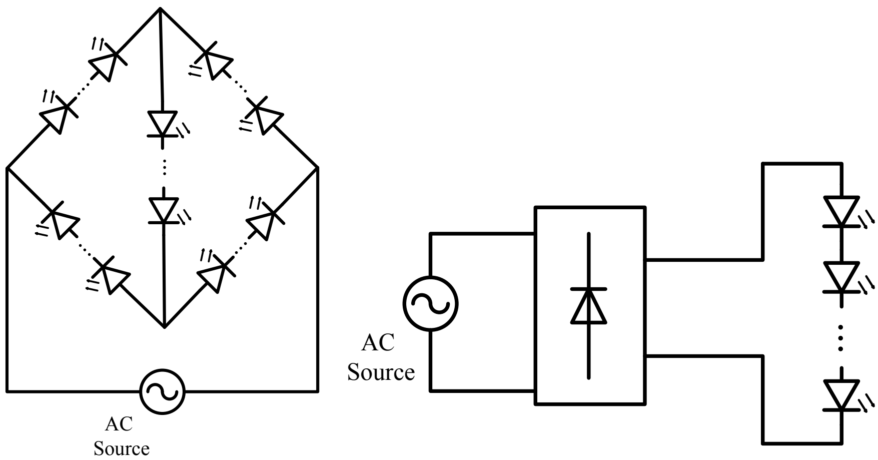

(a) Bridge-type ACLED. (b) Schottky-type ACLED.

Figure 1.2: Two configurations for direct AC driven LED circuit.

1.2.1.3 Direct AC Driving Topology

Due to the difficulty of applying DC current to LEDs from an AC-DC converters as mentioned above, the direct AC driven LEDs, or called ACLEDs, is invented where the LEDs are directly connected to AC input power source by adding a few passive components without power converters. Two possible configurations for this type of design are listed in Fig. 1.2. Figure 1.2(a) shows a configuration called bridge-type ACLEDs where the LEDs acted as a bridge rectifier. Figure 1.2(b) shows another configuration called Schottky-type ACLED. In the circuit, an additional bridge rectifier circuit is required. The earliest application of such method can be traced back to 1975 [32], where the researchers used ten pieces of bridge connected gallium phosphide (GaP) LEDs with a 10V AC input voltage source. Recent researchers have been using bridge connected LED array called AC operated LED (ACOLED) up to 230V AC input voltage [33]. There are several pros and cons with adopting such driving method. First, this driving method does not require electrolytic capacitors for energy storage for maintaining constant output power and hence the LED driving system would have a longer life time. Second, the design does not require a power converter and it contains the simplest circuit design with minimum component count in the power stage circuitry and hence the power efficiency can be improved. However, due to the fact that the direct AC driven LEDs are directly connected into the main power system, the LED current would vary with the line frequency, which is usually 50 or 60Hz. As a result, the electro-luminance intensity would vary with LED current and hence flickering effect may occur. Another disadvantage of this driving method is the poor utilization of LEDs. Since half (or a part) of the LEDs within a bridge connected LED array must be turned off such that more LEDs are required to deliver the same amount of average luminance intensity compared with DC current driving method. Furthermore, a current limit resistor should be connected to the LED string in series to achieve the current limit, where the power dissipation of the resistor contributes to power loss and hence reducing the power efficiency. Finally, the power factor would deteriorate due to the absence of power factor correction (PFC) regulators.

1.2.1.4 Other Topologies

Apart from the topologies discussed above, other ad hoc driving methods are proposed. R. Zane et al introduced a modular power converter architecture based on the series input connected converter cells with independent outputs that each drive a small series string of LEDs [34, 35]. The benefit of the design is that it allows the modulation of LED converters. In additions, the series cascade of power converters can maintain lower a voltage conversion ratio on each converter.

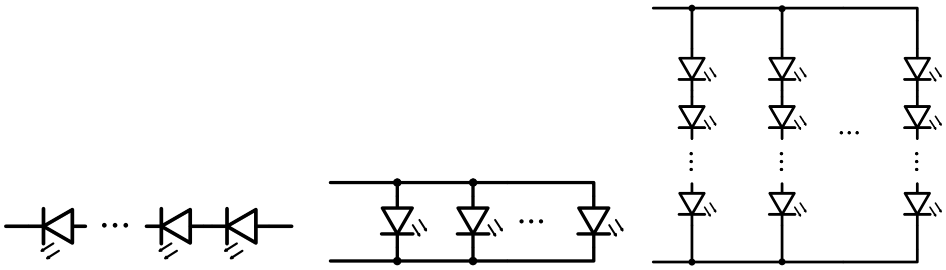

(a) series connected LEDs. (b) Parallel connected LEDs. (c) LEDs connected in array.

Figure 1.3: Different connection methods of LEDs.

1.2.2 Connections of LED Networks

There are different ways to combine LEDs to form a LED module, which is shown in Fig. 1.3. The LEDs can be connected in series, parallel and the combination of both [36]. In general, the forward voltage drop of a high-brightness LED is around 3 V to 4 V . In most of the applications, LEDs are configured in series connection so as to reduce the voltage conversion ratio of the power converter from the main voltage to the output voltage. On the order hand, some applications require a large number of LEDs such as backlight system of LCD display. It is preferred to connect in parallel or even in matrix array. However, the problem of imbalance current sharing among each LED strings leads to uneven luminance distribution. There are different ways to alleviate the problem. A linear regulator connected in series with strings of LED was suggested in [37]. The imbalance voltage among each LED string is handled with the linear regulator such that the overhead voltage of string would drop across the linear regulator. The trade off of the design is that the voltage drops across the linear regulator encountering power decapitation, resulting in reducing power efficiency. Another solution is to use inductors for current sharing [38]. Compared to the previous design, it does not attribute to conduction loss. Another approach is that a capacitor connected in each branch of ACLED to improve the current sharing [39].

1.2.3 Feedback Sensing Methods

The objective of using feedback control for the LED drivers is to maintain and control a stable luminance. Masahiro Nishikawa et al proposed using photo diode sensor to directly control the output luminance [40]. However, such method require a additional light sensor and the sensed value is easily affected by the external environment. Therefore, most power converters are designed to sense the output current in order to control the luminance because LED current has a high correlation with the luminance. Some researchers also proposed sensing and regulating the LED power instead of sensing LED current [41]. Another research found that there is a correlation between the average of LED current and LED junction temperature in PWM driving method [42]. Hence, luminance is controlled by sensing the case temperature of LEDs.

1.2.4 LED Driving Methods

For traditional DC output power converters, the ripples of output voltage and current are expected to be as small as possible. However, general lighting LED drivers would allow the output current containing relatively large ripples or even any kinds of current waveforms, provided that no flickering effect of light intensity would be observed by users due to the time variation of illuminance intensity.

When considering driving methods, dimming approach should be involved so that end users can adjust the desired light intensity to suit their needs. In general, the possible LED current driving methods existed in the literatures and commercial markets include (i) Amplitude mode (adjustable DC current), (ii) Pulse-width modulation and (iii) bi-level. The following section summaries the LED driving methods for LED systems. Heinz van der Broeckl et al summarized several LED current waveforms and list down the characteristics of different periodic current waveforms [43]. The following section briefly introduce the development status of those driving methods.

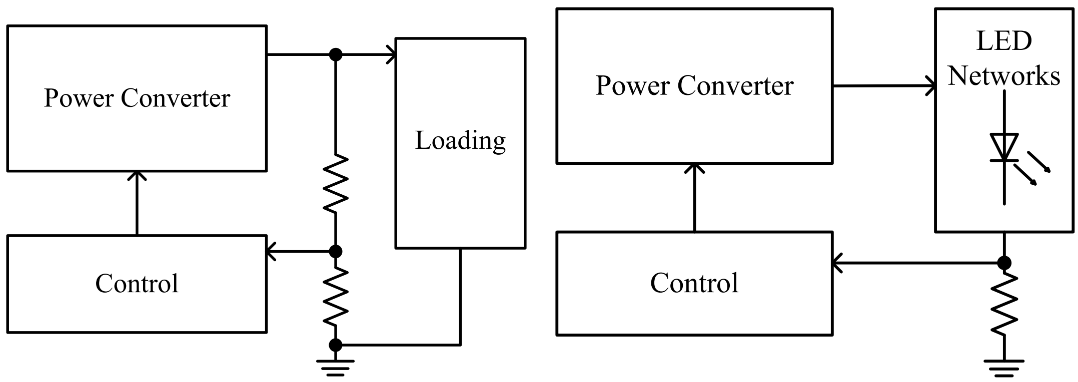

(a) Traditional converters senses output voltage.

(b) LED driver senses output current.

Figure 1.4: Two different sensing methods in DC output power converters.

1.2.4.1 Amplitude Mode (AM)

Most of the DC-DC or AC-DC power converters are suitably taken as LED drivers, which is the most straight-forward way to design such drivers with the minimum re-development procedures. One of the major differences between the traditional power converters and DC current LED drivers is that the former regulates the output voltage by means of feeding back the scaled output voltage signal to the controller circuit while the latter regulates the output current with the aid of an output current sensing resistor. Figure 1.4 illustrates those two feedback sensing methods. There are several advantages of using DC current to drive LED. First, DC current driving can provide the most stable luminance intensity emitted from LEDs since the instantaneous luminance intensity does not vary with time. Second, this driving method delivers the highest luminance efficacy due to the minimum influence on efficiency-droop effect property of LEDs [44, 45, 46]. However, such a constant DC output current cannot be easily achieved in AC-DC converter due to the requirement of large electrolytic capacitors as an energy store element, in which the life time of the power converter is reduced [22]. Another disadvantage of such driving method is that it is difficult to achieve an effective dimming approach due to the difficulty of controlling the precision of the output current level.

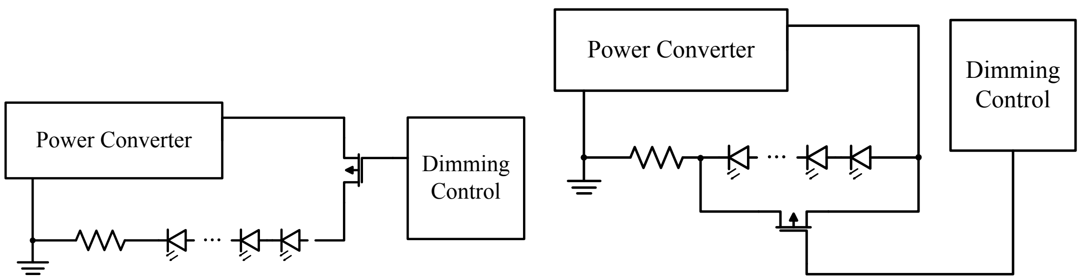

(a) Series switch PWM dimming approach. (b) Parallel switch PWM dimming approach.

Figure 1.5: Series switch and parallel switch PWM dimming approaches.

1.2.4.2 Pulse-width Modulation (PWM)

Apart from the AM driving method, pulse-width modulation driving approach is reviewed. The PWM driving method has been widely used in commercial market in recent decades. The main objective of using the driving method is the ease of implementation of dimming method. Dimming is adjusting the duty cycle of dimming frequency and the LED current changes with the duty cycle control signal. As a result, the average LED current as well as the average luminance intensity would vary with the duty cycle control signal. The PWM driving method implementation can be achieved by using a hard switch connected in series with LEDs to turn them on and off as shown in Fig. 1.5(a). A parallel switch dimming method is another option, where a hard switch is connected in parallel with LEDs [47, 48] as shown in Fig. 1.5(b). There are several disadvantages on this driving scheme. First, the luminance efficacy would not be as high as DC current driving. Second, there is flickering problem if the improper dimming period is chosen .

1.2.4.3 Bi-level

Bi-level driving method was developed from PWM driving method. The bi-level current waveform is similar to PWM one expect a DC offset. Such modification improves luminance efficacy compared with PWM [13, 14]. Sequential variable bi-Level driving approach is an enhanced driving technique that multiplex the current waveform to drive more than one LEDs operating in different power levels using only one power converter [49]. The performance of bi-level driving method is discussed in terms of color variation and junction temperature in [50, 51].

1.2.5 Other Related Issues

Today, there are issues and problems on LED drivers. A robust LED drive should be able to achieve dimming, high efficiency, long life time and maintaining a high quality of color and luminance stability. Previous section has discussed different dimming approaches using periodic current waveforms. PWM and bi-level are two of those examples that adjust the luminance by varying duty cycle. There are problems on dimming methods in terms of luminance efficacy, color stability, flickering effect, etc. The life of converters is another problem. The life time of a HB-LED claimed by manufacturers is usually 40,000 to 60,000 hours while that of the electrolytic capacitors inside the power converters would last a few thousand hours. The life time of the whole general lighting system would be shortened by the electrolytic capacitors. Researchers try to extend the life time of the hold systems by eliminating the electrolytic capacitors inside the converter while it can also provide a stable output current. Besides, the quality of color as well as the color and the luminance stability issues also affect the performance of the lighting system. Those quantities would vary non-linearly with changing the LED current and the junction temperature of LEDs. Different methods are discussed to minimize the variation of LED color and luminance [52, 53, 54, 55].

1.3 The Objective

Recent researches discovered the performance of LED driving systems can be affected by different driving approaches. Despite previous literatures conducted researches on analyzing the illuminance efficacy, color variations and illuminance intensity prediction on different driving methods, there are no standard modeling approach to identify the characterization on each of driving method. The objective of this research is to develop a generalized characteristic equations and a standard modeling approach on amplitude mode, pulse-width modulation and bi-level current driving methods.

In addition, It is also worth to investigate electrical characteristic of LED in terms of the relationship between the forward voltage, current and the junction temperature. It is able to examine how the property of LED affect the electrical behavior of the LED driving system. As a result, a systematic design tools can be developed for LED system optimization.

Finally, It is valuable to conduct a systematic study on the LED driving topologies starting from a fundamental electronic circuit consideration. It should develop a power converter synthesis method where it can devise different possible configurations of LED drivers and hence among those configurations to analyze their advantages and disadvantages of the suitability on the LED driving applications.

1.4 Outline of the Thesis

The thesis is organized as follows.

Chapter 1: Introduction Chapter 1 initially describes the motivation of the research work. It also provides a literature review of nowadays technologies and existing unsolved issues found in light-emitting driving systems. The objective of the research work is then stated.

Chapter 2: LED Characteristics and Electrical Behavior Chapter 2 provides an overview of the LED models, which are nowadays being used to characterize LED behavior. A proposed analytical model obtained from forward current, voltage and junction temperature is derived to enhance the accuracy of LED model. The model will be further extended to an LED network which contains multiple numbers of LEDs in rows and columns.

Chapter 3:Fundamentals and Implementation of LED Driving Methods The major LED current driving methods: amplitude mode, pulse-width modulation and bi-level are introduced. The pros and cons and the design trade-offs among those driving methods are discussed. Different circuit implementation methods applied to those driving approaches are examined. A general forward current time function equations and dimming factors on the three current driving methods are defined, which can help identify their electrical characteristics dimming performance.

Chapter 4:Modeling of LED Current Driving Systems The large and small signal models of LED driving systems were developed in Chapter 4. The large signal model is used for predicting the dc operating conditions among different current driving approaches. The small signal model is used to analyze the stability and dynamic performance issues. The affection of the Q-factor of the control-to-output transfer function in a second-order power converters due to the dynamic property of LED was investigated. The time-domain waveforms and bode plot of the closed loop gain of the system were compared with the simulation results from large signal and small models respectively.

Chapter 5:Current Output Converters for LED Driving Systems A systematic synthesis procedure is proposed to derive classes of DC-DC power converters by a set of basic converter structures obtained by duality transformation. A complete set of converters including those currently known DC-DC converters is generated by inter-connecting these structures. Some voltage-to-current uncovered power converters are derived based on the proposed method. Those are suitable for LED driving circuits, which are required to deliver constant output current.

Chapter 6:Conclusion Chapter 6 summarizes the thesis. A summary of the completed tasks is provided. Possible future research work related to this thesis is also stated.

Chapter 2

LED Characteristics and Electrical Behavior

2.1 Introduction

In this chapter, a review of the basic operation of light emitting diodes (LEDs) and LED modeling techniques is given. We will begin with a brief introduction to LED's operation. Then we will proceed to discuss different electrical models of LEDs. After that, a numerical model for determining the values of dc and ac resistances of an LED by using laboratory measured data is proposed. Finally, a method of finding the equivalent resistance in an LED connected network is suggested.

2.2 Operation of Light Emitting Diodes

The light emitting diode (LED) is a kind of p-n junction diode where semiconductor materials are doped with impurities. When an external voltage potential difference (v_{d}) is applied across the diode, the generation and recombination of electrons and holes produces forward diode drift and diffusion currents, resulting in a net flow of forward diode current (i_d) passing from the p-side to the n-side. Electrons combine with holes by falling from the conduction band to the valance band, and releases energy in the form of photons. Hence, light is emitted [56, 57, 58, 59].

2.3 Modeling of Light Emitting Diodes

Similar to other p-n junction diodes, the electrical properties of LEDs are non-linear. The relationship of forward voltage and current is not linear and it varies with junction temperature. When designing an LED driving system, the electrical behavior of the system is hard to predict due to the uncertainty of this non-linear behavior and the variation of the equivalent resistance of the LED. Different models are developed to help engineers investigate the LED electrical behavior. This section discusses two common analytical LED electrical models, namely, Piecewise Linear Model and Shockley Diode Model. The modeling methods, equations, benefits and drawbacks are discussed in the following sections.

2.3.1 Piecewise Linear Model

The Piecewise Linear Model is one of the models used to predict the electrical behavior of LEDs. The use of the Piecewise Linear Model for predicting the system electrical behavior was studied in [60]. According to the model, the forward voltage of an LED can be described by:

$$v_\mathrm{d} = V_\mathrm{th} + i_\mathrm{d} R_\mathrm{d} \tag{2.1}$$

where V_{th} is a constant voltage sink, regarded as a threshold voltage of the LED, and R_{D} is an ideal resistor. The relationship of the LED forward voltage and current is plotted in Fig. 2.1. It is obvious that the LED equivalent resistance is equal to R_{D}. This implies that the equivalent resistance is always the same in the entire operating range of forward current and junction temperature. Hence, this model does not provide the information on the dependency of forward current and junction temperature and it produces large error when an LED operates at different operating points, especially when the LED forward current is small.

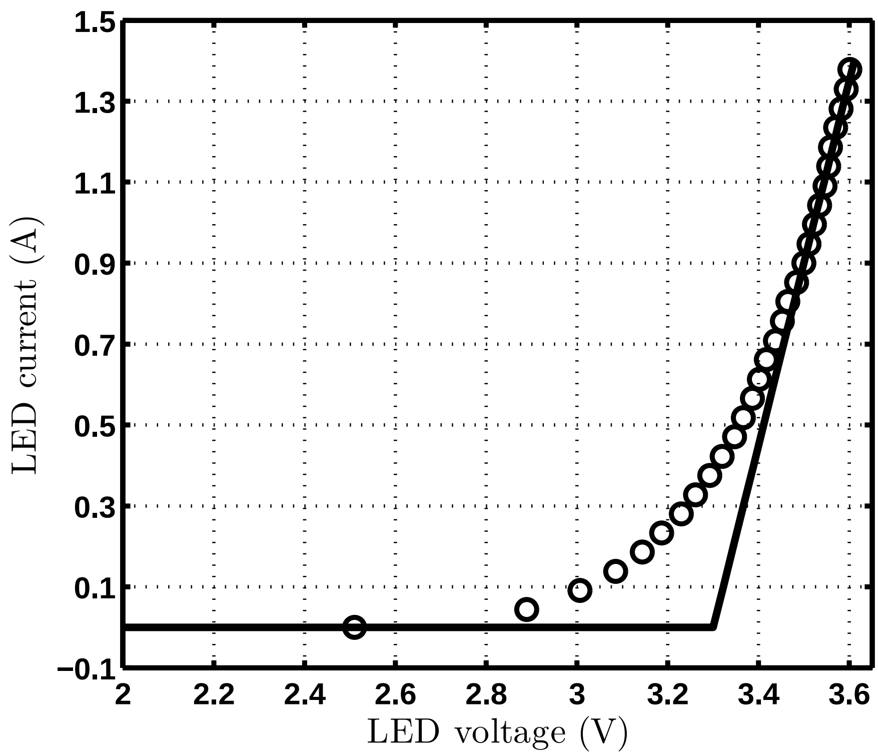

Figure 2.1: The Piecewise Linear Model

2.3.2 Shockley Diode Model

The Shockley Diode Model is another LED model which can be used to improve the temperature inaccuracy [61, 62]. The LED forward current in this model can be represented by:

$$i_{\mathrm{d}} = I_{\mathrm{S}}(e^{v_{\mathrm{d}}/nV_{\mathrm{T}}} - 1) \tag{2.2}$$

where I_{S} is the saturation current, n is the ideality factor and V_{T} is the thermal voltage defined by:

$$V_{\mathrm{T}} = \frac{k^{'}T_{\mathrm{j}}}{q} \tag{2.3}$$

where $k^{'}$ is Boltzmann constant, T_{j} is the junction temperature of the LED in Kelvin and q is the electrical charge of an electron. This model predicts that the LED forward current increases exponentially with the forward voltage and decreases with the junction temperature. Suppose an LED operates with a forward voltage and current of V_{d} and I_{d} respectively, and a junction temperature of T_{jo}. The dc resistance, R_{d}, of an LED can be represented by the ratio of the instantaneous voltage to its current:

$$R_{\mathrm{d}} = \frac{V_{\mathrm{d}}}{I_{\mathrm{d}}} \tag{2.4}$$

The ac resistance of an LED, $\hat{r_{\mathrm{d}}}$, is the inverse of the partial derivative of voltage at temperature T_{jo}:

$$
\begin{aligned}
\frac{1}{\hat{r_{\mathrm{d}}}} &= \left[\frac{\partial i_{\mathrm{d}}}{\partial v_{\mathrm{d}}}\right]_{i_{\mathrm{d}}=I_{\mathrm{d}},v_{\mathrm{d}}=V_{\mathrm{d}},T_{\mathrm{j}}=T_{\mathrm{jo}}} \\
\hat{r_{\mathrm{d}}} &= \left[\frac{qI_{\mathrm{S}}}{nkT_{\mathrm{jo}}}\exp\{\frac{qV_{\mathrm{d}}}{nkT_{\mathrm{jo}}}\}\right]^{-1}
\end{aligned}
\tag{2.5}
$$

Compared with the Piecewise Linear Model, the above equations includes the consideration of the junction temperature. Through the Piecewise Linear Model can be evaluated from LED's datasheets, the LED manufacturer's specification normally provides only a single $v_{\mathrm{d}} - i_{\mathrm{d}}$ curve at a specific temperature (usually 25 degree Celsius). In practices, accumulation of heat leads to increase in the junction temperature. Hence, the $v_{\mathrm{d}} - i_{\mathrm{d}}$ curve provided by the manufacturer cannot provide adequate information to predict the electrical behavior of the LED. Furthermore, the ideality factor and saturation current are also temperature dependent. This affects the accuracy of the model.

2.3.3 Drawbacks of the Models

The Piecewise Linear Model linearizes the equivalent resistance to a single R_{d} regardless of changes in the junction temperature. The major benefit of the model is simplicity, while the drawback is the inability to predict temperature dependence. The accuracy of the model is sufficient at a suitable V_{th} and R_{d} values if the LED operates at a single operation point, where the junction temperature is fixed. However, when an LED operates at different operating points such as in the dimming control or PWM driving schemes (to be discussed in the later section), this model fails to predict the system precisely. The Shockley Diode Model is an option that alleviates the problems mentioned above. However, the ideality factor and saturation current in Eq (2.2) are also temperature dependent, causing significant error in evaluating the equivalent resistance of LEDs. Furthermore, LED manufacturers usually do not provide the information of semiconductor and physical properties of the LED.

Due to the above drawbacks, a numerical model for the electrical behavior of LEDs is proposed. Engineers can construct a precise model based on the measured data from LED without considering the semiconductor behaviors. The details of the model will be introduced in the next section.

2.4 Numerical Modeling of Electrical Behavior of Light Emitting Diodes

In order to fully understand the relationship of the current, voltage and temperature of LEDs, this section studies the laboratory measured data to find out the electrical behavior of an LED. The proposed modeling method can be used to predict the ac and dc resistances of LEDs. These parameters will be incorporated in the model such that the system behaviors can be predicted.

An auto-measurement setup has been built to record the characteristics of an LED, as shown in Figure 2.2. The setup consists of three units: a linear current regulator, a thermal controller and a micro-controller. The micro-controller is used to control the thermal temperature of the heat-sink, where an LED is attached, and to control the current of the regulator, which provides the forward current to the LED under test such that the desirable heat-sink temperature and

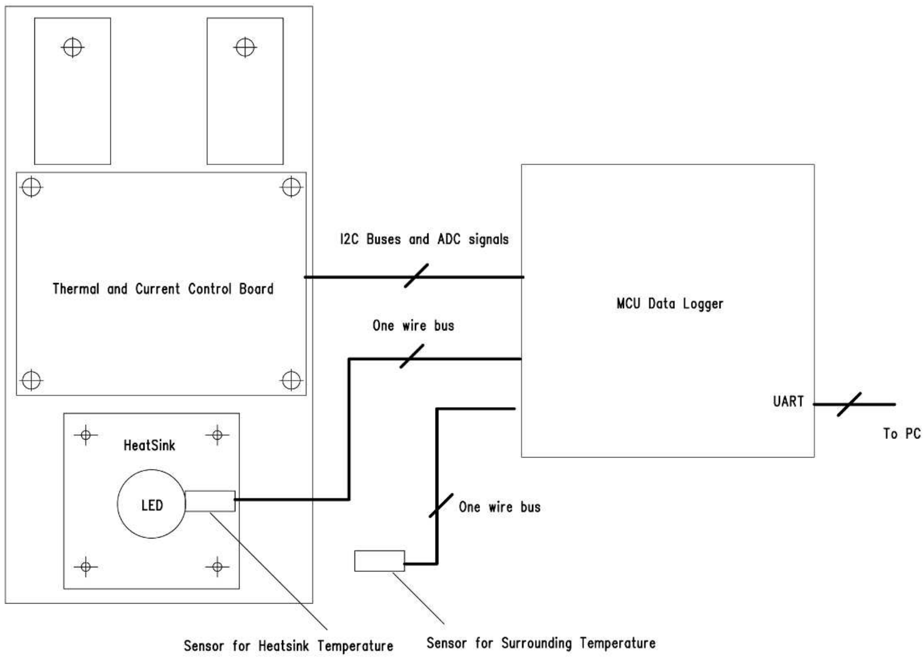

Figure 2.2: The Auto-measurement Setup

LED current are obtained. Before taking the measurement, the LED is turned off and the heater heats up the heat-sink for 10 minutes so as to ensure that the temperature becomes stable. The temperature sensor is put closed enough to the LED so that the measured temperature can be approximated to the junction temperature of the LED. During the measurement, the LED turns on in a short period of time (one to two seconds) such that the heat generated from the LED will not affect the measurement result. The room temperature is kept at 22 °C by the air conditioner. Since the measurement is automatic, the laboratory is vacant in order to minimize the affection of room temperature variation. The micro-controller records the measured temperatures, the LED voltages and the currents at different operating points. The details of the measurement setup is described in Appendix A.

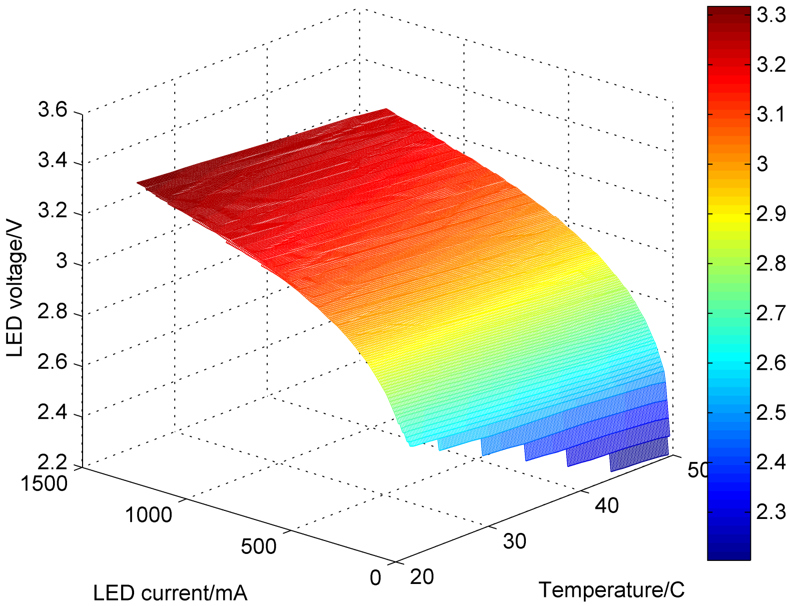

Figure 2.3: $v_{\mathrm{d}} - i_{\mathrm{d}} - T_{\mathrm{j}}$ relationship measurement result of LUXEON K2 LXK2-PW14-U00

An LED, LUXEON K2 LXK2-PW14-U00, was chosen in the measurement. The LED was operated at 20 to 50°C and the forward LED current from 0 mA to 1400 mA. A total of 870 measurement points were taken. All measurement points were analyzed using the 2-D linear interpolation method with the *griddata* command in MATLAB. The calculated result is presented as a surface in the $v_{\mathrm{d}} - i_{\mathrm{d}} - T_{\mathrm{j}}$ space, as shown in Fig. 2.3.

The LED forward current can be regarded as a function of v_{d} and T_{j}. This plane describes the characteristic of a specific LED, as each LED would have its own characteristic function describing its $v_{\mathrm{d}} - i_{\mathrm{d}} - T_{\mathrm{j}}$ behavior:

$$i_{\mathrm{d}} = f_i(T_{\mathrm{j}}, v_{\mathrm{d}}) \tag{2.6}$$

where f_i is defined as the the characteristic function of an LED using the numerical model shown in Fig. 2.3. The operating LED forward voltage (V_{d}) can be obtained, if both the forward current (I_{d}) and the junction temperature (T_{jo}) are known. Using these DC operating parameters, the dc and the ac equivalent resistances of the LED can be deduced by partial differentiation:

$$\begin{aligned}\frac{1}{\hat{r_{\mathrm{d}}}} &= \left[\frac{\partial i_{\mathrm{d}}}{\partial v_{\mathrm{d}}}\right]_{i_{\mathrm{d}}=I_{\mathrm{d}}, v_{\mathrm{d}}=V_{\mathrm{d}}, T_{\mathrm{j}}=T_{\mathrm{jo}}} \\ \hat{r_{\mathrm{d}}} &= \left[\frac{\partial f(T_{\mathrm{j}}, v_{\mathrm{d}})}{\partial v_{\mathrm{d}}}\right]_{i_{\mathrm{d}}=I_{\mathrm{d}}, v_{\mathrm{d}}=V_{\mathrm{d}}, T_{\mathrm{j}}=T_{\mathrm{jo}}}\end{aligned} \tag{2.7}$$

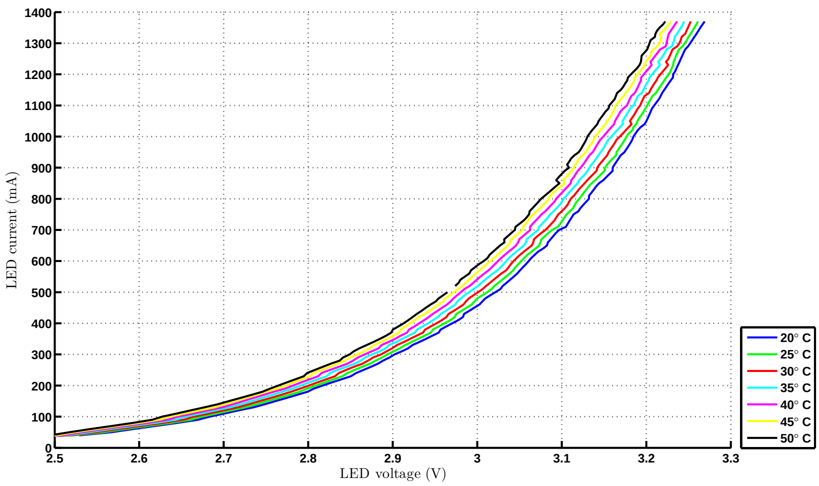

Figure 2.4: $v_{\mathrm{d}} - i_{\mathrm{d}}$ curves of the LED LUXEON K2 LXK2-PW14-U00 plotted from 20 to 60 °C at steps of 5 °C.

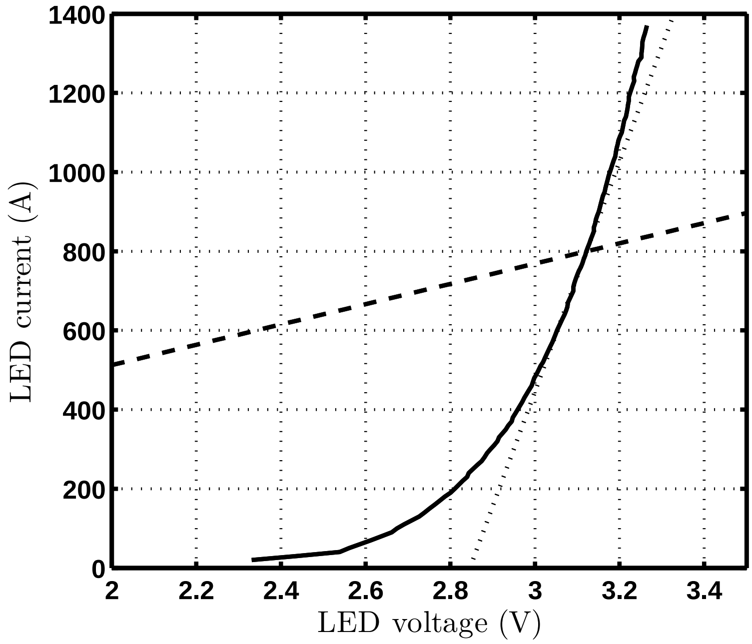

Figure 2.5: Estimation of the dc and ac resistance of the LED LUXEON K2 LXK2-PW14-U00 operated at 40 °C.

In order to show the trends of changes of the LED electrical behavior, Fig. 2.3 is rearranged to 2D plots as shown in Fig. 2.4. Five $v_{\mathrm{d}} - i_{\mathrm{d}}$ curves of the LED are plotted as the junction temperature changes from 25 to 60 °C at steps of 5 °C.

To illustrate the method of evaluating the dc and ac equivalent resistances of the LED, the $v_{\mathrm{d}} - i_{\mathrm{d}}$ curve of the LED operated at 40 °C junction temperature and 800 mA forward current is shown in Fig. 2.5. The operating forward voltage of the LED can be found from the $v_{\mathrm{d}} - i_{\mathrm{d}}$ curve using the *polyfit* and *polyval* functions in MATLAB. The dc resistance would be the ratio of V_{d} to I_{d}. The ac resistance is equal to the inverse of the slope of the tangent of the $v_{\mathrm{d}} - i_{\mathrm{d}}$ curve at point (V_{d}, I_{d}). Hence,

$$R_{\mathrm{d}} = \frac{V_{\mathrm{d}}}{I_{\mathrm{d}}} = \frac{3.12\ \mathrm{V}}{800\ \mathrm{mA}} = 3.9\ \Omega \tag{2.8}$$

$$
\begin{aligned}
\hat{r_\mathrm{d}} &= \left[\frac{\partial f(T_\mathrm{j}, v_\mathrm{d})}{\partial v_\mathrm{d}}\right]_{i_\mathrm{d}=I_\mathrm{d}, v_\mathrm{d}=V_\mathrm{d}, T_\mathrm{j}=T_\mathrm{jo}} \\
\hat{r_\mathrm{d}} &= 0.344\,\Omega
\end{aligned}
\tag{2.9}
$$

Figure 2.5 shows a line passing the origin (0, 0) and intersecting the dc operating point. The inverse of the slope is equal to the dc resistance of the LED. The ac resistance is the inverse of the slope of the tangent line of the $v_\mathrm{d} - i_\mathrm{d}$ curve at the operating point.

2.5 Modeling of Light Emitting Diodes Networks

In most applications, there are more than one LED in a system. For example, an LED light tube consists of a string of LEDs. The LED back-light used in LCD panels is usually made up of an array of LEDs [63]–[67]. In the previous sections, we discussed the dc and ac equivalent resistances of one LED. This section focuses on determining the equivalent resistance of an LED network. As mentioned in the literature review in Chapter 1, LEDs can be connected in series, parallel or a combination of both as shown in Fig. 1.3. Suppose an LED array has k LED strings in parallel. Each string has j LEDs connected in series operating at a junction temperature of T_jo. Assuming all LEDs are identical and the current passing each LED is I_d and the voltage across each LED is V_d, the voltage and the current of the LED network would be:

$$
V_{\mathrm{d},jk} = jV_\mathrm{d} \tag{2.10}
$$

$$I_{\mathrm{d},jk} = kI_{\mathrm{d}} \tag{2.11}$$

where $V_{\mathrm{d},jk}$ and $I_{\mathrm{d},jk}$ are the operating voltage and current of the LED network, respectively. Using Eq (2.10), Eq (2.11) and the characteristic function of the LED defined in Eq (2.6), the function $f_{i,jk}$ shown in Eq (2.12) can be obtained by using numerical operation in MATLAB.

$$i_{\mathrm{d},jk} = f_{i,jk}(T_{\mathrm{j}}, v_{\mathrm{d},jk}) \tag{2.12}$$

where subscript jk in the function indicates the number of rows and columns that the LED network contains. By applying the analysis described in the previous section, the dc and ac equivalent resistances of the LED networks can be obtained. Figures 2.6(a) and 2.6(b) correspond to LED networks with $j = 2$, $k = 1$ and $j = 1$, $k = 2$ respectively. Both of them operate at a forward current of 500 mA and a junction temperature of 40 °C. The estimated dc and ac resistances are $R_{\mathrm{d,jk}} = 12.37\,\Omega$, $r_{\hat{\mathrm{d,jk}}} = 0.917\,\Omega$ in the first example and $R_{\mathrm{d,jk}} = 5.709\,\Omega$, $r_{\hat{\mathrm{d,jk}}} = 0.427\,\Omega$ in the second example.

2.6 Summary

This chapter introduced the basic operation of LEDs. We then discussed the common LED models. A numerical model of LEDs is proposed in which $v_{\mathrm{d}} - i_{\mathrm{d}} - T_{\mathrm{j}}$ behaviors are recorded. Using this model, the ac and dc resistances can be estimated. The final section further developed the model and extended it to

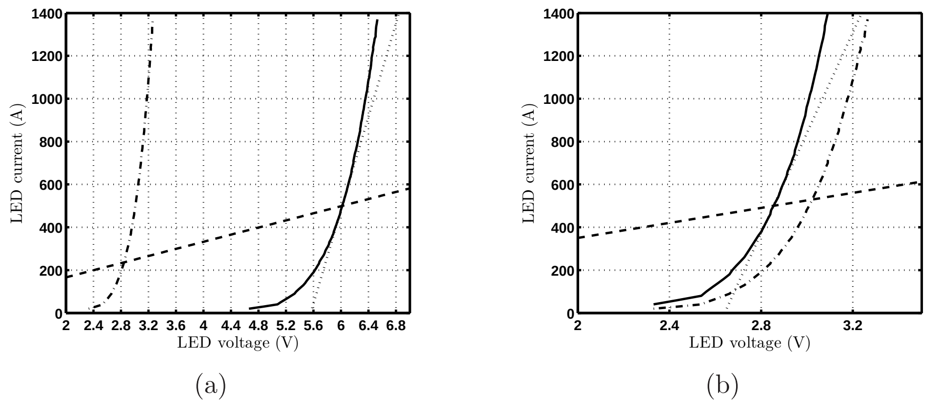

Figure 2.6: (a) $v_\mathrm{d} - i_\mathrm{d}$ curve of a LED network with $j = 2$, $k = 1$ operating at $T_\mathrm{jo} = 40\,^\circ\mathrm{C}$ with $I_{\mathrm{d},jk} = 500\,\mathrm{mA}$ and $V_{\mathrm{d},jk} = 6.018\,\mathrm{V}$ (b) $v_\mathrm{d} - i_\mathrm{d}$ curve of a LED network with $j = 1$, $k = 2$ operating at $T_\mathrm{jo} = 40\,^\circ\mathrm{C}$ with $I_{\mathrm{d},jk} = 500\,\mathrm{mA}$ and $V_{\mathrm{d},jk} = 2.854\,\mathrm{V}$.

an LED network containing multiple LEDs arranged in rows and columns. The model can be used in the later chapters to develop models for LED current driving systems.

Chapter 3

Fundamentals and Implementation of LED Driving Methods

3.1 Introduction

Three major LED current driving methods, namely, amplitude mode (AM), pulse width modulation (PWM) and bi-level PW are studied in this chapter. The definitions, current waveforms and dimming methods are discussed. Different available implementation circuits and control methods for each current driving approach are then introduced.

3.2 Sensing Methods for LED Driving Systems

The ultimate goal of an LED driving circuit is to drive LEDs such that a predictable luminance intensity or dissipated power can be controlled. Different feedback control methods are commonly found in the commercial market for controlling an LED lighting system delivering the required outputs for a varieties of applications. A System requiring highly accurate luminance intensity control such as back-light systems in Liquid Crystal Display (LCD) panel can employ luminance sensors as a kind of feedback sensing devices in the system. However, the expensive luminance intensity sensor increases the cost of the lighting system.

An alternative sensing technique is to sense dissipated power of LEDs in the system, where both LED forward current and voltage are being sensed. The instantaneous LED dissipated power can be predicted by multiplying the sensed current and voltage. Suitable control can then be applied to control the dissipated power. However, sensing both forward current and voltage increases the complexity of the controller while the multiplier circuit increases the cost.

According to the $v_\mathrm{d} - i_\mathrm{d}$ characteristics of the LED as indicated in Chapter 2, the small deviation of the forward voltage leads to a large change in the LED current and hence the luminance intensity. Therefore, sensing LED forward voltage is not a suitable method for LED driving systems. Instead, the LED forward current has a higher correlation to the LED dissipated power compared with the forward current. Further, the implementation of the sensing circuit can be achieved by using a simple current sensing resistor. Therefore, LED current sensing is widely used in nowadays LED driving systems, and has been widely adapted in the commercial products.

The following sections will focus on analyzing different current driving methods for LEDs. We will look into basic current waveforms and their circuit implementations. The benefits and drawbacks will be discussed. We also focus on the dimming approaches for these current driving methods.

3.3 Current Driving Methods and Circuit Implementation

Three major current driving methods namely, amplitude-mode (AM), pulse-width modulation (PWM) and bi-level PWM are discussed in detail in this section. The implementation circuits for each driving methods are analyzed. A unified set of driving current equations for the driving methods are introduced to help characterize the features of different driving systems. In this section, we assume that the driving circuits are implemented by switching power converters. Those circuits using linear converters will not be in discussed. In addition, we study the dimming approaches for luminance intensity control, which can be achieved by controlling the amount of current passing or/and the duration of conduction time of LEDs.

3.3.1 Amplitude-mode (AM) Driving Method

The amplitude-mode driving method is an LED current driving scheme where a constant current passes through an LED array. All traditional DC-DC switching regulators, which are able to deliver constant output power, are suitable for implementing this method. Some modification is required to be made in the traditional DC-DC switching regulators where the voltage feedback sensing resistor ladder (Fig. 1.4(a)) is omitted. Instead, a dc output current sensing circuit is inserted in order to provide a current sensing path for the controller. There are a few circuits for dc output current sensing. The simplest way is to add a low-side current sensing resistor in series with the LED array as shown in Fig. 1.4(b). Since an extra current sensing resistor is added the output power path of the power converter, it introduces a resistive power loss dissipated on that resistor. The percentage of the power loss compared to the input power would be:

$$\frac{P(\text{sensing resistor})}{P(\text{input})} = \frac{I_{\text{O}}^2 R_{\text{Sen}}}{I_{\text{O}}^2 (R_{\text{Sen}} + R_{\text{d}})} \tag{3.1}$$

where I_{O} is the current passing the LED array and R_{Sen} is the current sensing resistor. To minimize this power loss, the LEDs inside the LED array are usually connected in series instead of in parallel. According to Eq (2.10) and Eq (2.11), based on the condition that the same number of LED are used, increasing the number of LEDs connected in series, j, results in a larger $V_{\text{d,jk}}$ and smaller $I_{\text{d,jk}}$. Hence, the loss can be reduced.

Since the output of the power converter is connected to the LED array, the output current I_{O} is identical to the input current of the LED array $I_{\text{d,jk}}$. Besides, a current sensing resistor is connected to the LED array in series, the output voltage of the power converter is:

$$\begin{aligned} I_{\mathrm{O}} &= I_{\mathrm{d,jk}} \\ V_{\mathrm{O}} &= V_{\mathrm{Sen}} + V_{\mathrm{d,jk}} \\ &= I_{\mathrm{d,jk}} R_{\mathrm{Sen}} + V_{\mathrm{d,jk}} \end{aligned} \tag{3.2}$$

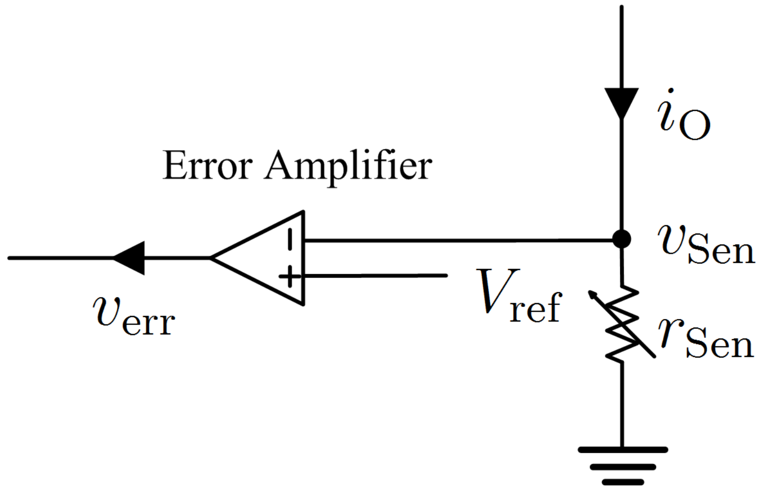

Figure 3.1: Using variable resistor to control load current.

The current sensing circuit shown in Fig. 1.4(b) only allows the system to operate at one specific load current. In order to achieve dimming, the load current must be adjustable. The way to achieve such aim is to use a variable current sensing resistor as the sensing circuit which is shown in Fig. 3.1. The amount of load current can be calculated by:

$$i_{\mathrm{O}} = \frac{V_{\mathrm{ref}}}{r_{\mathrm{Sen}}} \tag{3.3}$$

where V_{ref} is a constant reference voltage and r_{Sen} is the adjustable sensing resistor value.

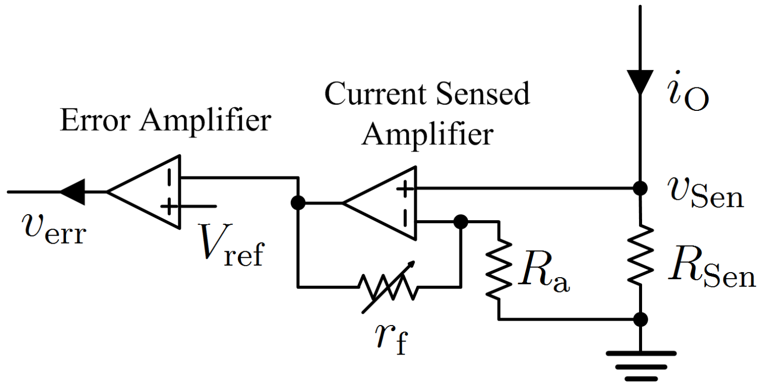

Figure 3.2: Using adjustable-gain current sensed amplifier to control load current.

In most cases, the values of sensing resistor should be as low as possible, normally less than 0.5 Ω, so as to minimize the above-mentioned power loss. However, a variable resistor in such a range of values are not easily found in the market. In addition, using a variable resistor for current sensing causes a large percentage error and hence output current inaccuracy. Therefore, a possible solution is adopted by inserting a variable gain current sense amplifier in the the current sensing node and the error amplifier input. As a result, the variable resistor is located at the control signal path instead of the power path. The value of the variable resistor can now be much higher and it can easily be found in the commercial market. The implementation circuit shown in Fig. 3.2 describes the proposed method where a feedback resistor of the current sensing amplifier uses a variable resistor of tens of kilo-ohms. Hence, the gain, G_{Sen}, of the amplifier is adjustable and the value of the output current is:

$$
\begin{aligned}
i_{\mathrm{O}} &= \frac{V_{\mathrm{ref}}}{G_{\mathrm{Sen}} R_{\mathrm{Sen}}} \\
i_{\mathrm{O}} &= \frac{V_{\mathrm{ref}}}{\left(\frac{r_{\mathrm{f}}}{R_{\mathrm{a}}} + 1\right) R_{\mathrm{Sen}}}
\end{aligned}
\tag{3.4}
$$

The major disadvantage of those two current sensing methods is that the LED driving system is not permitted to communicate with a digital controller, such as an embedded system controller in an LCD panel controlling LED back-light illuminance intensity, because there is not easy to control the value of the variable resistor via a digital interface. Instead of varying the current sensing resistor's value or gain of the current sensed amplifier, an adjustable voltage reference signal can be used. A programmable voltage reference IC (e.g. X60250 of *Intersil Corporation*) or a digital controllable resistor ladder (e.g. TPL0102-100 of T*exas Instruments Inc.*) collaborating with constant voltage reference can fulfil such aim. The corresponding circuit diagrams are shown in Fig. 3.3 and Fig. 3.4, respectively. By using those ICs, the dimming level can be easily controlled by a digital controller.

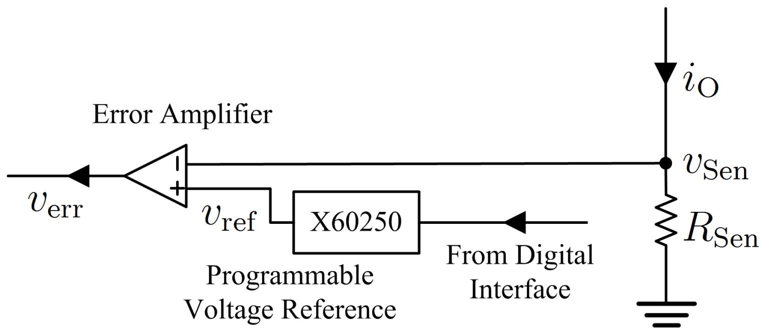

Figure 3.3: Variable voltage reference signal based on X60250.

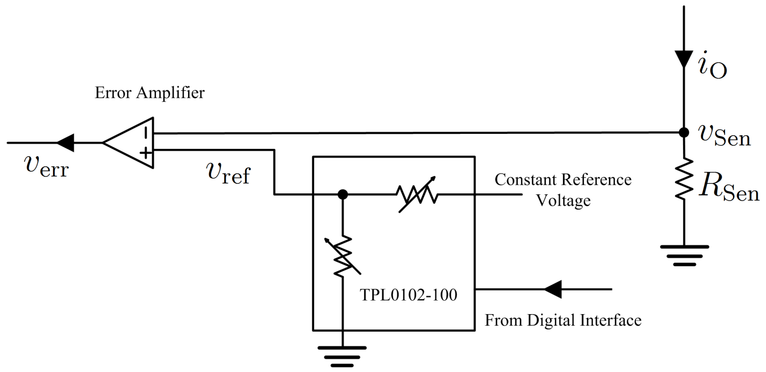

Figure 3.4: Variable voltage reference signal based on TPL0102-100.

In Fig. 3.3, the load current is:

$$i_{\mathrm{O}} = R_{\mathrm{Sen}} \frac{x}{255} V_{\mathrm{refo}} \tag{3.5}$$

The dimming resolution and the allowable dimming steps depend on the programmable resolution and the multiplier steps of the IC. The programmable voltage reference IC X60250 provides a maximin voltage reference level, (V_{refo}), of 1.25 V with 8-bit resolution steps, which implies that the system can deliver 255 controllable load current levels. The variable x from Eq (3.5) is a value ranging from 0 to 255. Eq (3.5) can also be used in the circuit of Fig. 3.4 to calculate the output current.

In general, Eq (3.3), Eq (3.4) and Eq (3.5) can be represented by the unified equation Eq (3.6), where I_{OH} is the maximin allowable load current in the system and k_{d} is defined as the dimming factor. Noted that k_{d} is always lower than or equal to one, since it is the ratio of the dimmed current compared to the maximin current I_{OH} that the power converter can deliver. Fig. 3.5 explains the meanings of these parameters.

$$i_{\mathrm{O}}(t) = k_{\mathrm{d}} I_{\mathrm{OH}} \tag{3.6}$$

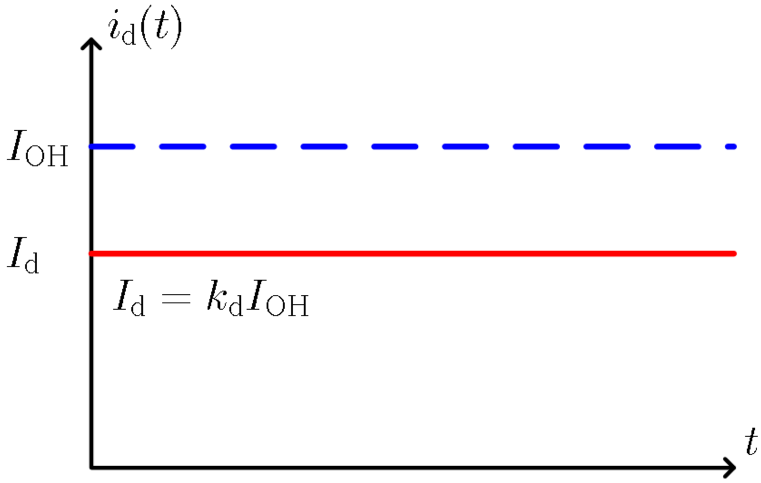

Figure 3.5: Illustration of ideal LED forward current timing waveform under amplitude-mode (AM) driving method.

3.3.2 Pulse-width Modulation (PWM) Driving Method

Apart from delivering constant current to LEDs, the pulse-width modulation (PWM) driving method is also popularly used in LED driving circuits [65]–[70]. Fig. 3.6 shows the ideal LED current waveform based on this driving method, where the current is periodically switched between a constant level I_{OH} and zero level at a period of T_{d}. The duty cycle of the periodic output current, controlling the dimming level, rang from zero to one, contains the same property of the dimming factor k_{d} as defined in Section 3.3.1. Since the output current changes with time, the current time function can be represented by:

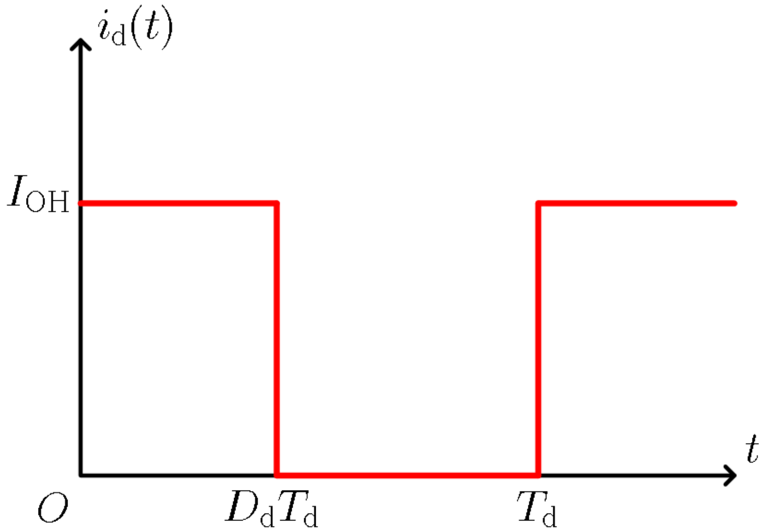

Figure 3.6: Illustration of ideal LED forward current timing waveform under pulse-width modulation (PWM) driving method.

$$i_\mathrm{O}(t) = I_\mathrm{OH} \sum_{n=1}^{+\infty} [u(nt) - u(nt - nT_\mathrm{d}D_\mathrm{d})] \tag{3.7}$$

where $u(t)$ is a unit step function. Also, D_d is the dimming duty cycle, where the sub-letter "*d*" is added to avoid confusion with the switching duty cycle, D of the power converter. The dimming frequency f_d as defined by $1/T_\mathrm{d}$ is the number of cycles that the current waveform repeats per second. Since the current switches either to I_OH or zero repeatedly, the luminance intensity emitted from LEDs would switch also. If the dimming frequency is not fast enough, flickering problem may exist while users can observe the effect [71, 72]. This flickering problem can be alleviated by increasing the dimming frequency, but the rise and fall times of the LED current (limited by the response of the system) limits the possibility of increasing the dimming frequency. Different methods were proposed to improve the response of the LED driving systems [69, 47].

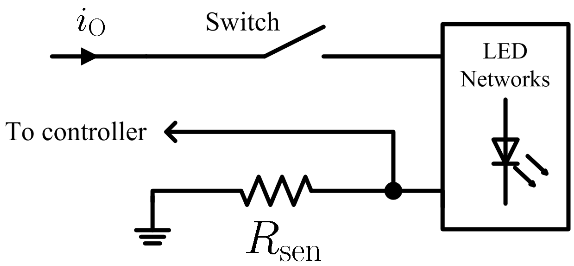

Figure 3.7: PWM circuit using converter output switch.

The simplest way to implement the PWM driving method is to add an analog switch in series with the LED network which is shown in Fig.3.7. When the switch is on, a load current is delivered to LEDs from the power converter controlled by the controller, where the operation principle is the same with the AM mode. When the switch is off, LEDs are disconnected from the power converter. Since no current flows to R_{sen}, v_{Sen} changes to zero. The switching duty cycle of the power converter (d) would reach to the maximum level and eventually the converter may be damaged. An extra circuit should be required to be added to the controller in order to either turn off the whole system or reduce the switching duty cycle to zero.

Another way to achieve this driving method is to control the PWM output signal of the controller. Some PWM controllers contain an enable pin for disabling the PWM gate signal, so that the power converter can be turned off. A PWM dimming signal can be fed to the enable pin of the PWM controller in order to achieve the PWM driving approach. Figure 3.8 shows the diagram to implement this concept.

The PWM driving method can also be implemented by controlling the voltage

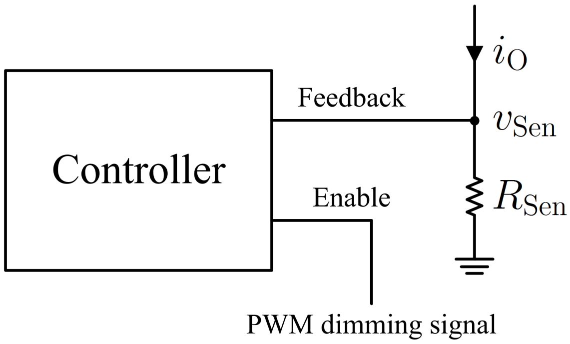

Figure 3.8: PWM circuit using PWM sinal fed to enable pin of PWM controller.

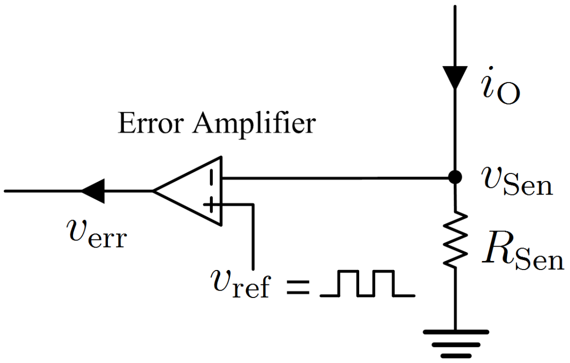

Figure 3.9: PWM circuit using reference voltage control approach.

reference signal. Figure 3.9 shows that an PWM dimming signal which is used as the voltage reference signal. v_{ref} is at zero level when i_O is desired to be 0 A and v_{ref} is at V_{refH} when i_O is desired to be I_{OH}.

In general, the average output current in the PWM driving method can be found by averaging the current time function:

$$
\begin{aligned}
\bar{I_O} &= \frac{1}{T_d}\int_{\delta}^{\delta+T_d}\left\{I_{OH}\sum_{n=1}^{+\infty}[u(nt)-u(nt-nT_dD_d)]\right\}dt \\
\bar{I_O} &= I_{OH}D_d \\
\bar{I_O} &= I_{OH}k_d
\end{aligned}
\tag{3.8}
$$

The above equation indicates that the dimming factor is equal to the dimming duty cycle. Usually, the dimming duty cycle can range from zero to one and the possible dimmed output current level of the PWM driving method can reach zero when the dimming duty cycle is equal to zero.

3.3.3 Bi-level PWM Driving Method

The bi-level PWM driving method is a generalized method of PWM and AM. It extends the driving method of PWM where the PWM current waveform is offset by a dc current such that the current switches between two current levels I_{OL} and I_{OH} as shown in Fig. 3.10. One of the major advantages of using the bi-level PWM driving scheme is that the luminance efficacy of the LED driving system can be enhanced during dimming while the flexibility of controlling dimming by means of adjusting the dimming duty cycle can be maintained. The load current time function for this driving method can be represented by:

$$i_{\mathrm{O}}(t) = (I_{\mathrm{OH}} - I_{\mathrm{OL}}) \sum_{n=1}^{+\infty} [u(nt) - u(nt - nT_{\mathrm{d}}D_{\mathrm{d}})] + I_{\mathrm{OL}} \tag{3.9}$$

The theory of the luminance efficacy improvement was widely discussed in [13, 14]. This section would specializes in the implementation methods. One possible implementation is to use two power converters delivering two output voltage levels to LEDs [73]. This method is cost ineffective as it requires twice as many electronic components to construct the system. In addition, those two converters deliver energy to LEDs in turn during each dimming states. This implies either one of them states idle while another is operating. Hence, the utilization of the

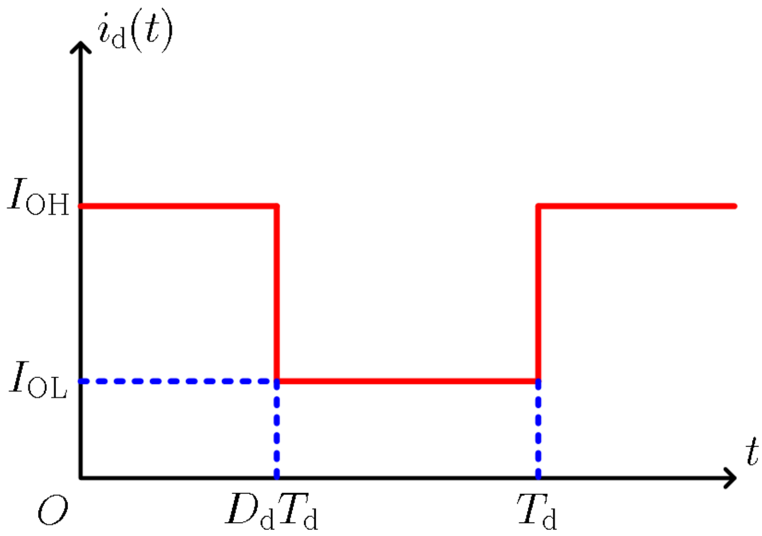

Figure 3.10: Illustration of ideal LED forward current timing waveform under bi-level PWM driving method.

system is reduced. Furthermore, this approach uses a voltage driven method to drive LEDs which is not the main focus of our study here. Therefore, the two-converter driving method would not be considered in our discussion.

There are other possible circuitries that can utilize the system without using two converters for this bi-level PWM method. The idea of controlling the changes of the voltage reference signal is proposed in [73]. In this circuit, the voltage reference signal changes according to the following equation:

$$v_{\mathrm{ref}}(t) = (V_{\mathrm{refH}} - V_{\mathrm{refL}}) \sum_{n=1}^{+\infty} [u(nt) - u(nt - nT_{\mathrm{d}}D_{\mathrm{d}})] + V_{\mathrm{refL}} \tag{3.10}$$

Another approach requires a switch-controlled current sensing resistor network, which is shown in Fig. 3.11. The switch S_1 is turned on in the duration $D_{\mathrm{d}}T_{\mathrm{d}}$ in every dimming period and turned off during the remaining time of the period such that the current sensing resistance value changes with time:

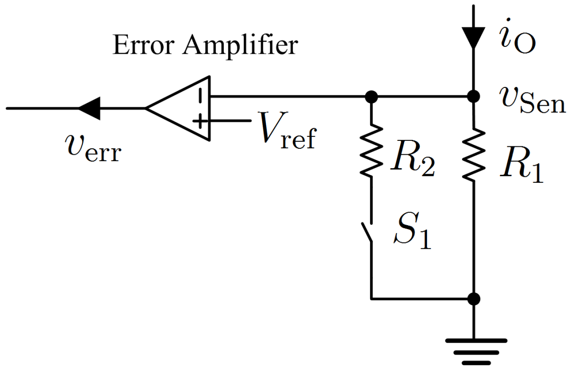

Figure 3.11: Switch-controlled current sensing resistor used in bi-level PWM method.

$$r_{\mathrm{sen}}(t) = [(R_2 \setminus\!\!\setminus R_1) - R_1] \sum_{n=1}^{+\infty} [u(nt) - u(nt - nT_{\mathrm{d}}D_{\mathrm{d}})] + R_1 \tag{3.11}$$

In general, the average output current in this driving method is:

$$\begin{aligned} \bar{I_{\mathrm{O}}} &= \frac{1}{T_{\mathrm{d}}} \int_{\delta}^{\delta+T_{\mathrm{d}}} \left\{ [I_{\mathrm{OH}} - I_{\mathrm{OL}}] \sum_{n=1}^{+\infty} [u(nt) - u(nt - nT_{\mathrm{d}}D_{\mathrm{d}})] + I_{\mathrm{OL}} \right\} dt \\ \bar{I_{\mathrm{O}}} &= \frac{1}{T_{\mathrm{d}}} [D_{\mathrm{d}} I_{\mathrm{OH}} + (1 - D_{\mathrm{d}}) I_{\mathrm{OL}}] \\ \bar{I_{\mathrm{O}}} &= I_{\mathrm{OH}} \left[D_{\mathrm{d}} + \frac{I_{\mathrm{OL}}}{I_{\mathrm{OH}}} (1 - D_{\mathrm{d}}) \right] \end{aligned} \tag{3.12}$$

Hence, the dimming factor in the bi-level PWM driving method is:

$$k_{\mathrm{d}} = D_{\mathrm{d}} + \frac{I_{\mathrm{OL}}}{I_{\mathrm{OH}}} (1 - D_{\mathrm{d}}) \tag{3.13}$$

The above equation implies that the minimum dimming factor value is found when D_{d} is chosen to be zero such that $k_{\mathrm{d}} = I_{\mathrm{LL}}/I_{\mathrm{LH}}$. This implies that the

Table 3.1: Current Time Function and Dimming Factor on each LED Current Driving Method

Method	Current Time Function	Dimming Factor
AM	$i_{\mathrm{L}}(t) = k_{\mathrm{d}} I_{\mathrm{Lo}}$	k_{d}
PWM	$i_{\mathrm{L}}(t) = I_{\mathrm{Lo}} \sum_{n=1}^{+\infty} [u(nt) - u(nt - nT_{\mathrm{d}} D_{\mathrm{d}})]$	D_{d}
Bi-level	$i_{\mathrm{L}}(t) = I_{\mathrm{Lo}} \sum_{n=1}^{+\infty} [u(nt) - u(nt - nT_{\mathrm{d}} D_{\mathrm{d}})]$	$D_{\mathrm{d}} + \frac{I_{\mathrm{LL}}}{I_{\mathrm{LH}}}(1 - D_{\mathrm{d}})$

dimming factor in the bi-level PWM driving method cannot reach zero as long as I_{OL} is non-zero. Thus, the trade off of the bi-level PWM driving method is the reduction of the dimming range.

3.4 Summary

This chapter re-visits three major LED current driving methods, namely, amplitude-mode, pulse-width modulation mode and bi-level pulse-width modulation mode. The benefits and drawbacks of each of these driving methods are discussed. Different implementation circuits for each deriving method are studied and analyzed. The output current time functions and the dimming factors are defined to describe the properties for each LED current driving method, which is listed in TABLE 3.1.

Chapter 4

Modeling of LED Current Driving Systems

4.1 Introduction

In Chapter 3, three LED current driving methods are introduced. This Chapter focuses on constructing models for those driving methods. The motivation of this chapter is to develop a modeling method which can be used in computer simulation so as to predict the small-signal and large-signal's behaviors of the entire system, such as evaluating output voltage and current levels between two dimming states in PWM and bi-level driving methods. In Section 4.2, we starts with analyzing the method of constructing the large-signal model. Experimental waveforms are compared with the simulated waveforms generated from the proposed model. We then look into the small-signal model and stability issues in Section 4.3, where the measured loop gain of the experimental prototype of an LED driving system is compared with the simulation results.

4.2 Large Signal Modeling of LED Current Driving Systems

The large-signal model of an LED current driving system is being studied in this section. Figure 4.1 shows a general block diagram of the model. We will divide the whole LED system into several sub-blocks and discuss how to formulate each sub-block individually. All the sub-blocks will be eventually combined together to form the entire model of the whole system. The details of the construction of each sub-block will be discussed.

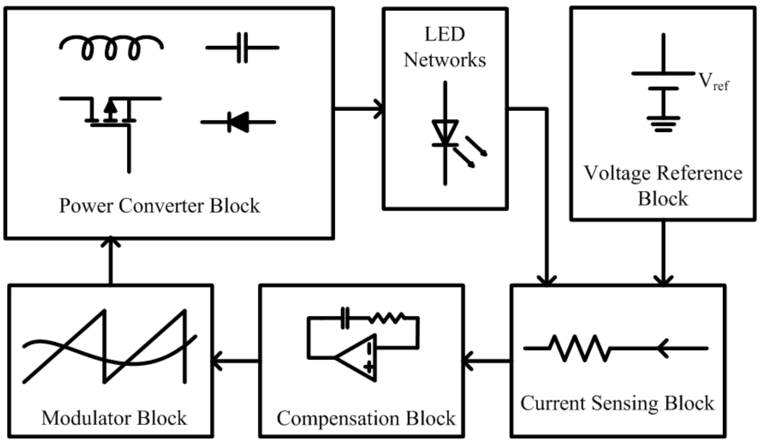

Figure 4.1: Sub-blocks in the model of LED driving system.

4.2.1 Formation of Sub-Blocks in Large-Signal Model

4.2.1.1 Sensing Circuit Model and Voltage Reference

Different current sensing methods are used in LED current driving circuits as discussed in Section 3.3. These sensing circuits, according to the circuit modeling approach, can be categorized into two types: i) based on changing the voltage reference signals and ii) based on changing the gain of the sensing block . An example of the first approach is to adjust the output level of the programmable voltage reference IC in the AM driving method as indicated in Fig. 3.3. The corresponding model is revealed in Fig. 4.2.

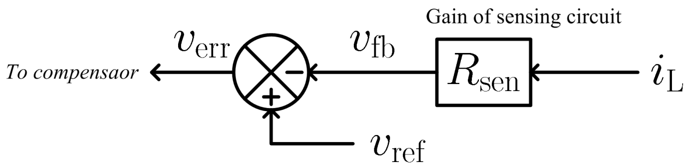

Figure 4.2: Block diagram of the current sensing circuit shown in Fig 3.3.

One of the examples in the second approach is to change the equivalent resistance of the current sensing resistor network in the bi-level driving method. Taking the circuit shown in Fig. 3.11 as an example, the equivalent circuit model is revealed in Fig. 4.3. In this circuit, the voltage reference signal remains unchanged while the gain of the sensing block changes in time periodically according to Eq. (3.11), where the transfer function of the current sensing block, $h_{\mathrm{sen}}(s)$, is equal to the Laplace transform of $r_{\mathrm{sen}}(t)$ in Eq. (3.11).

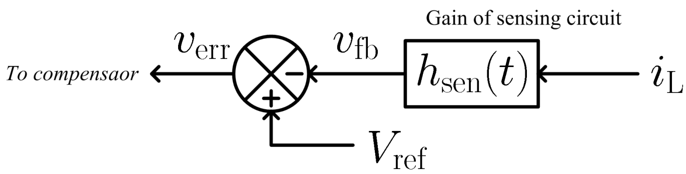

Figure 4.3: Block diagram of the current sensing sensing circuit shown in Fig 3.11.

In order to unify the model of the sensing block among all different sensing methods, a unified model is proposed as shown in Fig. 4.4, in which the gain of

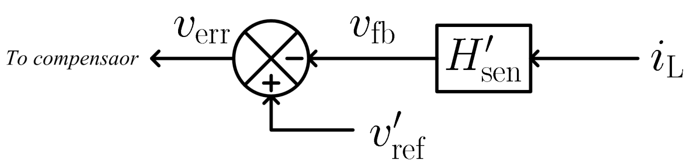

Figure 4.4: The unified block diagram for current sensing circuit.

the current sensing block, H'_S, is kept at constant and the transformed voltage reference signal, $v'_{ref}(t)$, is allowed to change. If the current sensing circuit is achieved by varying the voltage reference signal, the original block is identical to the unified block. Taking Fig. 4.2 as an example, H'_S is equal to R_{sen} while $v'_{ref}(t)$ is equal to $v_{ref}(t)$. If the gain of a sensing circuit varies, a transformation procedure ies required to convert the model into a unified form. The following procedure shows how to transform the model shown in Fig. 4.3 into a unified form. As the summing block's inputs in the model represent the input of an error amplifier in the system, we can assume that the inventing input and non-inventing input of the error amplifier would be equal during the steady state provided that the steady state error is neglected in the ideal case. Hence, the following two equations represent the relationship of the two input levels of the error amplifier during two dimming states in the bi-level driving method:

$$\begin{cases} V_{\mathrm{ref}} = (R_2 \mathbin{\backslash\backslash} R_1) i_{\mathrm{L}} & \text{During } D_{\mathrm{d}} T_{\mathrm{d}} \\ V_{\mathrm{ref}} = R_1 i_{\mathrm{L}} & \text{During } (1 - D_{\mathrm{d}}) T_{\mathrm{d}} \end{cases} \tag{4.1}$$

Comparing Eq. (4.1) and Eq. (3.11), we conclude:

$$v'_{\mathrm{ref}}(t) = \left[\frac{(R_2 \mathbin{\backslash\backslash} R_1) - R_1}{H'_S} \right] \sum_{n=1}^{+\infty} [u(nt) - u(nt - nT_{\mathrm{d}} D_{\mathrm{d}})] + \frac{R_1}{H'_S} \tag{4.2}$$

Table 4.1: General Unified Equation for $v'_{ref}(t)$.

Method	$v'_{ref}(t)$ Equation
AM	$v'_{\mathrm{ref}}(t) = k_{\mathrm{d}} V'_{\mathrm{refo}}$
PWM	$v'_{\mathrm{ref}}(t) = (V'_{\mathrm{refo}}) \sum_{n=1}^{+\infty} [u(nt) - u(nt - nT_{\mathrm{d}} D_{\mathrm{d}})]$
Bi-level	$v'_{\mathrm{ref}}(t) = (V'_{\mathrm{refH}} - V'_{\mathrm{refL}}) \sum_{n=1}^{+\infty} [u(nt) - u(nt - nT_{\mathrm{d}} D_{\mathrm{d}})] + V'_{\mathrm{refL}}$

Since H'_S is the scaled ratio between the transformed voltage reference signal and the load current, it can be any trivial number chosen in the model. Similar transformation procedures can be performed in the variable gain control circuits such as the variable sensing resistor circuit shown in Fig. 3.1 and the variable gain of the current sense amplifier circuit shown in Fig. 3.2. The routine transform procedure for each of the following circuits will not be shown in this discussion.

In this unified form, there is a general format for the equation of the transformed voltage reference signal $v'_{ref}(t)$ in AM, PWM and bi-level driving methods. The general equation is indicated in TABLE 4.1.

4.2.1.2 Modulator Model

The modeling of the modulator circuit will follows traditional method. This section will take the fixed-frequency variable-duty-cycle controller model as an example. The basic mechanism of this control scheme is shown in Fig. 4.5, in which the ramp signal is being compared with the error voltage generated from the error amplifier. The desired switching duty cycle d is generated. They can be related by:

$$\frac{v_{\mathrm{err}} - V_{\mathrm{L}}}{V_{\mathrm{H}} - V_{\mathrm{L}}} = d \tag{4.3}$$

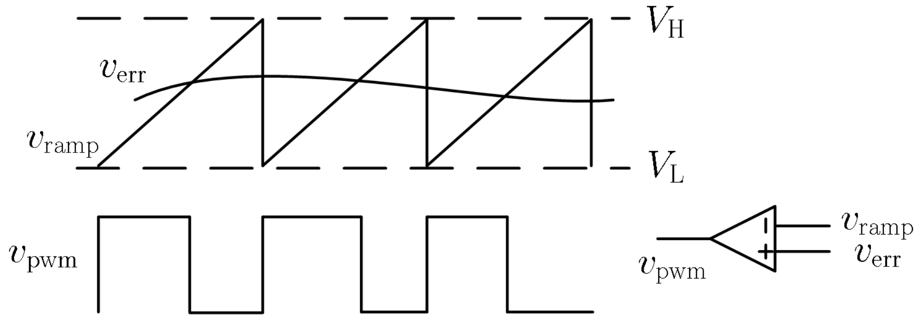

Figure 4.5: Illustration waveforms of the PWM modulator.

The gain of the PWM modulator block would be:

$$G_{\mathrm{M}} = \frac{\hat{v_{\mathrm{err}}}}{\hat{d}} = \frac{1}{V_{\mathrm{H}} - V_{\mathrm{L}}} \tag{4.4}$$

4.2.1.3 Load Resistance Model

The dc resistance of the load viewed from the power converter, R_{O}, is needed to obtain in order to deduce steady-state solution of the power converter, which will be discussed in Section 4.2.2. This equivalent dc resistance can be evaluated by calculating the ratio of the V_{O} to I_{O}. Using Eq. (3.2), we can obtain:

$$\begin{aligned} R_{\mathrm{O}} &= \frac{V_{\mathrm{O}}}{I_{\mathrm{O}}} \\ &= R_{\mathrm{Sen}} + \frac{V_{\mathrm{d,jk}}}{I_{\mathrm{d,jk}}} \\ &= R_{\mathrm{Sen}} + R_{\mathrm{d,jk}} \end{aligned} \tag{4.5}$$

The load dc resistance, R_{O}, is the sum of the current sensed resistor value,

R_{Sen}, and the dc resistance of the LED network, $R_{\mathrm{d,jk}}$. As discussed in Chapter 2, the characteristic model of the LED connected network can be used for finding $R_{\mathrm{d,jk}}$. Since LED manufacturers undergo a binning process for their products, the characteristic variation of LEDs in the same binning can be minimized. In our analysis, we assume that all LEDs used in the connected network are in the same binning and that all LEDs are identical. The procedure of determining the equivalent dc resistance is as follows:

1. Obtain the LED characteristic model discussed in Chapter 2.
2. Identify the number of LEDs, j, connected in an LED string and the number of string, k, used in the LED connected network.
3. Transform the LED characteristic model to the model of the LED connected network according to j and k.
4. Define and measure the steady state operation point(s) (one point for AM-mode and two points for PWM and bi-level modes) in the system (such as the load current and junction temperature)
5. Calculate the dc resistance using the method discussed in Chapter 2.

4.2.1.4 Power Converter Model

It is important to find a set of averaged equivalent differential equations to represent the properties of a switching mode power converter used in the system. Any traditional modeling methods, such as state-space averaged model, averaged switch model, MISSCO model, current-injected model, etc, can be used in our LED driving system's model. The details of forming an equivalent model are well discussed in the literature and will not be discussed in this thesis.

4.2.2 Example of the Proposed Large Signal Modeling Approach

The construction method of the model of an LED driving system is discussed in Section 4.2.1. An example is given in this section to illustrate the concept of constructing the model of an LED driving system based on the technique discussed in Section 4.2.1. An experimental LED driving circuit has been built and the schematic is shown in Fig. 4.6. The circuit can be configured as either AM, PWM or bi-level current driving method by means of adjusting an appropriate voltage reference signal. The power stage used a buck converter operating in continuous inductor current conduction mode with the switching frequency of 500 kHz. The voltage reference signal is generated according to TABLE 4.1. The specification of the systems is listed in TABLE 4.3. The computer simulation is conducted by using MATLAB Simulink. To compare the simulated results with experimental measurement, the circuits operated on these driving methods and the conditions are shown in TABLE 4.2. The steps of forming the models are discussed in details as follows:

Table 4.2: Specifications in Each of Conditions.

Condition	Driving Method	j	k	I_{OH}	I_{OL}	V_{refH}	V_{refL}	T_{C}
1	AM	1	1	1 A	N/A	0.5 V	N/A	45 °C
2	PWM	1	1	1 A	0 A	0.5 V	0 V	35.5 °C
3	Bi-level	1	1	1 A	0.5 A	0.5 V	0.25 V	41.5 °C
4	AM	2	1	1 A	N/A	0.5 V	N/A	45.5 °C
5	PWM	2	1	1 A	0 A	0.5 V	0 V	36 °C
6	Bi-level	2	1	1 A	0.5 A	0.5 V	42.5 V	40 °C

Gain of Current Sensing Network The current sensing circuit uses a current sensing resistor and the current sensing amplifier U1. The current sensing block's transresistance gain H'_{s} can be calculated by the multiplication of the current sensing resistor value and the gain of the current sensing amplifier:

$$\begin{aligned}
H'_{\mathrm{S}} &= \frac{v_{\mathrm{fb}}}{i_{\mathrm{L}}} \\
H'_{\mathrm{S}} &= \left(\frac{R_{\mathrm{f1}}}{R_{\mathrm{a1}}}\right) R_{\mathrm{sen}} \\
H'_{\mathrm{S}} &= \left(\frac{2\ \mathrm{k\Omega}}{1\ \mathrm{k\Omega}}\right) 0.5\ \Omega \\
H'_{\mathrm{S}} &= 1\ \Omega
\end{aligned} \tag{4.6}$$

Voltage Reference Signal The way of generating a voltage reference signal depends on the driving method. The voltage reference generator consists of two voltage reference digital controller ICs, X60250, (U2) and (U3), and an analog multiplexer, SN74LVC1G3157, (U4). The I^{2}C bus and the PWM dimming signal

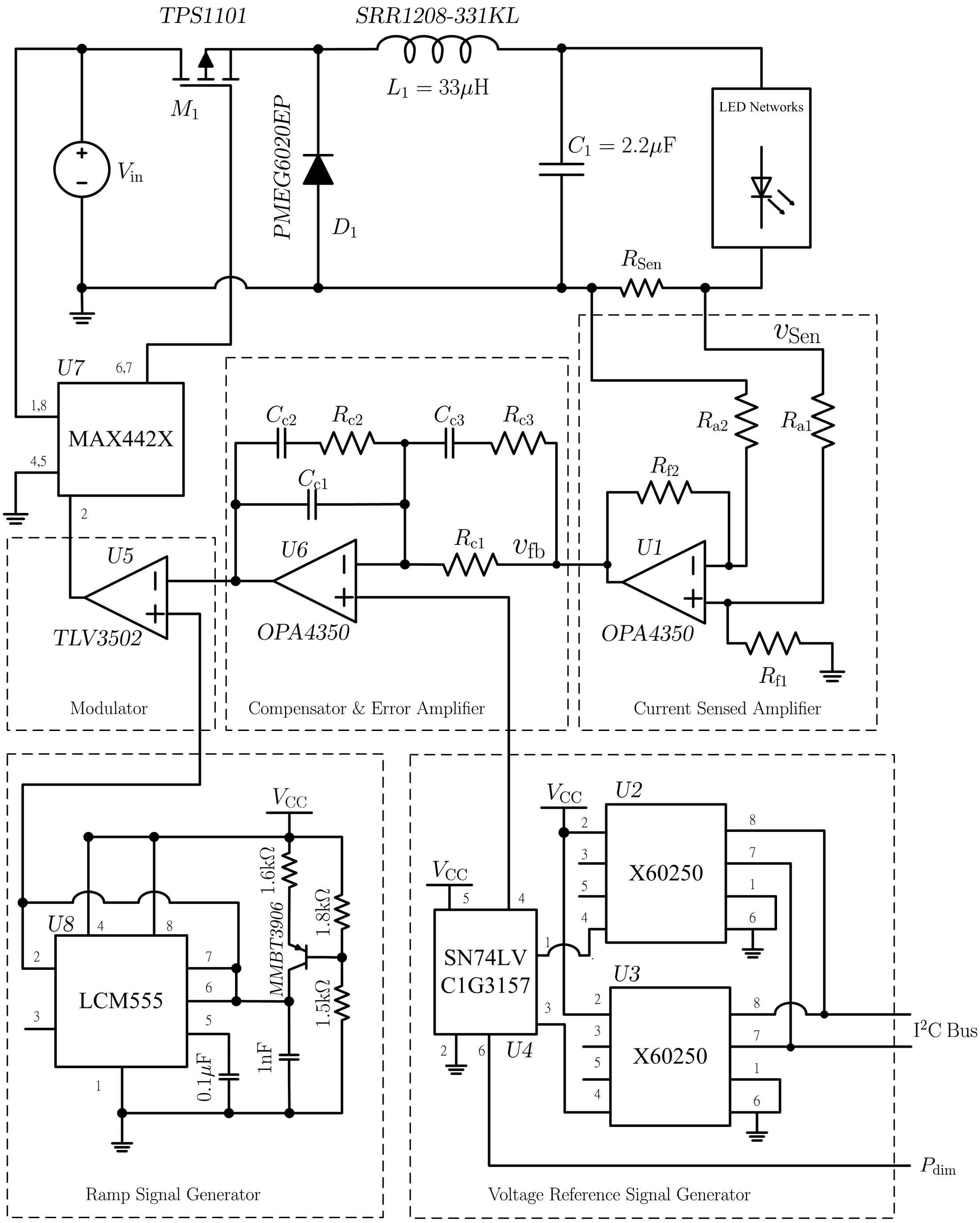

Figure 4.6: Schematic of the experimental LED driving circuit.

Table 4.3: Specifications of the Experimental LED Current Driving Circuit.

Description	Symbol	Value
General System Parameters		
Power converter	N/A	Buck
Current driving method	N/A	†
Output low current	i_{OL}	†
Output high current	i_{OH}	†
Number of LED used in string	j	†
Number of LED string used	k	†
Dimming frequency	f_{d}	1 kHz
Nominal dimming duty cycle	D_{d}	0.5
Measured Case Temperature	T_{C}	†
Power Converter Parameters		
Switching frequency	f_{SW}	500 kHz
Inductance	L_1	22 μH
Capacitance	C_1	10 μF
Controller Parameter		
Current sensing resistor	R_{sen}	0.5 Ω
Feedback resistor of current sensed amplifier	R_{f}	10 kΩ
Input resistor of current sensed amplifier	R_{a}	1 k
Low reference voltage	V_{refL}	†
High reference voltage	V_{refH}	†
Ramp signal high voltage	V_{H}	2.4 V
Ramp signal low voltage	V_{L}	0 V

† Those values depends on different conditions shown in TABLE 4.2.

P_{dim} are connected to a micro-controller to adjust the voltage reference levels and generate PWM dimming signals, respectively.

Under AM-mode, the PWM dimming signal is turned off such that the analog multiplexer U4 always select U2 as an output and the voltage reference signal time function is always constant:

$$v'_{\mathrm{ref}}(t) = 0.5\,\mathrm{V} \tag{4.7}$$

Under PWM or bi-level mode, U4 selects two voltage reference levels generated from U2 and U3 in turn. The voltage reference signal can be expressed as:

For PWM:

$$\begin{aligned} v'_{\mathrm{ref}}(t) &= (V'_{\mathrm{refH}}) \sum_{n=1}^{+\infty} [u(nt) - u(nt - nT_{\mathrm{d}}D_{\mathrm{d}})] \\ v'_{\mathrm{ref}}(t) &= 0.5 \sum_{n=1}^{+\infty} \left[u(nt) - u(nt - n\frac{0.5}{1000}) \right] \end{aligned} \tag{4.8}$$

For bi-level

$$\begin{aligned} v'_{\mathrm{ref}}(t) &= (V'_{\mathrm{refH}} - V'_{\mathrm{refL}}) \sum_{n=1}^{+\infty} [u(nt) - u(nt - nT_{\mathrm{d}}D_{\mathrm{d}})] + V'_{\mathrm{refL}} \\ v'_{\mathrm{ref}}(t) &= (0.5 - 0.25) \sum_{n=1}^{+\infty} \left[u(nt) - u(nt - n\frac{0.5}{1000}) \right] + 0.25 \end{aligned} \tag{4.9}$$

In the simulation tool, Simulink, a constant term can be represented by a "Constant" block for the AM method. A "Repeating Sequence" block can be used to realize the voltage time functions for the PWM and bi-level driving methods. These blocks are multiplexed using a "Multiport Switch" block while a "Vref Control" the constant input block is used to select the appropriate reference signal for each of the simulation conditions. The whole voltage reference block is shown in Fig. 4.7.

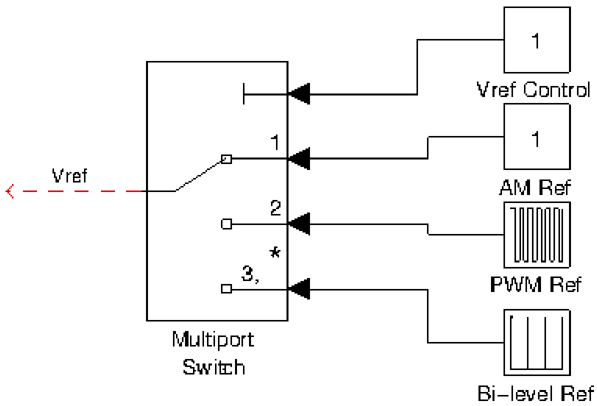

Figure 4.7: Simulation block for voltage reference signal.

Modulator Model Since the control scheme of this circuit uses a fixed-frequency duty-cycle-control, the zero-crossing comparator block is used to model the modulator and the saw-sooth waveform block is used for the ramp signal. The full simulation diagram of the modulator model is shown in Fig. 4.8. The comparator U5 is realized in the model using the "Relay" block and the ramp signal generator is modeled using the "Repeating Sequence" block.

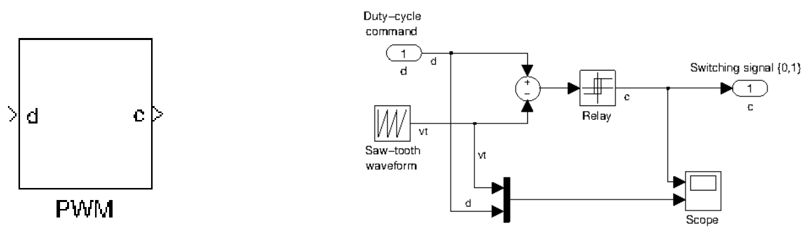

(a) Block mask

(b) Block diagram

Figure 4.8: Simulation block for modulator.

Load Resistance Model The dc resistance can be found by adopting the method discussed in Section 4.2.1.3. Figure 4.9 shows the operating $v_\mathrm{d} - i_\mathrm{d}$ curve of the LED array operated in AM, PWM and bi-level operation, respectively. The calculated output voltages, dc resistances of the LED array and the output resistance are listed in TABLE 4.4.

Table 4.4: Evaluation of DC Load Resistance in Different Conditions.

Condition	I_OH	V_OH	I_OL	V_OL	$R_\mathrm{d,jkH}$	R_OH	$R_\mathrm{d,jkL}$	R_OL
1	1000 mA	3.1597 V	N/A	N/A	3.1597 Ω	3.6597 Ω	N/A	N/A
2	1000 mA	3.1952 V	N/A	N/A	3.1952 Ω	3.6952 Ω	N/A	N/A
3	1000 mA	3.1724 V	500 mA	3.004 V	3.1724 Ω	3.6724 Ω	6.008 Ω	6.508 Ω
4	1000 mA	6.3156 V	N/A	N/A	6.3156 Ω	6.8156 Ω	N/A	N/A
5	1000 mA	6.3866 V	N/A	N/A	6.3866 Ω	6.8866 Ω	N/A	N/A
6	1000 mA	6.3556 V	500 mA	6.0183 V	6.3556 Ω	6.8556 Ω	12.0366 Ω	12.5366 Ω

Power Converter Model The state space averaging method is used to derive the state equations representing the buck converter used in the LED driving circuit. The inductor (L_1) current, i_L, and capacitor (C_1) voltage, v_C, will be put into the state vector $\mathbf{x}$. The load current, i_L is the output variable y and the input voltage, v_in, is the input variable u, such that:

$$\begin{cases} \mathbf{x} & = [v_\mathrm{C}\ i_\mathrm{L}]^\mathrm{T} \\ y & = i_\mathrm{O} \\ u & = v_\mathrm{in} \end{cases} \tag{4.10}$$

A set of differential equations will be formulated in the following calculation to describe the behavior of the power converter, where n is the number of states of the converter during operation. In this example, n is equal to 1 or 2 when S_1 turns on or off, respectively.

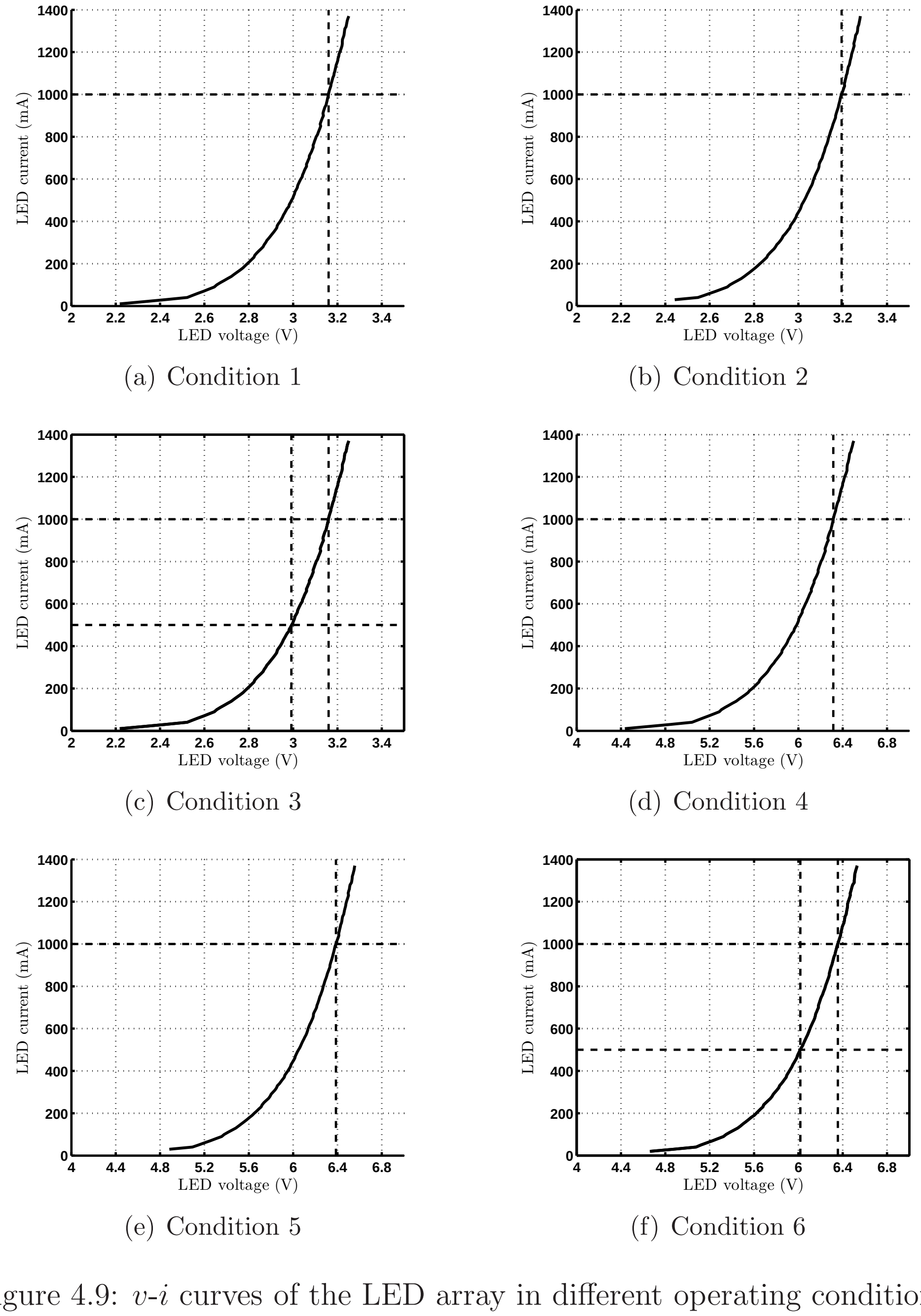

(a) Condition 1

(b) Condition 2

(c) Condition 3

(d) Condition 4

(e) Condition 5

(f) Condition 6

Figure 4.9: v-i curves of the LED array in different operating conditions.

$$\begin{cases} \dot{\mathbf{x}} & = \mathbf{A}_n\mathbf{x} + \mathbf{B}_n u \\ y & = \mathbf{C}_n\mathbf{x} + \mathbf{E}_n u \end{cases} \tag{4.11}$$

$\mathbf{A}_n$, $\mathbf{B}_n$, $\mathbf{C}_n$ and $\mathbf{E}_n$ are the state matrix, input matrix, output matrix and feed-forward matrix respectively.

During the period that transistor S_1 is turned on ($n = 1$), the power converter becomes the circuit network as shown in Fig. 4.10 and the differential equations describing this state are:

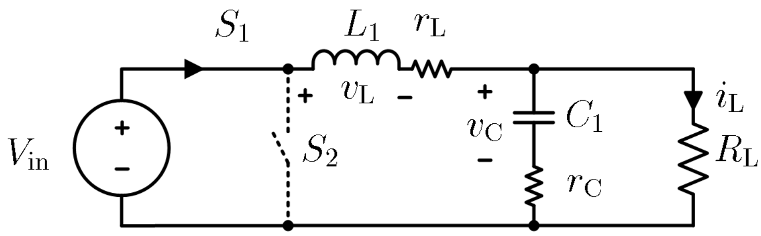

Figure 4.10: Circuit corresponding to S_1 being turned on.

$$\begin{cases} \frac{dv_C}{dt} & = \frac{1}{(r_O+r_C)C_1}v_C + \frac{r_O}{r_O+r_C}i_L \\ \frac{di_L}{dt} & = -\frac{r_O}{(r_O+r_C)L_1}v_C + \frac{1}{L_1}(\frac{r_Or_C}{r_O+r_C} + r_L)i_L + \frac{1}{L_1}v_{in} \\ i_O & = \frac{1}{r_O+r_C}v_C + \frac{r_O}{r_C+r_C}i_L \end{cases} \tag{4.12}$$

Comparing with Eq. (4.10) and Eq. (4.12), we have:

$$\mathbf{A}_1 = \begin{bmatrix} -\frac{1}{(r_O+r_C)C_1} & \frac{r_O}{(r_O+r_C)C_1} \\ -\frac{r_O}{(r_O+r_C)L_1} & \frac{1}{L_1}(\frac{r_Or_C}{r_O+r_C} + r_L) \end{bmatrix} \tag{4.13}$$

$$\mathbf{B}_1 = \begin{bmatrix} 0 \\ \frac{1}{L_1} \end{bmatrix} \tag{4.14}$$

$$\mathbf{C}_1 = \begin{bmatrix} \frac{1}{(r_\mathrm{O}+r_\mathrm{C}} & \frac{r_\mathrm{O}}{(r_\mathrm{O}+r_\mathrm{C}} \end{bmatrix} \tag{4.15}$$

$$\mathbf{D}_1 = 0 \tag{4.16}$$

Similarly, during the period that transistor S_1 is turned off ($n = 2$), the power converter becomes the circuit network as shown in Fig. 4.11 and the differential equations describing this state are:

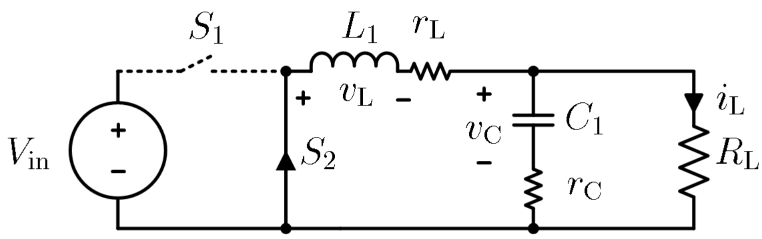

Figure 4.11: Circuit corresponding to S_2 being turned on.

$$\begin{cases} \frac{dv_\mathrm{C}}{dt} &= \frac{1}{(r_\mathrm{O}+r_\mathrm{C})C_1} v_\mathrm{C} + \frac{r_\mathrm{O}}{r_\mathrm{O}+r_\mathrm{C}} i_\mathrm{L} \\ \frac{di_\mathrm{L}}{dt} &= -\frac{r_\mathrm{O}}{(r_\mathrm{O}+r_\mathrm{C})L_1} v_\mathrm{C} + \frac{1}{L_1}(\frac{r_\mathrm{O} r_\mathrm{C}}{r_\mathrm{O}+r_\mathrm{C}} + r_\mathrm{L}) i_\mathrm{L} \\ i_\mathrm{O} &= \frac{1}{r_\mathrm{O}+r_\mathrm{C}} v_\mathrm{C} + \frac{r_\mathrm{C}}{r_\mathrm{O}+r_\mathrm{C}} i_\mathrm{L} \end{cases} \tag{4.17}$$

Comparing with Eq. (4.10) and Eq. (4.17), we have:

$$\mathbf{A}_2 = \mathbf{A}_1 \tag{4.18}$$

$$\mathbf{B}_2 = 0 \tag{4.19}$$

$$\mathbf{C}_2 = \mathbf{C}_1 \tag{4.20}$$

$$\mathbf{D}_1 = 0 \tag{4.21}$$

By using the state-space averaging method, we obtain:

$$\begin{aligned} \bar{\mathbf{A}} &= d\mathbf{A}_1 + (1-d)\mathbf{A}_2 \\ \bar{\mathbf{B}} &= d\mathbf{B}_1 + (1-d)\mathbf{B}_2 \\ \bar{\mathbf{C}} &= d\mathbf{C}_1 + (1-d)\mathbf{C}_2 \\ \bar{\mathbf{D}} &= d\mathbf{D}_1 + (1-d)\mathbf{D}_2 \end{aligned} \tag{4.22}$$

$$\bar{\mathbf{A}} = \begin{bmatrix} -\frac{1}{(r_{\mathrm{O}}+r_{\mathrm{C}})C_1} & \frac{r_{\mathrm{O}}}{(r_{\mathrm{O}}+r_{\mathrm{C}})C_1} \\ -\frac{r_{\mathrm{O}}}{(r_{\mathrm{O}}+r_{\mathrm{C}})L_1} & \frac{1}{L_1}\left(\frac{r_{\mathrm{O}}r_{\mathrm{C}}}{r_{\mathrm{O}}+r_{\mathrm{C}}} + r_{\mathrm{L}}\right) \end{bmatrix} \tag{4.23}$$

$$\bar{\mathbf{B}} = \begin{bmatrix} 0 \\ \frac{d}{L_1} \end{bmatrix} \tag{4.24}$$

$$\bar{\mathbf{C}} = \begin{bmatrix} \frac{1}{(r_{\mathrm{O}}+r_{\mathrm{C}}} & \frac{r_{\mathrm{O}}}{(r_{\mathrm{O}}+r_{\mathrm{C}}} \end{bmatrix} \tag{4.25}$$

$$\bar{\mathbf{D}} = 0 \tag{4.26}$$

Hence,

$$\begin{cases} \frac{dv_{\mathrm{C}}}{dt} & = \frac{1}{(r_{\mathrm{O}}+r_{\mathrm{C}})C_1} v_{\mathrm{C}} + \frac{r_{\mathrm{O}}}{(r_{\mathrm{O}}+r_{\mathrm{C}})C_1} i_{\mathrm{L}} \\ \frac{di_{\mathrm{L}}}{dt} & = -\frac{r_{\mathrm{O}}}{(r_{\mathrm{O}}+r_{\mathrm{C}})L_1} v_{\mathrm{C}} + \frac{1}{L_1}(\frac{r_{\mathrm{O}} r_{\mathrm{C}}}{r_{\mathrm{O}}+r_{\mathrm{C}}} + r_{\mathrm{L}}) i_{\mathrm{L}} + \frac{d}{L_1} v_{\mathrm{in}} \\ i_{\mathrm{O}} & = \frac{1}{r_{\mathrm{O}}+r_{\mathrm{C}}} v_{\mathrm{C}} + \frac{r_{\mathrm{C}}}{r_{\mathrm{O}}+r_{\mathrm{C}}} i_{\mathrm{L}} \end{cases} \tag{4.27}$$

Using the fact that $r_{\mathrm{O}} \gg r_{\mathrm{C}}$ and $r_{\mathrm{O}} \gg r_{\mathrm{L}}$, Eq. (4.27) can be simplified as

$$\begin{cases} \frac{dv_{\mathrm{C}}}{dt} & = \frac{1}{C_1}\left(-\frac{v_{\mathrm{C}}}{r_{\mathrm{O}}} + i_{\mathrm{L}}\right) \\ \frac{di_{\mathrm{L}}}{dt} & = \frac{1}{L_1}\left(-v_{\mathrm{C}} - (r_{\mathrm{C}} + r_{\mathrm{L}}) i_{\mathrm{L}} + d v_{\mathrm{in}}\right) \\ i_{\mathrm{O}} & = \frac{1}{r_{\mathrm{O}}}\left(v_{\mathrm{C}} + r_{\mathrm{C}} i_{\mathrm{L}}\right) \end{cases} \tag{4.28}$$

As for the large-signal analysis, the variable r_{O} can be replaced by the dc output resistance R_{O}. Substituting the known parameters defined in TABLE 4.3, Eq. (4.28) becomes

$$\begin{cases} \frac{dv_{\mathrm{C}}}{dt} & = \frac{1}{10\ \mu\mathrm{F}} \left(-\frac{v_{\mathrm{C}}}{R_{\mathrm{O}}} + i_{\mathrm{L}} \right) \\ \frac{di_{\mathrm{L}}}{dt} & = \frac{1}{33\ \mu\mathrm{H}} \left(-v_{\mathrm{C}} - (0.1\ \Omega) i_{\mathrm{L}} + d v_{\mathrm{in}} \right) \\ i_{\mathrm{O}} & = \frac{1}{R_{\mathrm{O}}} \left(v_{\mathrm{C}} + 0.05\ \Omega i_{\mathrm{L}} \right) \end{cases} \tag{4.29}$$

The variables v_{C} and i_{L} are the state variables in the system, r_{O}, d, v_{in} are the input variables, and i_{O} is the output variable. Equation (4.29) is a set of linearized differential equations for the power converter. It can be used in the simulation model to describe the behavior of the system. This model can be built by the Simulink blocks, such as the "Product", "Gain", 'Integrator", as shown in Fig. 4.12.

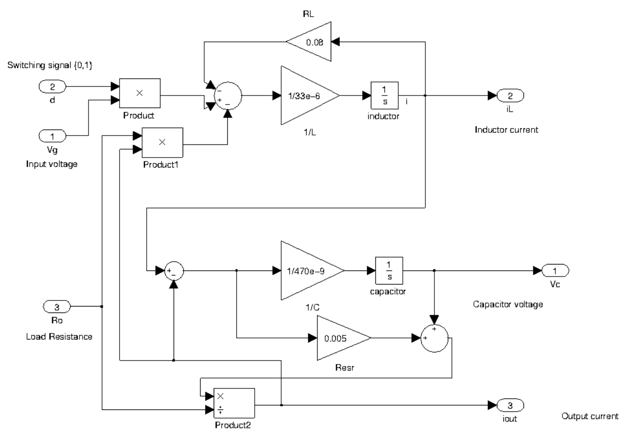

Figure 4.12: Simulation block for the power converter.

The Entire System Model The above simulation sub-blocks are combined together to form a complete model of the whole LED current driving system. The simulation block diagram is shown in Fig. 4.13. Since the design of the compensation network involves the ac modeling technique, the details of the compensation block will be discussed in Section 4.3.

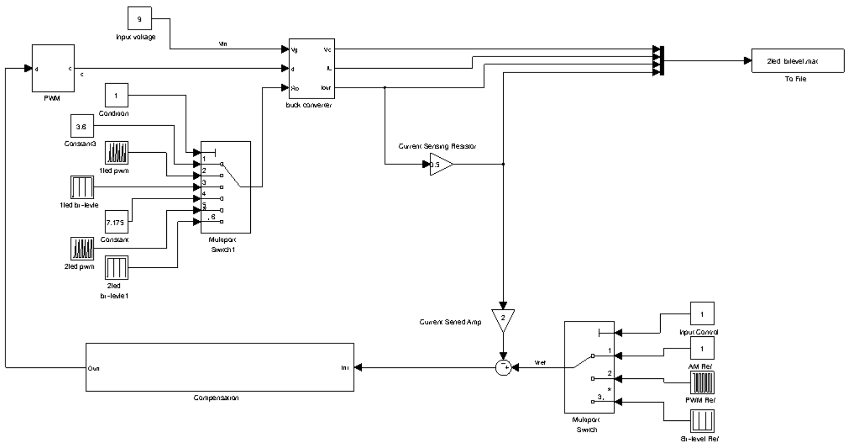

Figure 4.13: The completed simulation block for the whole LED driving system.

4.2.3 Large Signal Simulation and Experimental Waveforms

The previous section has discussed in detail the method of formation of an LED driving system under AM, PWM and bi-level current driving methods. This section discusses the simulation results. A prototype of an LED driving system is constructed. The measurement and simulation results are compared in order to reflect the validity of the simulation model.

An experimental LED driving circuits are constructed according to the six operating conditions shown in TABLE 4.2. In order to prove the validity of the simulation results, the measured output current, output voltage and the voltage sensing signal waveforms are compared with the simulation waveforms. The results are shown in Figs. 4.14 through 4.19. The results show that the simulation model can accurately predict different signals in different LED current driving methods.

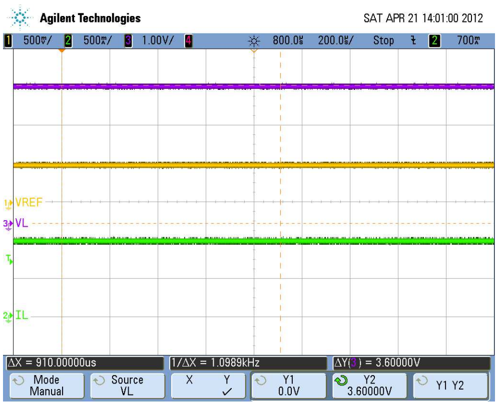

(a)

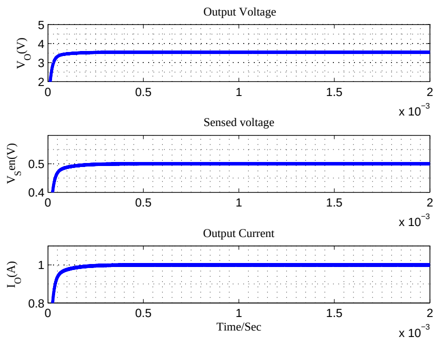

(b)

Figure 4.14: Experimental and simulated waveforms in condition 1.

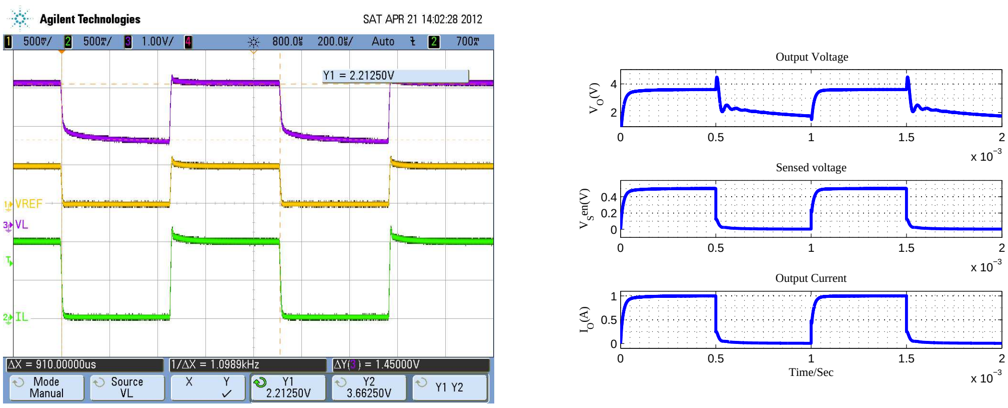

(a) (b)

Figure 4.15: Experimental and simulated waveforms in condition 2.

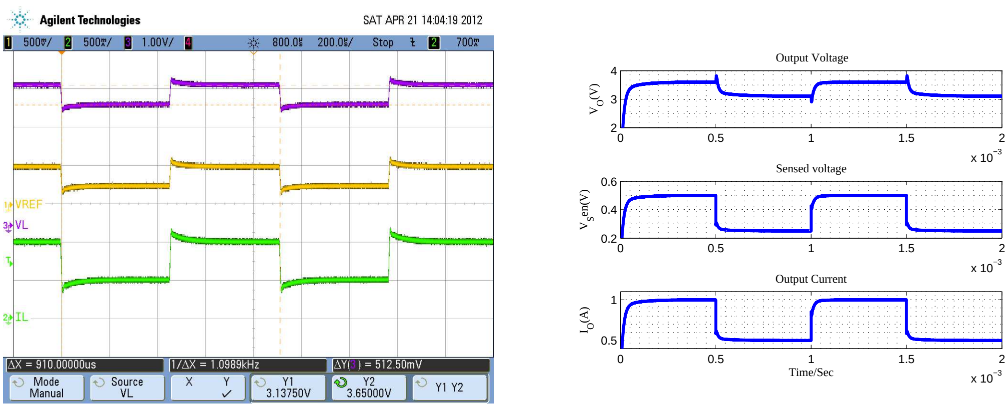

(a) (b)

Figure 4.16: Experimental and simulated waveforms in condition 3.

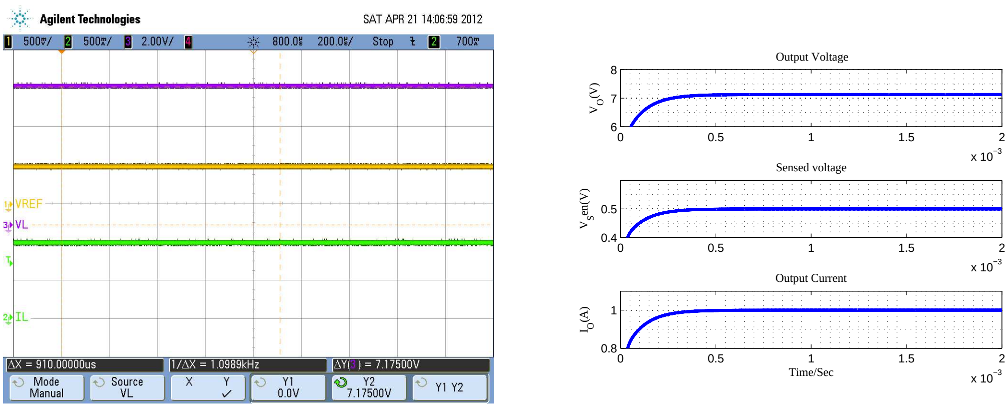

(a) (b)

Figure 4.17: Experimental and simulated waveforms in condition 4.

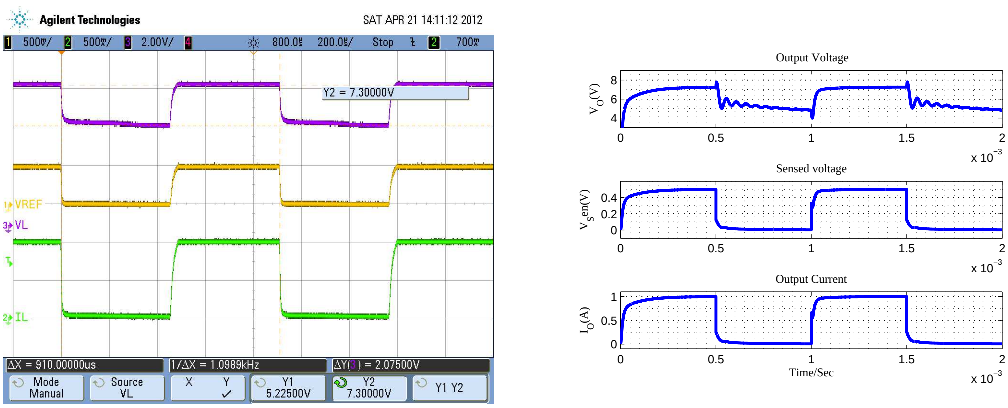

(a) (b)

Figure 4.18: Experimental and simulated waveforms in condition 5.

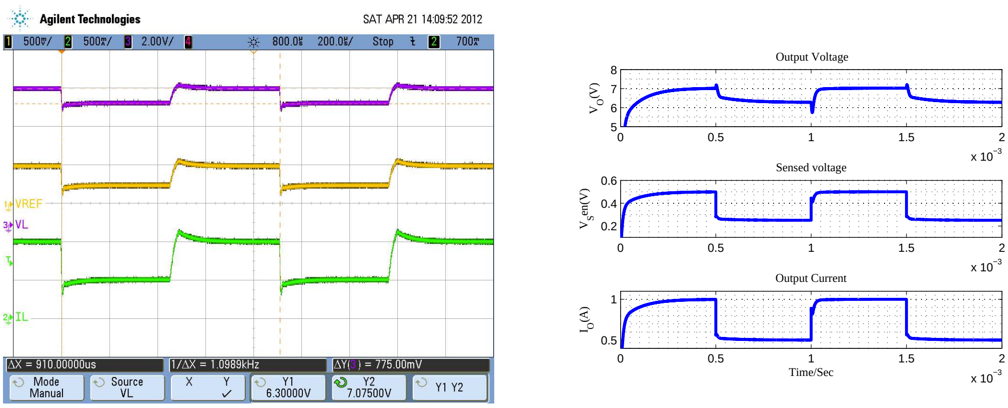

(a) (b)

Figure 4.19: Experimental and simulated waveforms in condition 6.

4.3 Small Signal Modeling of LED Driving Systems

This section provides an example of calculating the ac small signal transfer functions of the power converter, compensator, modulator and current sensing circuit. The loop gain of an LED driving system can be determined. The discussion on the design of an appropriate compensation network is provided in order to optimize the system bandwidth and DC gain. The experimental circuit studied in Section 4.2.2, which is shown in Fig. 4.6, will be considered again in this section to investigate its ac properties. We begin with discussing the specific issues of the LED driving systems raised in Section 4.3.1. Section 4.3.2 provides an example discussing the method of determining the transfer functions of the sub-system and the closed-loop transfer function from an prototype LED driving system. The loop gain measurement on the prototype circuit is compared with the simulation results in Section 4.3.3.

4.3.1 Transfer Functions of LED Driving Systems

In an LED current driving system, there is a converter output current (LED current) feedback loop for regulating a desired output current irrespective of the changes of circuit variations such as input voltage disturbance, thermal variation of components' values and variation of LED junction temperature. The current feedback loop consists of the feed-forward and feedback paths. The former is composed of the control-to-output transfer function of the power converter (plant transfer function), the compensator transfer function, and the modulator transfer function. The latter is composed of the transresistnace gain of the circuit sensing circuit (for example, the value of current sensing resistor) and the gain of the current sensed amplifier. Fig. 4.20 shows the small signal block diagram of an LED driving system. Hence, the small signal reference signal to output closed loop transfer function is

$$\frac{\hat{i_{\mathrm{O}}}}{\hat{v_{\mathrm{ref}}}} = \frac{G_{\mathrm{C}}G_{\mathrm{M}}G_{\mathrm{do}}}{1 + G_{\mathrm{C}}G_{\mathrm{M}}G_{\mathrm{do}}G_{\mathrm{sen}}R_{\mathrm{sen}}} \tag{4.30}$$

The loop gain of the system is

$$T_{\mathrm{lg}} = G_{\mathrm{C}}G_{\mathrm{M}}G_{\mathrm{do}}G_{\mathrm{sen}}R_{\mathrm{sen}} \tag{4.31}$$

When designing an LED driving system, the loop gain of the system is taken into account for analyzing the stability problem and optimizing the dynamic response. In the AM-mode current driving method, there is only one operating point while there is only one loop gain transfer function representing the state of this system. However, the situation in the bi-level driving method is different, in

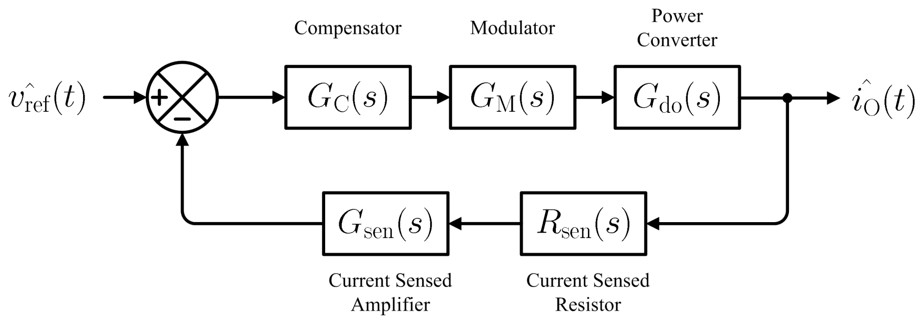

Figure 4.20: Illustration of the small signal model of an LED driving system.

that the system operates in two operating points for two dimming states in turn. The system is required to be stable for both operating points. For the PWM driving method, the system operates either at zero current or another operating point. The design approach is the same with the AM-mode as the operating point at zero can be omitted.

4.3.2 Example of Constructing Transfer Functions

4.3.2.1 Power Converter Transfer Functions

In Section 4.2, we developed a set of differential equations (Eq (4.27)) to describe the large-signal electrical properties of the power converter. We will make use of this set of equations to derive the small-signal behavior of the power converter. We apply small perturbation to the following signals:

$$
\begin{aligned}
i_{\mathrm{L}} &= I_{\mathrm{L}} + \hat{i_{\mathrm{L}}} \\
v_{\mathrm{C}} &= V_{\mathrm{C}} + \hat{v_{\mathrm{C}}} \\
d &= D + \hat{d} \\
v_{\mathrm{in}} &= V_{\mathrm{in}} + \hat{v_{\mathrm{in}}} \\
i_{\mathrm{O}} &= I_{\mathrm{O}} + \hat{i_{\mathrm{O}}}
\end{aligned}
\tag{4.32}
$$

The variables in capital letters represents the DC terms of the signals while the variables with a " ^ " represents the small perturbation signal. Putting Eq. (4.32) into Eq. (4.27),we get

$$
\begin{aligned}
\frac{dV_{\mathrm{C}}}{dt} + \frac{d\hat{v_{\mathrm{C}}}}{dt} &= -\frac{V_{\mathrm{C}}}{(r_{\mathrm{O}}+r_{\mathrm{C}})C_1} - \frac{\hat{v_{\mathrm{C}}}}{(r_{\mathrm{O}}+r_{\mathrm{C}})C_1} + \frac{r_{\mathrm{O}}I_{\mathrm{L}}}{(r_{\mathrm{O}}+r_{\mathrm{C}})C_1} + \frac{r_{\mathrm{O}}\hat{i_{\mathrm{L}}}}{(r_{\mathrm{O}}+r_{\mathrm{C}})C_1} \\
\frac{di_{\mathrm{L}}}{dt} + \frac{d\hat{i_{\mathrm{L}}}}{dt} &= -\frac{r_{\mathrm{O}}V_{\mathrm{C}}}{(r_{\mathrm{O}}+r_{\mathrm{C}})L_1} - \frac{r_{\mathrm{O}}\hat{v_{\mathrm{C}}}}{(r_{\mathrm{O}}+r_{\mathrm{C}})L_1} - \\
&\quad \frac{1}{L_1}\left(\frac{r_{\mathrm{O}}r_{\mathrm{C}}}{r_{\mathrm{O}}+r_{\mathrm{C}}} + r_{\mathrm{L}}\right)I_{\mathrm{L}} - \frac{1}{L_1}\left(\frac{r_{\mathrm{O}}r_{\mathrm{C}}}{r_{\mathrm{O}}+r_{\mathrm{C}}} + r_{\mathrm{L}}\right)\hat{i_{\mathrm{L}}} + \frac{DV_{\mathrm{in}}}{L_1} + \frac{D\hat{v_{\mathrm{in}}}}{L_1} + \frac{\hat{d}V_{\mathrm{in}}}{L_1} + \frac{\hat{d}\hat{v_{\mathrm{in}}}}{L_1} \\
I_{\mathrm{O}} + \hat{i_{\mathrm{O}}} &= \frac{V_{\mathrm{C}}}{r_{\mathrm{O}}+r_{\mathrm{C}}} + \frac{\hat{v_{\mathrm{C}}}}{r_{\mathrm{O}}+r_{\mathrm{C}}} + \frac{r_{\mathrm{C}}I_{\mathrm{L}}}{r_{\mathrm{O}}+r_{\mathrm{C}}} + \frac{r_{\mathrm{C}}\hat{i_{\mathrm{L}}}}{r_{\mathrm{O}}+r_{\mathrm{C}}}
\end{aligned}
\tag{4.33}
$$

Equation (4.33) contains DC terms, first order terms and higher order terms. To linearize the equation, we remove all those high order terms. The DC terms and first order terms can then be separated into two sets of equations. The DC equations are used to predict the averaged DC values of the state variables, input and output signals in the steady state. The output resistance r_{O} in those equations should be replaced by the DC equivalent output resistance, R_O, as defined in Eq. (4.5).

$$
\begin{aligned}
0 &= -\frac{V_C}{(R_O + r_C)C_1} + \frac{R_O I_L}{(R_O + r_C)C_1} \\
0 &= -\frac{R_O V_C}{(R_O + r_C)L_1} - \frac{1}{L_1}\left(\frac{R_O r_C}{R_O + r_C} + r_L\right)\hat{I_L} + \frac{DV_{in}}{L_1} \\
I_O &= \frac{V_C}{R_O + r_C} + \frac{r_C I_L}{R_O + r_C}
\end{aligned}
\tag{4.34}
$$

For the first-order equations, r_O should be replaced by the ac equivalent output resistance, $\hat{r_O}$, which is derived from Eq. (4.5):

$$\hat{r_O} = R_{Sen} + \hat{r_{d,jk}} \tag{4.35}$$

Hence,

$$
\begin{aligned}
\frac{d\hat{v_C}}{dt} &= -\frac{\hat{v_C}}{(\hat{r_O} + r_C)C_1} + \frac{\hat{r_O}\hat{i_L}}{(\hat{r_O} + r_C)C_1} \\
\frac{d\hat{i_L}}{dt} &= -\frac{\hat{r_O}\hat{v_C}}{(r_O + r_C)L_1} - \frac{1}{L_1}\left(\frac{\hat{r_O} r_C}{\hat{r_O} + r_C} + r_L\right)\hat{i_L} + \frac{D\hat{v_{in}}}{L_1} + \frac{\hat{d}V_{in}}{L_1} \\
\hat{i_O} &= \frac{\hat{v_C}}{\hat{r_O} + r_C} + \frac{r_C\hat{i_L}}{\hat{r_O} + r_C}
\end{aligned}
\tag{4.36}
$$

We now apply Laplace transform to Eq. (4.36) and substitute the results from Eq. (4.34) to get

$$G_{\mathrm{od}}(s) = \frac{\hat{i_{\mathrm{O}}}(s)}{\hat{d}(s)} = \frac{(V_{\mathrm{in}}/\hat{r_{\mathrm{O}}})(1 + sr_{\mathrm{C}}C_1)}{1 + s\left[r_{\mathrm{C}}C_1 + (\hat{r_{\mathrm{O}}} \parallel r_{\mathrm{L}})C_1 + \frac{L_1}{\hat{r_{\mathrm{O}}}+r_{\mathrm{L}}}\right] + s^2L_1C_1\left(\frac{\hat{r_{\mathrm{O}}}+r_{\mathrm{C}}}{\hat{r_{\mathrm{O}}}+r_{\mathrm{L}}}\right)} \tag{4.37}$$

$$G_{\mathrm{oi}}(s) = \frac{\hat{i_{\mathrm{O}}}(s)}{\hat{v_{\mathrm{in}}}(s)} = \left(\frac{D}{\hat{r_{\mathrm{O}}}(\hat{r_{\mathrm{O}}} + r_{\mathrm{L}})}\right)\frac{1 + sr_{\mathrm{C}}C_1}{1 + s\left[r_{\mathrm{C}}C_1 + (\hat{r_{\mathrm{O}}} \parallel r_{\mathrm{L}})C_1 + \frac{L_1}{\hat{r_{\mathrm{O}}}+r_{\mathrm{L}}}\right] + s^2L_1C_1\left(\frac{\hat{r_{\mathrm{O}}}+r_{\mathrm{C}}}{\hat{r_{\mathrm{O}}}+r_{\mathrm{L}}}\right)} \tag{4.38}$$

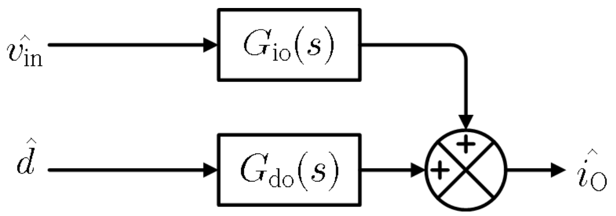

Figure 4.21: Illustration of the small signal model of a power converter.

In Eqs. (4.37) and (4.38), $G_{\mathrm{do}}(s)$ is the control-to-output transfer function and $G_{\mathrm{io}}(s)$ is the input-to-output transfer function. The small signal model of the power converter is indicated in Fig. 4.21. Referring to Fig. 4.20, the closed loop gain involves only $G_{\mathrm{do}}(s)$ and we would neglect $G_{\mathrm{io}}(s)$ when considering system stability analysis. The output ac resistance of the power converter is the function of the ac equivalent resistance of the LED networks, which has a non-linear resistive load property as described in Chapter 2. Since $G_{\mathrm{do}}(s)$ and $G_{\mathrm{io}}(s)$ are second order, containing double poles with a Q-factor equals to

$$Q = \frac{\sqrt{L_1 C_1}}{\left[r_{\mathrm{C}} C_1 + (\hat{r_{\mathrm{O}}} \parallel r_{\mathrm{L}}) C_1 + \frac{L_1}{\hat{r_{\mathrm{O}}} + r_{\mathrm{L}}}\right]} \tag{4.39}$$

By using the fact that $\hat{r_{\mathrm{O}}} \gg r_{\mathrm{C}}$ and $\hat{r_{\mathrm{O}}} \gg r_{\mathrm{L}}$, the Q factor can be simplified to

$$Q = \hat{r_{\mathrm{O}}} \sqrt{\frac{C_1}{L_1}} \tag{4.40}$$

The value of the Q-factor in the second order system affects the phase and gain variations of the control-to-output transfer functions located around the resonant frequency of the power converter f_{LC}. The values of the output capacitor and the switching inductor are determined at the beginning of the large signal design process. The value of ac load resistance, $\hat{r_{\mathrm{O}}}$, changes according to the operating conditions. The value of $\hat{r_{\mathrm{O}}}$ is determined by the output current (iO), output voltage (vO), the value of current sensed resistor (RSen), the operating junction temperature of LEDs (Tjo), the property of $v - i$ curve of LEDs, the number of LED in series (j) and the number of LED strings in parallel (j).

In the next section, we will provide an insight into how the value of the ac resistance of LED would affect the Q-factor of the power converter. Precautions will be emphasized for the design process of the LED driving system.

4.3.2.2 Q-factor Evaluation

Section 4.3.2.1 described the various parameters affecting the values of the ac resistance of LEDs and the Q-factor of G_{od} of the power converter. In order to fully investigate the relationship of $\hat{r_{\text{O}}}$ to different parameters, Fig. 4.22 plots $\hat{r_{\text{O}}}$ under different conditions.

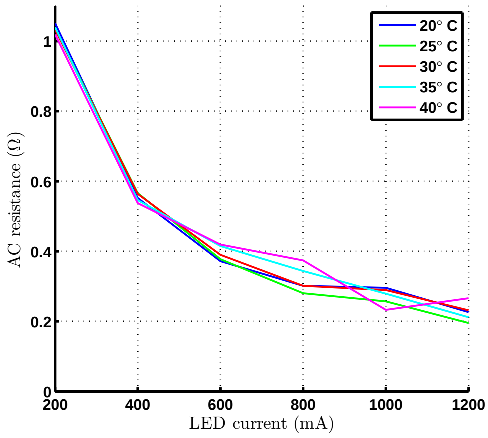

(a) $j = 1$

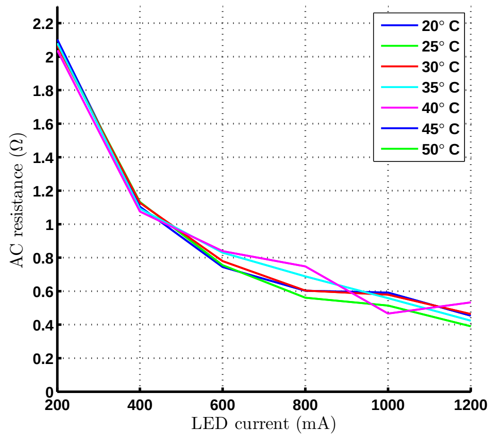

(b) $j = 2$

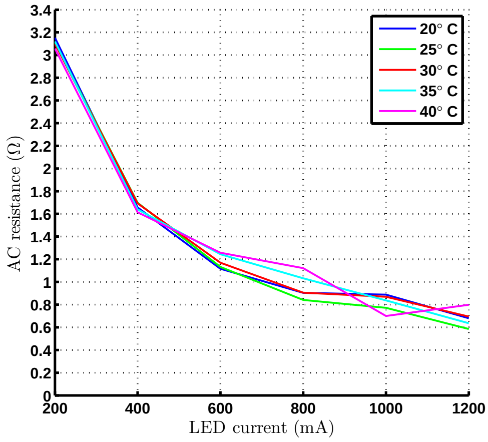

(c) $j = 3$

Figure 4.22: Dynamic resistance of LED array versus loading current under different conditions.

According to Fig. 4.22, $r_{\hat{\mathrm{d,jk}}}$ versus Tjo has been plotted for $j = 1$, $j = 2$ and $j = 3$. The result indicates that $\hat{r_{\mathrm{O}}}$ does not correlate to the operating junction temperature. The results also reveal that $\hat{r_{\mathrm{O}}}$ monolithically (but not linear) decreases with increasing i_{O}. This is due to the exponential changes of the slope of the v-i curve of LED. In addition, it can be found that the total ac resistance of the LED string is equal to the individual sum of each ac resistance of LEDs. In particular, we have

$$r_{\hat{\mathrm{d,j1}}} = j r_{\hat{\mathrm{d,11}}} \tag{4.41}$$

4.3.2.3 Loop Gain Transfer Function and Compensator Design

This section describes the construction of the loop gain transfer function of the system by using the results derived previously. The modulator transfer function can be found by using Eq. (4.4). G_{sen} and R_{sen} can be found by using the controller's parameters shown in TABLE 4.3. Hence,

$$\begin{aligned} G_{\mathrm{M}} &= \frac{1}{V_{\mathrm{H}} - V_{\mathrm{L}} = \frac{1}{2.4}} \\ G_{\mathrm{sen}} &= \frac{R_{\mathrm{f1}}}{R_{\mathrm{a1}}} = 2 \\ R_{\mathrm{sen}} &= 0.5 \end{aligned} \tag{4.42}$$

$$T_{\mathrm{lg}} = \frac{G_{\mathrm{C}} V_{\mathrm{in}}}{2.4} \frac{(1 + s r_{\mathrm{C}} C_1)}{1 + s\left[r_{\mathrm{C}} C_1 + (\hat{r_{\mathrm{O}}} \parallel r_{\mathrm{L}}) C_1 + \frac{L_1}{\hat{r_{\mathrm{O}}} + r_{\mathrm{L}}}\right] + s^2 L_1 C_1 \left(\frac{\hat{r_{\mathrm{O}}} + r_{\mathrm{C}}}{\hat{r_{\mathrm{O}}} + r_{\mathrm{L}}}\right)} \tag{4.43}$$

If the compensator is not present in the system ($G_\mathrm{C} = 1$), the uncompensated loop gain is shown in Eq. (4.43). Figure 4.23 reveals the Bode plots of the uncompensated loop gain of the system. The dc gain of the uncompensated closed loop system is 11.1 dB, which introduces a large steady-state error [74, 74]. A compensator is required to enhance the dc gain of the loop gain and increase the zero-dB bandwidth so as to improve the dynamic performance.

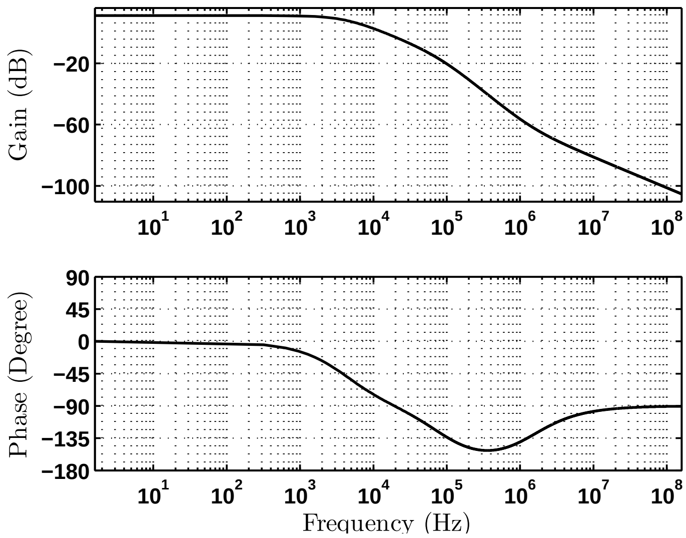

Figure 4.23: The Bode plot of the uncompensated loop gain.

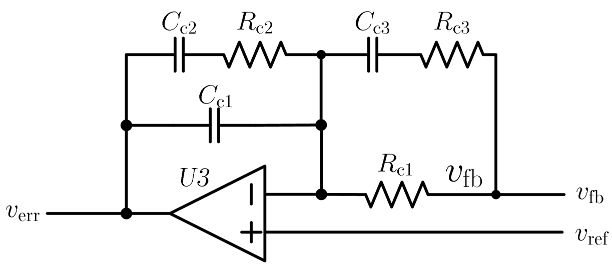

Figure 4.24: The schematic of type III error amplifier.

A type-III error amplifier has been adopted in the experimental circuit. The schematic diagram of the error amplifier circuit is extracted from Fig.4.6 and shown in Fig. 4.24. The transfer function of the error amplifier is

$$\frac{\hat{v_{\text{err}}}}{\hat{v_{\text{fb}}}} = \frac{\left(s+\frac{1}{R_{c2}C_{c2}}\right)\left(s+\frac{1}{(R_{c1}+R_{c3})C_{c3}}\right)}{\left(s\frac{R_{c1}C_{c1}R_{c3}}{R_{c1}+R_{c3}}\right)\left(s+\frac{C_{c1}+C_{c2}}{R_{c2}C_{c1}C_{c2}}\right)\left(s+\frac{1}{R_{c3}C_{c3}}\right)} \tag{4.44}$$

The error amplifier is able to produce one dominant pole, two poles and two zeros. In order to boost up the phase around the resonant frequency, the two zeros should be located at a location before the resonant frequency while the poles are put after that. Figure 4.25 shows the Bode plots of the error amplifier. The Bode plots of the uncompensated loop gain of the system also plotted as reference. The corresponding parameters of the error amplifier are shown in TABLE 4.5.

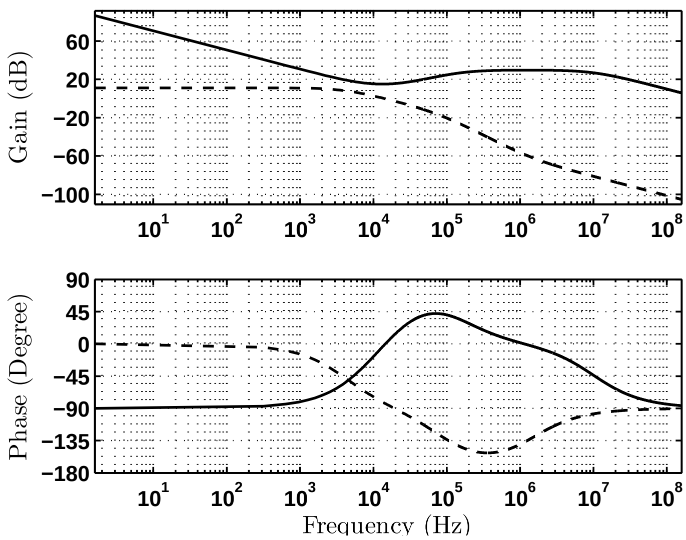

Figure 4.25: The transfer function of the error amplifier compared with the uncompensated loop gain.

Table 4.5: The Specification of the Error Amplifier.

Component	Value
C_{c1}	3.9 pF
R_{c1}	1 kΩ
C_{c2}	4.7 nF
R_{c2}	4 kΩ
C_{c3}	6.8 nF
R_{c3}	150 Ω
Poles/Zeros	Location
Dominant pole	313 MHz (0-dB frequency)
First Zero	8.47 kHz
Second Zero	20.4 kHz
First pole	156 kHz
Second pole	10.2 MHz

4.3.3 Loop Gain Simulation and Experimental Results

This section compares the simulated and measured loop gain Bode plots to verify the validity of the modeling method.

The method of measuring loop gain by voltage injection method for the LED driving system is discussed. For the traditional voltage-output power converters, the injection break point is usually chosen at a point between the output port of the power converter and the feedback resistor leader [75, 76]. In contrast to the current-output power converters, a current sense resistor is always used instead of the voltage feedback resistor ladder. The injection break point chosen at the current sense resistor do not fulfill the impedance constraint in which the impedance looking backward from the voltage injection break point must sufficiently smaller than the impedance looking forward from the point [77]. Moreover, the voltage level at the low-side current sense resistor is usually only a hundreds of mini-volts, which introduce large errors in measurement and the injected voltage will cause the system be unstable. Considering the above reasons, a suitable injection brake point must be chosen correctly in the LED driving system. Figure 4.26 indicates the injection point chosen in our measurement setup. The point is broken at the output of the current sense amplifier and the input of the compensator [78].

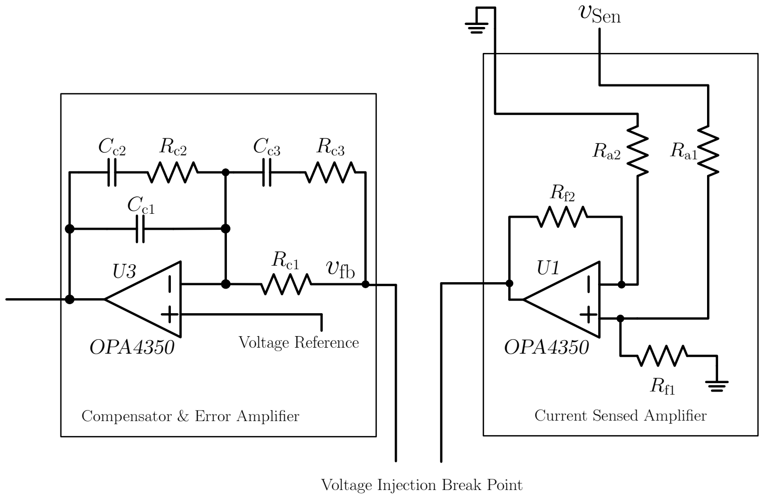

Figure 4.26: Illustration of voltage injection brake point in loop-gain measurement setup.

The loop-gain experiment was conducted using the the prototype LED driving system shown in Fig. 4.6 operating at 1 A output current with one LED. A frequency response analyzer NFA5097 was adopted in the measurement.The measured and simulated Bode plots of the system loop gain are plotted in Fig. 4.27. The result indicates a consistency between the simulation model and the experimental data.

4.3.4 Different AC Property Between LED Drivers and Traditional Power Converters

In the traditional power converter design where the converter drives a pure resistive load, the ac load resistance is identical to the dc load resistance which is

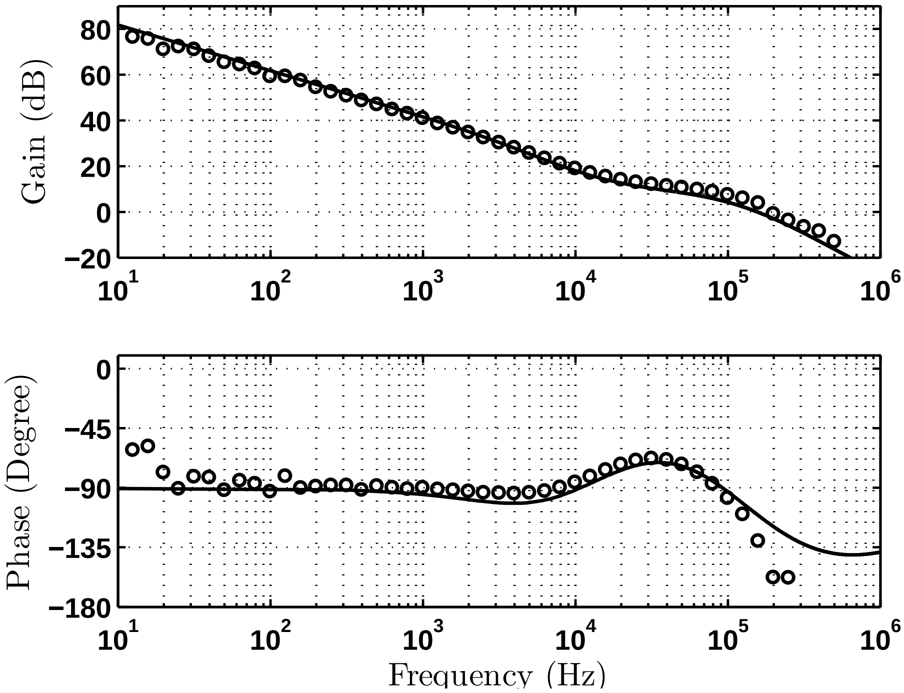

Figure 4.27: The measured and simulated loop gain of the LED driving system.

the ratio of the output voltage to the output current. In the LED driving system, since the ratio of LED forward current and voltage is not a constant term, the value of the ac load resistance changes according to the operating condition. Some previous works have overlooked the implication of the ac LED resistance that affects the Q-factor calculation during the design process. For example, a pure resistance [79] or a piecewise linear model [80] of LED is used to simplify the calculation process. Hence, the inappropriate evaluation of the ac load resistance of LED results in errors in deriving the closed loop gain transfer function during stability investigation of the LED driving system design process.

In order to show the phase and the gain difference of the power-converter control-to-output transfer function between a pure resistive load and LEDs, Fig. 4.28

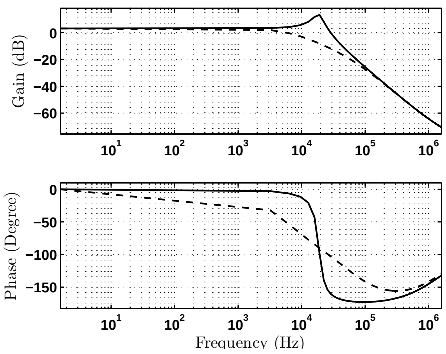

(a) $\{V_{\mathrm{O}}, I_{\mathrm{O}}\} = \{2.81\mathrm{V}, 200\mathrm{mA}\}$, Dotted line: $\hat{r_{\mathrm{d}}} = 1.04\Omega$ with Q-factor $= 0.28$, Solid line: $R_{\mathrm{dc}} = 14.03\Omega$ with Q-factor $= 3.33$.

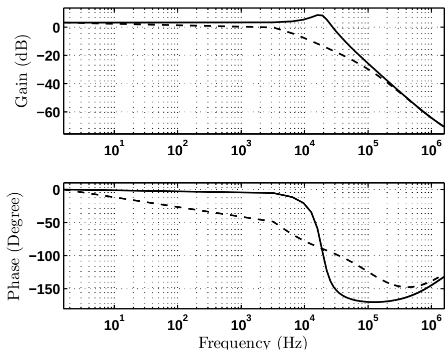

(b) $\{V_{\mathrm{O}}, I_{\mathrm{O}}\} = \{2.96\mathrm{V}, 400\mathrm{mA}\}$, Dotted line: $\hat{r_{\mathrm{d}}} = 0.55\Omega$ with Q-factor $= 0.15$, Solid line: $R_{\mathrm{dc}} = 7.40\Omega$ with Q-factor $= 1.83$.

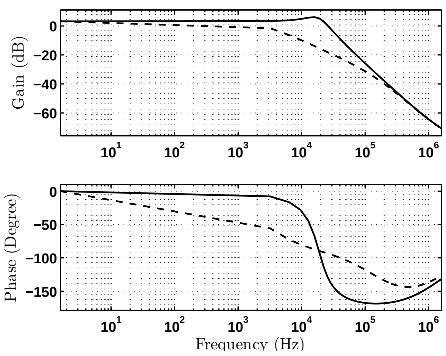

(c) $\{V_{\mathrm{O}}, I_{\mathrm{O}}\} = \{3.05\mathrm{V}, 600\mathrm{mA}\}$, Dotted line: $\hat{r_{\mathrm{d}}} = 0.41\Omega$ with Q-factor $= 0.12$, Solid line: $R_{\mathrm{dc}} = 5.09\Omega$ with Q-factor $= 1.28$.

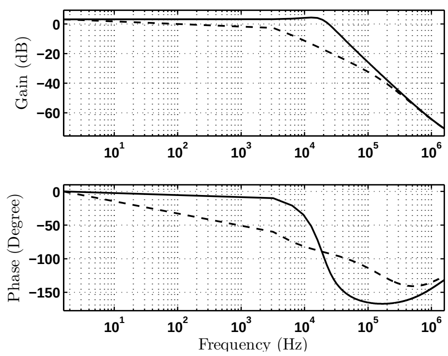

(d) $\{V_{\mathrm{O}}, I_{\mathrm{O}}\} = \{3.12\mathrm{V}, 800\mathrm{mA}\}$, Dotted line: $\hat{r_{\mathrm{d}}} = 0.34\Omega$ with Q-factor $= 0.10$, Solid line: $R_{\mathrm{dc}} = 3.90\Omega$ with Q-factor $= 0.99$.

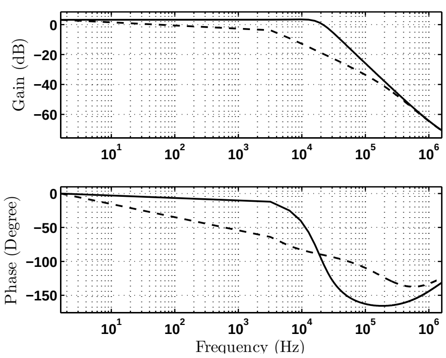

(e) $\{V_{\mathrm{O}}, I_{\mathrm{O}}\} = \{3.18\mathrm{V}, 1000\mathrm{mA}\}$, Dotted line: $\hat{r_{\mathrm{d}}} = 0.28\Omega$ with Q-factor $= 0.08$, Solid line: $R_{\mathrm{dc}} = 3.18\Omega$ with Q-factor $= 0.82$.

Figure 4.28: Comparison of control-to-output transfer functions between a pure resistive load (blue line) and an LED (green line) with output current from 200 mA to 1000 mA in steps of 200 mA.

shows the Bode plots of the transfer functions around the resonant frequency region using the buck converter with the configuration shown in TABLE 4.3. The dotted line in the figures indicates the case of a pure resistive load while the solid line indicates the case of an LED. Both the resistive load and LED operate at the same voltage and current. The figures indicate that there are differences between the LED and the resistive load. It is required to consider the deviation when designing a compensator for an LED driving system.

4.4 Summary

In the first part of this chapter, the techniques for constructing a large-signal model for the LED current driving system is proposed to predict the large-signal electrical behaviors. The second part provides a guideline for formulating the small signal model of the system and the prediction of the loop gain transfer function for analyzing the stability of the feedback system. Both the large signal and small signal models are compared with the laboratory experimental results. A high degree of consistency has been achieved. These models can provide a guidance for LED system designers in predicting the behaviors of the system as well as a reference tool for the design process.

Chapter 5

Current Output Converters for LED Driving Systems

5.1 Introduction

This chapter focuses on developing a procedure to derive classes of DC-DC power converters. A systematic synthesis approach is used based on the fundamental duality principle on voltage and current sources to formulate DC-DC power converters in the possible configurations. The method can identify uncovered basic power converter structures including those voltage-to-current power converters which is potentially suitable for LED driving systems.

The proposed synthesis procedure starts with the definition of a set of basic converter structures obtained by duality transformation. A complete set of converters including those currently known PWM DC-DC converters is generated by inter-connecting the structures. In this chapter, we will define how these structures can be connected and present an orderly search method that can expose a large number of converter topologies.

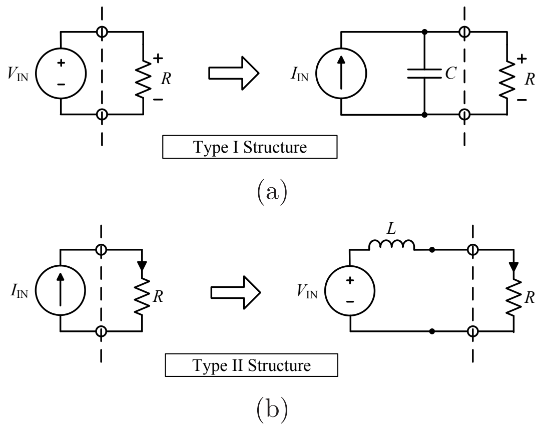

Figure 5.1: Duals of current and voltage sources: (a) Ideal voltage source and its dual and (b) Ideal current source and its dual.

5.2 Basic Structures and General Rules

5.2.1 Basic Converter Structures

The duals of current and voltage source networks are defined in this section. By inserting two complementary single-pole single-throw (SPST) switches into these networks, two basic cells are obtained to form, along with the duals, the four basic converter structures that can be employed to derive different converter topologies. It is shown that more complex and high-order power converters can be obtained from these four basic structures with the aid of a systematic synthesis procedure.

Fig. 5.1(a) shows an ideal voltage source connected to a load. According to the duality principle, the voltage source can be replaced by an ideal current source with a parallel-connected capacitor to have a sufficiently large value, of

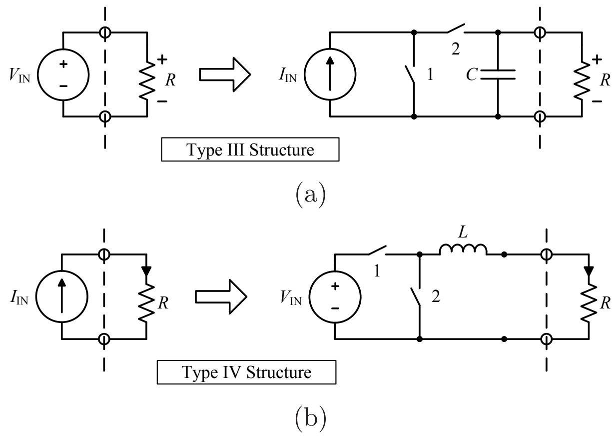

Figure 5.2: Two switches are inserted into Type I and Type II structures to form (a) Type III structure and (b) Type IV structure

which we define it as Type I structure in this chapter. Similarly, an ideal current source connected to a load as shown in Fig. 5.1(b) can be replaced by an ideal voltage source with an inductor connected in series, of which we define it as Type II. These two structures can be regarded as converting a voltage input to a current input, or a current source to a voltage source, respectively. The two structures have an input-output conversion ratio that depends on the value of the resistance of the load R. Two ideal SPST switches are now inserted into these two structures to form Type III and Type IV, as shown in Fig. 5.2(a) and Fig. 5.2(b) respectively. The two switches are designed to operate with two switch intervals (for continuous current conduction) and the switches are inserted in such a way that the resulting networks operates with (i) constant output voltage or current, (ii) continuous capacitor voltage and inductor current, and (iii) non-zero current or voltage from the source. The conversion ratio (M) of Type III structure can be obtained by using the capacitor charge balance principle,

$$\begin{aligned} \int_0^{T_\mathrm{s}} i_C(t)dt &= 0 \\ \int_0^{DT_\mathrm{s}} i_C(t)dt + \int_{D'T_\mathrm{s}}^{T_\mathrm{s}} i_C(t)dt &= 0 \\ -D\frac{V_\mathrm{O}}{R} + D'I_\mathrm{IN} - D'\frac{V_\mathrm{O}}{R} &= 0 \\ M = \frac{V_\mathrm{O}}{I_\mathrm{IN}} &= D'R \end{aligned} \tag{5.1}$$

where i_C is the current through the capacitor, D is the duty cycle, D' is the defined as $1-D$, and T_s is the switching period. Similarly, the conversion ratio of Type IV can be obtained by using the inductor volt-second balance principle,

$$M = \frac{I_\mathrm{O}}{V_\mathrm{IN}} = \frac{D}{R}. \tag{5.2}$$

The conversion ratio of any converter formed by these structures can be derived by Eqs. (5.1) and (5.2). It is obvious that Type III structure converts a current input to a voltage output while Type IV structure converts a voltage input to a current output. These four structures form the basis of the framework to obtain more complex and higher order DC-DC converters with the aid of a systematic synthesis procedure.

5.2.2 Derivation of Higher-Order Converters

The fundamental requirement of a DC-output power converter is to maintain a constant output in such a way that the output voltage or current must be able to retain its desirable value after undergoing line or load variations. For such requirement, a storage element is usually required for energy buffering under different operating conditions. Generally, a capacitor is connected in parallel to the load forming a voltage-output power converter, whereas an inductor connected in series forms a current-output converter [81, 82]. Depending on the input source, these two types of converters can be classified as either voltage-to-voltage, voltage-to-current, current-to-current, or current-to-voltage converter. In combining two converters to form a new one, it is necessary to ensure that the output of first converter must have the same type as the input of second converter. That is, only a converter with voltage (current) input can connect to a converter with voltage (current) output.

In synthesizing voltage-to-voltage and current-to-current converters, we shall consider only even-order networks which only have practical importance [83]. Adding an additional inductor at the input or at the output of a voltage-to-voltage converter, the converter becomes a current-to-voltage or a voltage-to-current converter, which has an order of odd number. Table 5.1 summarizes the formation of these four types of DC-DC converters by a possible combination of four basic structures and their derivatives. As indicated in Table 5.1, higher-order converters can be derived by connecting these four structures in series. For example, a second-order current-to-current converter can be obtained by connecting a Type II structure to a Type IV structure. A third-order is made by further connecting a Type I onto the newly-formed converter. Fig. 5.3 shows the four well-known basic converters that are readily to be constructed in this way.

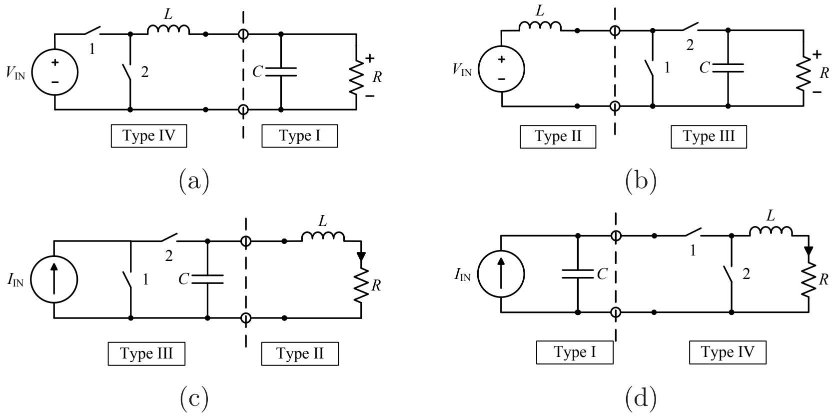

Figure 5.3: Four basic power converters can constructed by cascading four basic structures: (a) voltage buck, (b) voltage boost, (c) current buck, and (d) current boost

Table 5.1: Classification of four types of DC-DC converters

Type	**Input stage**	**Output stage**	**Order**
Voltage-to-voltage	Type II, IV or derivatives with voltage input	Type II, IV or derivatives with input having same type as the output of input stage and voltage output	Even
Voltage-to-current	Type II, IV or derivatives e with voltage input	Type I, III or derivatives with input having same type as the output of input stage and current output	Odd
Current-to-current	Type I, III or derivatives with current input	Type I, III or derivatives with input having same type as the output of input stage and current output	Even
Current-to-voltage	Type I, III or derivatives with current input	Type II, IV or derivatives with input having same type as the output of input stage and voltage output	Odd

5.2.3 Reduction of Redundant Cases

Since a topology is formed by inter-connecting different converter structures, redundancies arise in the synthesis procedure. A CLC network (π–network) and LCL network (T–network) shown in Fig. 5.4 may appear in initial circuits after formation and before circuit minimization. In such cases, the π–network or T–network should be simplified to a single capacitor or inductor to reduce the complexity of the final circuit. The simplification is valid by the fact that the natural frequency of the LC filter is much lower than the switching frequency,

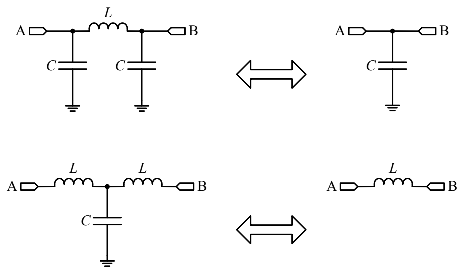

Figure 5.4: Reduction of storage element.

i.e.

$$\frac{1}{2\pi\sqrt{LC}} \ll f_S \tag{5.3}$$

where L and C are the inductance and capacitance value of LC filter and f_S is the switching frequency [81, 82].

Similarly, the switch networks shown in Fig. 5.5 as a result of connecting different converter structures should also be simplified. Considering the switch network shown in Fig. 5.5(a), the network contains three switches, with Switch "1" and "2" operating in a complementary manner. When Switch "1" is on and two Switches "2" are off, Port A and B have the same voltage potential. When Switch "1" is off and two Switches "2" are on, Port A and B are connected to ground. Intuitively, this switch network is simply equivalent to a single switch "2" network as shown in Fig. 5.5(a). Same rationale applies to the other three switch networks and their results are shown in Fig. 5.5(b) to Fig. 5.5(d).

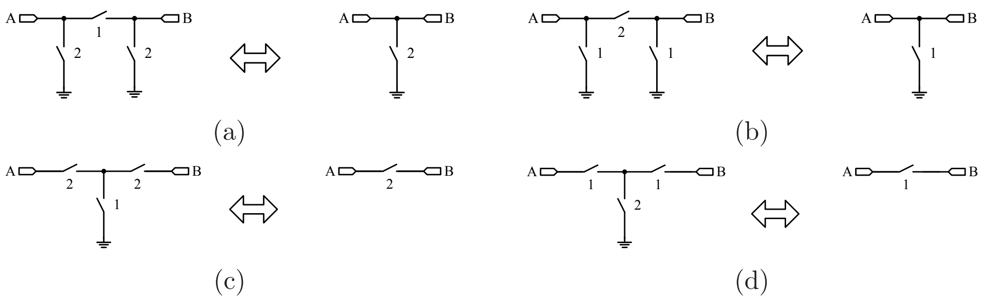

Figure 5.5: Reduction of switches.

5.2.4 Position Exchange for Circuit Elements

The position of switches and reactive elements can be interchanged without affecting their original functions [84]. If the situations arise as shown in Fig. 5.6(a) to Fig. 5.6(d), the switches and the reactive element can be exchanged as indicated. This position exchange approach allows us to uncover other possible configurations and, along with the reduction of reactive elements and switches, greatly simplifies the derivation of higher order converters with minimum configurations. This idea will be illustrated with examples in the next section.

5.3 Synthesis Procedure

The proposed synthesis method can be applied to all DC-DC ladder-structured power converters which share the common input and output ground. This class of converters has four possible structures in which it contains only π–network or T–network structures as shown in Fig. 5.7 [85]. As mentioned before, the new topologies can be synthesized by connecting two converters following the rules that are stated in the previous section. To illustrate the synthesis procedure, we make use of two examples here to show how a converter with the same order or a

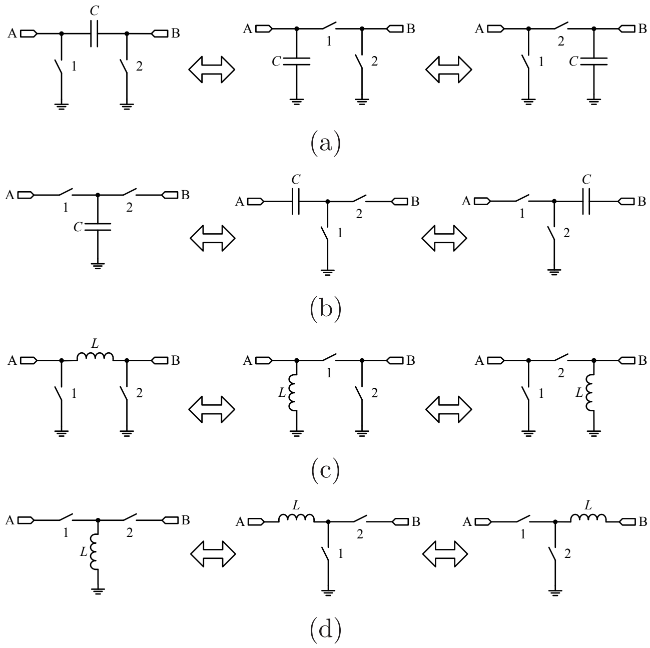

Figure 5.6: Position exchange for switches and reactive elements.

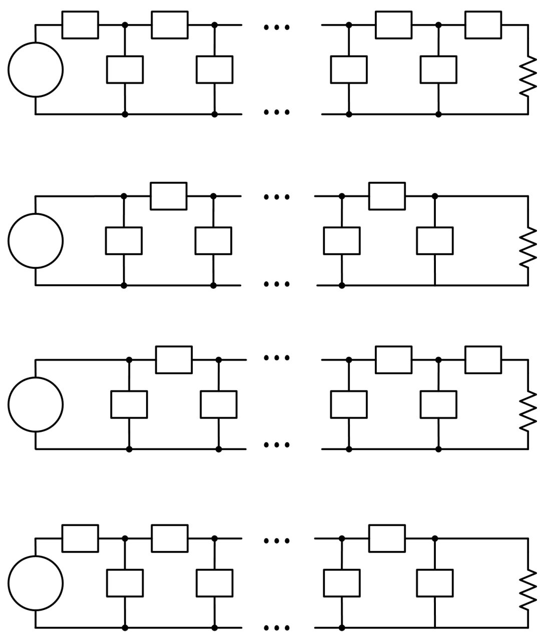

Figure 5.7: Four types of ladder-structured power converters.

higher order can be derived by exchanging circuit elements position and reducing excessive switches.

Considering the circuit shown in Fig. 5.8, in which a buck converter is connected to a boost converter, it can be seen that the LC filter can be reduced to a single inductor L. After exchanging the position of the inductor L and the Switch “2”, the circuit can be further simplified by reducing excessive switches as shown. Subsequently, a second-order buck-boost converter is resulted.

Considering the circuit shown in Fig. 5.9, an inverted buck-boost converter is connected to a type-IV structure. By interchanging the position of capacitor C and the switch “2”, it results in a circuit where three switches can be integrated into one. As a result, a third-order voltage-to-current converter is generated. In this way, different converter topologies can be synthesized by connecting the four basic structures and performing subsequent reduction by interchanging position of circuit elements.

In order to illustrate further on the number of converters that can be synthesized by the proposed method, the procedure is employed to search all possible configurations by interconnecting the four basic structures and their derivatives for second-order and third-order converters. Fig. 5.10 and Fig. 5.11 show the respective generic structures by the proposed method. In the figures, "A", "B", "C" and "D" represent the possible positions of switches and the reactive elements. Table 5.2 and Table 5.3 indicate the positions of those elements for a practical converter which is either well-known, cited in References [86]–[87], or

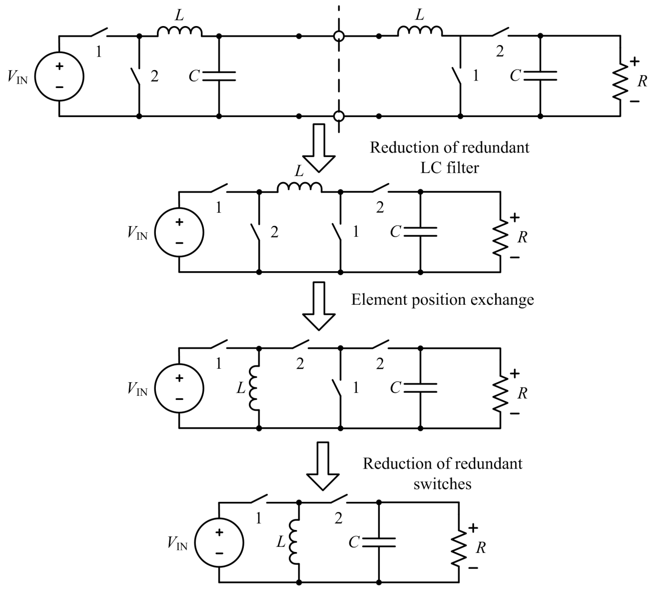

Figure 5.8: Construction of a buck-boost converter by the proposed method.

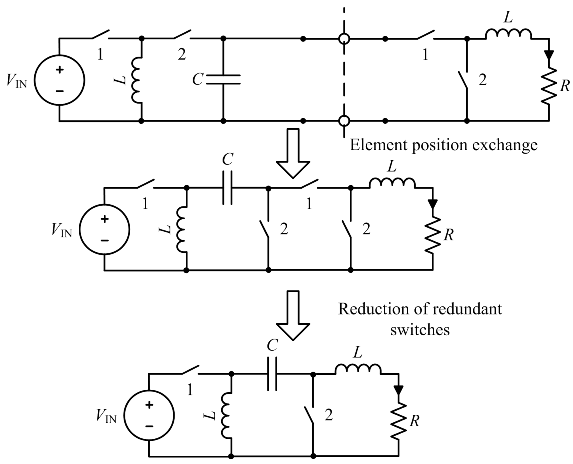

Figure 5.9: Construction of a third-order V-to-I converter.

never cited in literature before.

The modes of power converters indicated in Table 5.2 and Table 5.3 represent different topologies. It is worth noting that power converters having the same mode number in the category of the same order is the dual circuit of each other ,

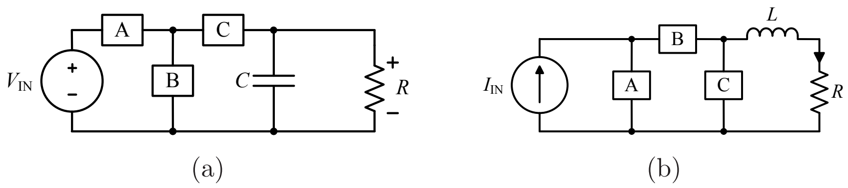

Figure 5.10: Generic structures of second-order converters: (a) voltage-to-voltage converter and (b) current-to-current converter.

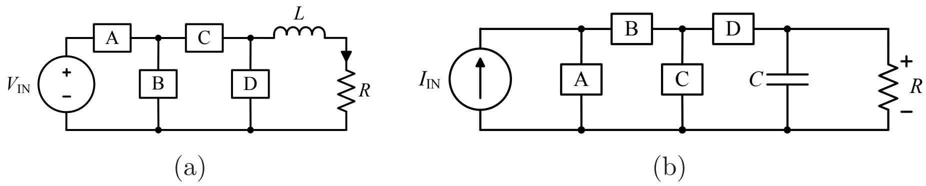

Figure 5.11: Generic structures of third-order converters: (a) voltage-to-current converter and (b) current-to-voltage converter.

Table 5.2: Six possible combinations of second-order converters

Mode	Type	**A**	**B**	**C**		Literatures
1	V-to-V	S	$\overline{S}$	L	C	Well-known
2	V-to-V	L	S	$\overline{S}$	C	Well-known
3	V-to-V	S	L	$\overline{S}$	C	Well-known
1	I-to-I	S	$\overline{S}$	C	L	[86], [87]
2	I-to-I	C	S	$\overline{S}$	L	[86], [88], [87]
3	I-to-I	S	C	$\overline{S}$	L	[86], [87]

which can be derived using di-graph [89]. For example, the duality circuit of the voltage-buck converter (second-order V-to-V mode-1) is the dual of current buck converter (second-order I-to-I mode-1).

In summary, using the proposed synthesis method, a two-state ladder-structured power converter has 2 possible configurations for first-order, 6 for second-order, 12 for third-order, 20 for fourth-order, and N configurations for n-order calculated

Table 5.3: Twelve possible combinations of third-order converters

Mode	Type	A	B	C	D		Literatures
1	V-to-I	S	$\overline{S}$	L	C	L	Not cited before
2	V-to-I	L	S	$\overline{S}$	C	L	[86]
3	V-to-I	L	C	S	$\overline{S}$	L	[86]
4	V-to-I	S	L	$\overline{S}$	C	L	Not cited before
5	V-to-I	L	S	C	$\overline{S}$	L	[86], [88]
6	V-to-I	S	L	C	$\overline{S}$	L	(not cited before)
1	I-to-V	S	$\overline{S}$	C	L	C	Not cited before
2	I-to-V	C	S	$\overline{S}$	L	C	Not cited before
3	I-to-V	C	L	S	$\overline{S}$	C	Not cited before
4	I-to-V	S	C	$\overline{S}$	L	C	Not cited before)
5	I-to-V	C	S	L	$\overline{S}$	C	[88]
6	I-to-V	S	C	L	$\overline{S}$	C	Not cited before

by the equation,

$$\begin{aligned} N &= 2 \times \sum_{i=1}^{n} i \\ &= n(n+1) \end{aligned} \tag{5.4}$$

where n represents the order of power converters. The details of each of the configuration is shown in Appendix B. Although fourth-order power converters are the highest order converters that can be found in most practical applications, it is worth mentioning that the proposed synthesis method is also applicable to formulate higher order converters. Table 5.4 and Table 5.5 show the possible configurations for n-order two-state power converters.

The proposed method is not only limited to formulate two-switch power con-

Table 5.4: List of possible combinations for n-order voltage-input converters

$$
\begin{array}{rl}
 & \overbrace{\hphantom{S \quad \overline{S} \quad L \quad C \quad L \quad C\ldots}}^{(n+2)\text{ in total}} \\
n\text{ in total} & \left\{\begin{array}{llllll}
S & \overline{S} & L & C & L & C\ldots \\
L & S & \overline{S} & C & L & C\ldots \\
L & C & S & \overline{S} & L & C\ldots \\
\vdots & & & \ddots & & \ldots \\
L & C & L & C & L & C\ldots
\end{array}\right. \\
(n-1)\text{ in total} & \left\{\begin{array}{llllll}
S & L & \overline{S} & C & L & C\ldots \\
L & S & C & \overline{S} & L & C\ldots \\
L & C & S & L & \overline{S} & C\ldots \\
\vdots & & & \ddots & & \ldots \\
L & C & L & C & L & C\ldots
\end{array}\right. \\
(n-2)\text{ in total} & \left\{\begin{array}{llllll}
S & L & C & \overline{S} & L & C\ldots \\
L & S & C & L & \overline{S} & C\ldots \\
L & C & S & L & C & \overline{S}\ldots \\
\vdots & & & \ddots & & \ldots \\
L & C & L & C & L & C\ldots
\end{array}\right. \\
 & \begin{array}{llllll}
\vdots & & & \ddots & & \ldots \\
 & & & & & \\
L & C & L & C & L & C\ldots
\end{array}
\end{array}
$$

verters. It can also be applied to converters with switches of even number such as non-inverting voltage-buck-boost converter [90]. The formation details of that kind of power converters will not be mentioned in this chapter as it is similar to the previous discussion but the possible combinations of four-switch DC-DC ladder-structured power converters are listed in Table 5.6.

Table 5.5: List of possible combinations for n-order current-input converters

$$
\begin{array}{rl}
 & \overbrace{\hphantom{S \quad \overline{S} \quad C \quad L \quad C \quad L\ldots}}^{(n+2)\text{ in total}} \\
n \text{ in total} & \left\{ \begin{array}{llllll} S & \overline{S} & C & L & C & L\ldots \\ C & S & \overline{S} & L & C & L\ldots \\ C & L & S & \overline{S} & C & L\ldots \\ \vdots & & & \ddots & & \ldots \\ C & L & C & L & C & L\ldots \end{array} \right. \\
(n-1) \text{ in total} & \left\{ \begin{array}{llllll} S & C & \overline{S} & L & C & L\ldots \\ C & S & L & \overline{S} & C & L\ldots \\ C & L & S & C & \overline{S} & L\ldots \\ \vdots & & & \ddots & & \ldots \\ C & L & C & L & C & L\ldots \end{array} \right. \\
(n-2) \text{ in total} & \left\{ \begin{array}{llllll} S & C & L & \overline{S} & C & L\ldots \\ C & S & L & C & \overline{S} & L\ldots \\ C & L & S & C & L & \overline{S}\ldots \\ \vdots & & & \ddots & & \ldots \\ C & L & C & L & C & L\ldots \end{array} \right. \\
 & \begin{array}{llllll} \vdots & & & \ddots & & \ldots \\ & & & & & \\ C & L & C & L & C & L\ldots \end{array}
\end{array}
$$

Table 5.6: Possible combinations for four-switch converters

Four-switch converters	**Possible Combinations**
First-order	2
Second-order	10
Third-order	30
Fourth-order	70

5.4 Simulation Results on Third-order LED Drivers

This section analyze the suitability on using the current-output power converters, which derived from the previous sections, for LED drivers. The differences between the voltage-output and current-output power converters are discussed. The advantages of using current-output power converters for LED drivers are highlighted. Simulation results indicates the validity of the third-order LED drivers.

5.4.1 Properties of Current-output Power Converters

Previous sections proposed a synthesis procedures for formulating power converters in a systematic way, in which those voltage-input current-output power converters can be derived. The possible schematics of the power stages of those converters in first-order and third-order forms are indicated in Fig. 5.12 and Fig. 5.13. In terms of there topological structures, there are some common grounds on those power converter which the voltage-output power converters never existed. First, as observed from Fig. 5.12 and Fig. 5.13, the output current of those converters are relating to the output inductor current. Second, there are two possible output storage component configuration during the discharging period, which is shown in Fig 5.14(a) and Fig 5.14(b). During the discharging period, the output component configurations will be in either two forms: (i) the output inductor connect the loading in parallel or (ii) the output capacitor and inductor connect to the loading in series. Third, All current-output power converters can deliver non-pulsating output current. Their differences are summarized in TABLE 5.7.

The first-order current-output LED driver is widely used in commercial market [91]. This is because it can provide the easiest and simplest way to deliver

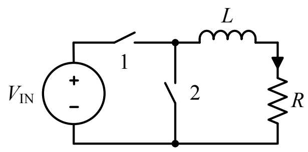

Figure 5.12: First-order voltage-to-current converter.

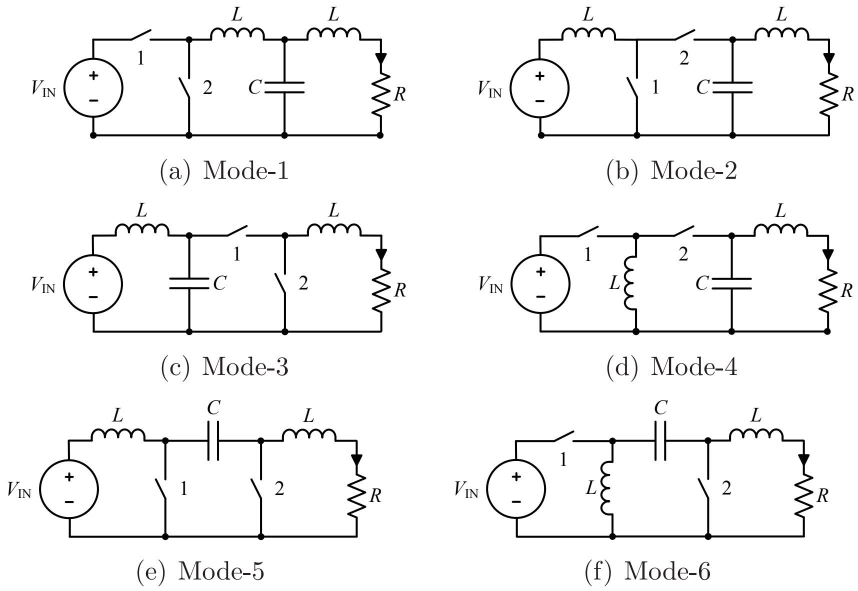

(a) Mode-1
(b) Mode-2
(c) Mode-3
(d) Mode-4
(e) Mode-5
(f) Mode-6

Figure 5.13: Third-order current-to-voltage converters

Table 5.7: Differences between the voltage-output and current-output converters

Voltage-output Converters	**Current-output Converters**
The output voltage is relating to output capacitor voltage.	The output current is relating to output inductor current.
Two possible output element configurations during discharging period are shown in Fig 5.14(c) and Fig 5.14(d).	Two possible output element configurations during discharging period are shown in Fig 5.14(a) and Fig 5.14(b) .
Some configurations deliver pulsating output current.	All configurations deliver non-pulsating output current.

constant output current with minimum component count. However, this converter can only achieve step-down function. This means that the converter is not suitable in the applications requiring step-up or wide-range conversion such as automotive and portable devices. In such a case, the third-order current-output

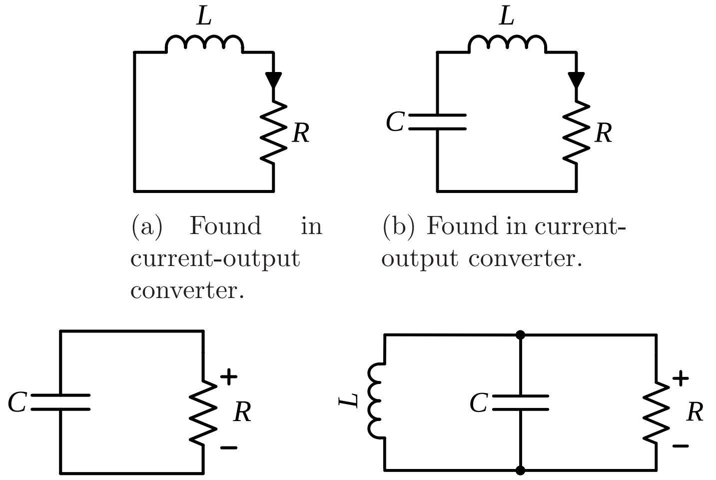

(a) Found in current-output converter.

(b) Found in current-output converter.

(c) Found in voltage-output converter.

(d) Found in voltage-output converter.

Figure 5.14: Possible output component configurations during discharging period.

LED driver is the other solution.

5.4.2 Simulation Results on the Third-order LED Drivers

In order to investigate the performance of the third-order LED driver, the mode-2 third order converter is taken into analysis in the simulation. This converter is compared with the second-order voltage-boost converter. Those two converter were operated at the same specification expected the value of output storage components, which is shown in TABLE 5.8. The simulation was done by using OcCAD PSPICE. The simulation is trying to adjust the output inductance value of the mode-2 third order converter and the output current ripples are being recorded. The simulated output current waveforms were shown from Fig. 5.15. Comparing the output capacitor value of the boost converter, the result shows that the value of the output capacitor in the third order converter is greatly reduced, while the output current ripple can be kept the same with a suitable

Table 5.8: Specifications of Power Converters in PSPICE Simulation.

Description	Third-order mode-2	Second-order boost
Input Voltage	6V	6V
Output current	1000mA	1000mA
Switching frequency	200 kHz	200 kHz
Input Inductance	33 μH	33 μH
Output Inductance	63 to 300 μH	N/A
Output Capacitance	1 μF	30 μF
Loading resistance	24 Ω	24 Ω

output inductor value. This result shows that the third order converter can eliminate the use of electrolytic capacitor by choosing suitable value of output inductance. However, the tradeoff of using smaller value of output capacitor is the use of larger size of output inductor. Designers can adjust a suitable values of the output capacitor and inductor for their needed.

5.5 Summary

The proposed synthesis method starts from applying duality transformation on voltage and current sources and subsequently developing four basic structures as building blocks for more complex configurations. The general rules for reduction and position exchange of circuit elements are detailed to uncover higher order converters with minimum configurations. Examples are given to illustrate the derivation procedure for two-state ladder-structured power converters. The proposed method provides a new alternative way for the formulation of DC-DC switch-mode power converters.The proposed synthesis method derived first-order and third-order voltage-to-current power converters have the potential to be used

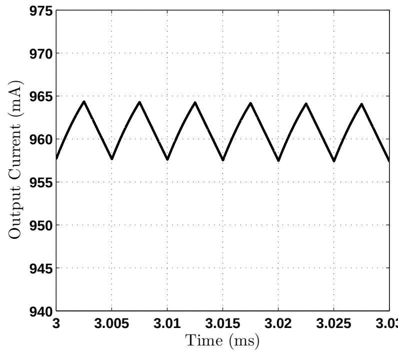

(a) Second-order boost. Ripple =6mA

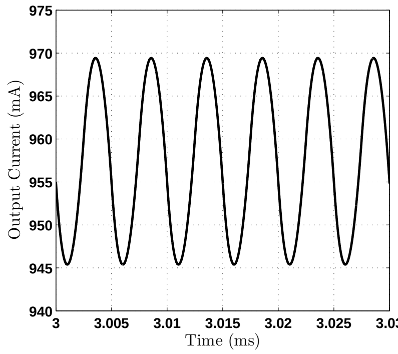

(b) Third-order mode-2.(L_O = 63 μH) Ripple =24mA

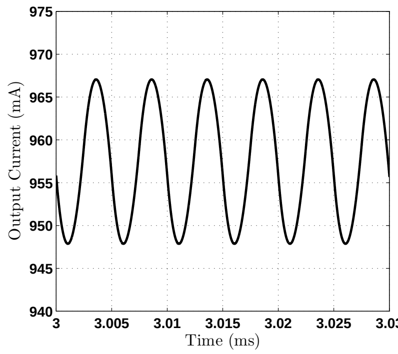

(c) Third-order mode-2.(L_O = 79 μH) Ripple =19mA

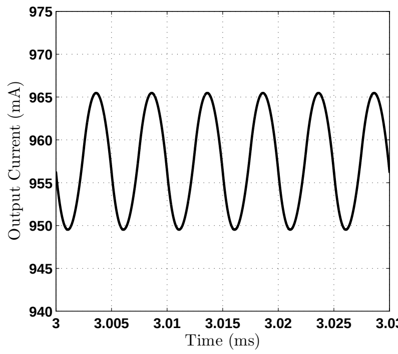

(d) Third-order mode-2.(L_O = 95 μH) Ripple =16mA

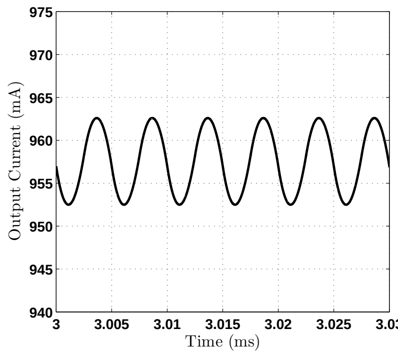

(e) Third-order mode-2.(L_O = 150 μH) Ripple =10mA

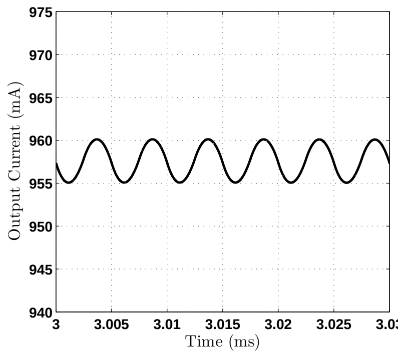

(f) Third-order mode-2.(L_O = 300 μH) Ripple =5mA.

Figure 5.15: PSPICE output current simulation waveforms of the mode-2 third order converter and second-order voltage-boost converter.

in LED applications, in which constant current sources are required. The simulation results that the third-order mode-2 voltage-to-current power converter can be used for driving LED which minimizes the output capacitance value in a step-up voltage application.

Chapter 6

Conclusion

This chapter concludes the tasks that have been completed in this research work. In addition, possible future research works are proposed. Finally, the contributions of the thesis are summarized.

6.1 Work Accomplished

6.1.1 Electrical Characterization on LED

An electrical model of light-emitting diode was formed based on the $v_\mathrm{d} - i_\mathrm{d} - T_\mathrm{j}$ experimental measurement result. Compared with the traditional Piecewise Linear Model and Shockley Diode Model, the proposed model can precisely predict the electrical behavior of LEDs. The proposed model can evaluate the dc and ac resistance of an LED in different operation points. Furthermore, the $v_\mathrm{d} - i_\mathrm{d}$ curves under different operating junction temperature are obtained such that the curve drift can be predicted due to the temperature change. The model was further extended to an LED network which contains multiple number of LEDs in rows and columns. The electrical characterization of LED networks can provide information for developing a modeling method for LED driving systems.

6.1.2 Modeling of LED Driving Systems

A modeling approach of LED driving systems was derived in both static (dc) and dynamic (ac) aspects. This modeling approach focuses on characterizing three different LED current driving approaches: amplitude mode, pulse-width modulation and bi-level method. A systematic equation model was formed which describes the LED forward current in mathematical form.

In the large-signal modeling approach, the system was divided into several sub-blocks. The formulation of each block was discussed. An example was given to illustrate the formulation of the various blocks. A MATLAB-based simulation result was compared to the data from experiment.

In the small-signal modeling approach, the small-signal closed loop transfer function of the LED driving system was constructed. The Q-factor of the control-to-output transfer function of a buck power converter affected by the dynamic resistance of LEDs was emphasized. The derivation of the dynamic resistance was discussed. The comparison of loop gain measurement result and the analytical calculation showed a high degree of consistency. The proposed calculation can be used to analyze an LED driving system during the stage of the design process.

6.1.3 Power Converter Synthesis Procedures

A power converter synthesis method was proposed which was based on the duality transformation on voltage and current sources and subsequently generated four basic switching structures. The proposed method provides a new way for formulating classes of DC-DC power converters. This method can uncover some voltage-to-current power converters which are potentially suitable for LED driving circuits.

6.2 Future Research

Although an electrical model of LED was derived in this research work where the forward voltage, current and junction temperature are interrelated, both the forward current and the junction temperature are required to be measured when applying the model to evaluate the DC and AC resistances of an LED.

A thermal model that has the relationship between the thermal behavior of the LED cooling system and electrical behavior of LED can help anticipate the expected operating junction temperature of LEDs in the driving system. Although the General Photo-Electro-Thermal Theory and Dynamic Photo-Electro-Thermal Theory have been developed [92, 93], the theories can only be used for constant power driving methods, which are not applicable to the current driving technique (amplitude) or driving methods where the forward current of LED changes dynamically (pulse-width modulation and bi-level). Dynamic current models are worth developing in order to predict the expected junction temperature of LED for the PWM and bi-level current driving methods.

Moreover, the averaged luminance intensity cannot be evaluated using the General Photo-Electro-Thermal Theory and Dynamic Photo-Electro-Thermal Theory for the PWM and bi-level current driving methods. It is still worthwhile to develop a new model and to investigate the expected averaged luminance intensity under those current driving methods.

Appendix A

This appendix provides the information and raw captured data of the LED measurement setup described in Chapter 2.

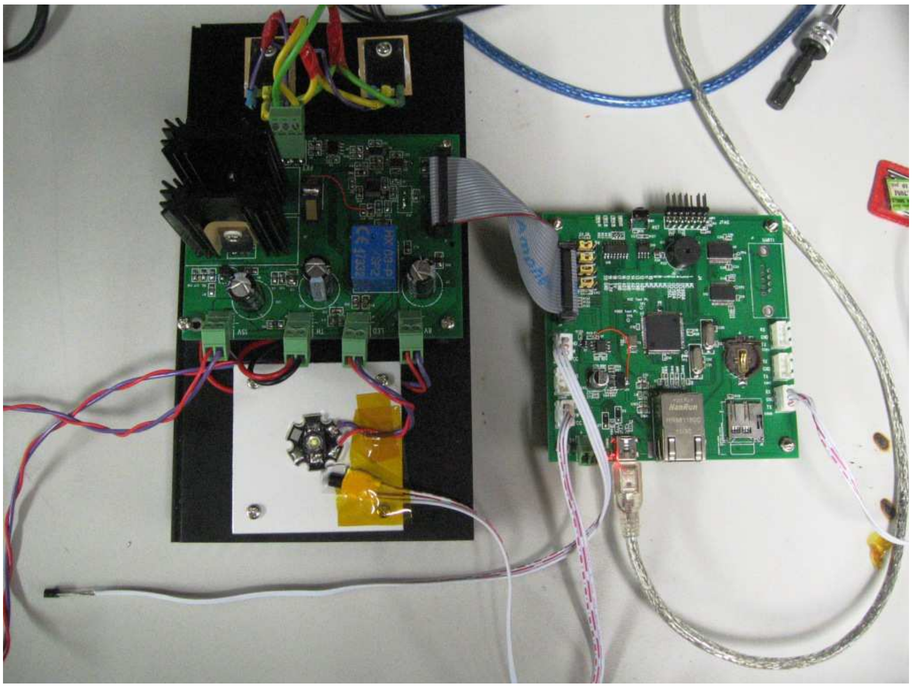

Figure 1: The hardware setup of the measurement.

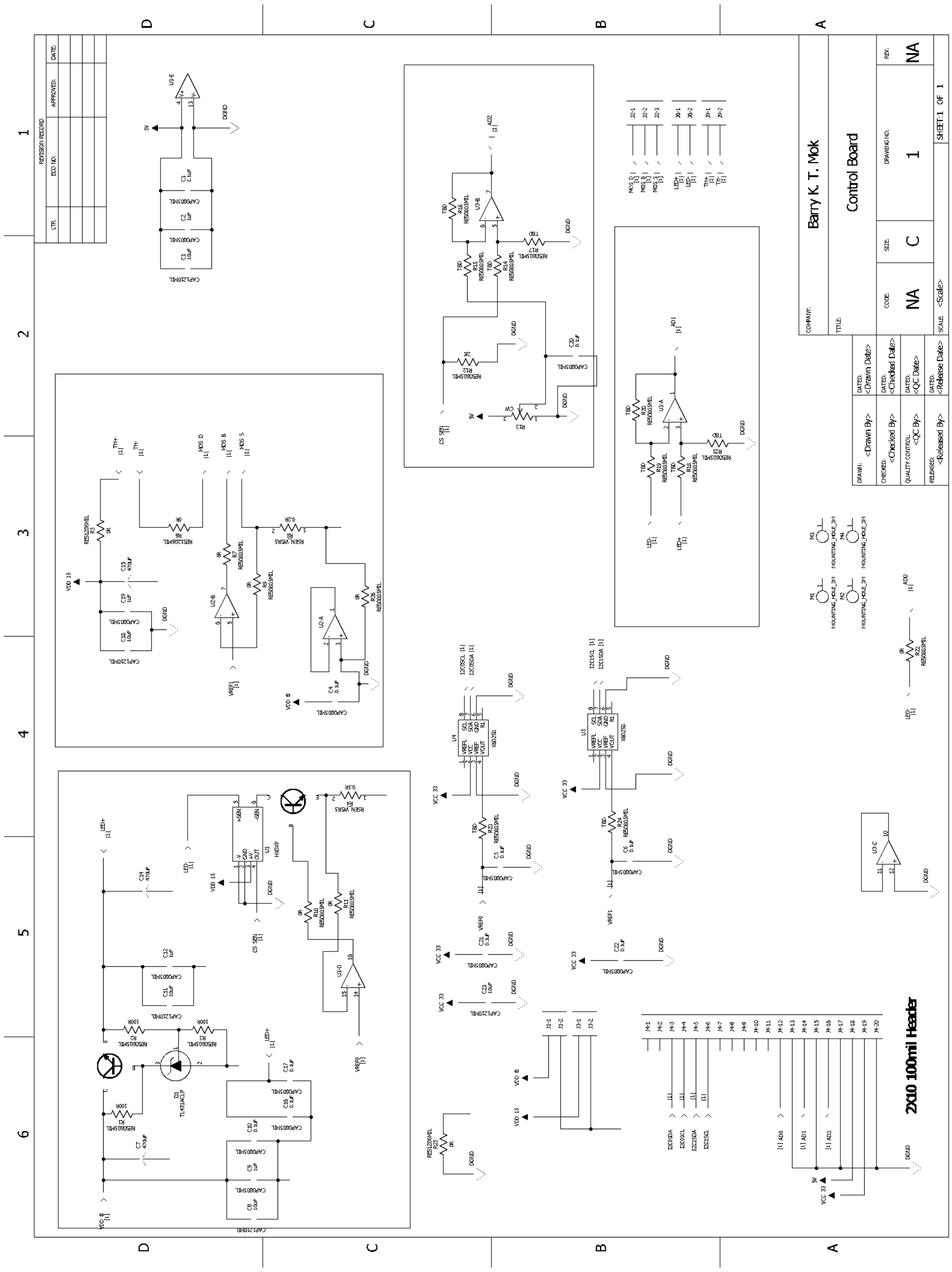

Figure 2: Full schematic diagram of the current and temperature control board.

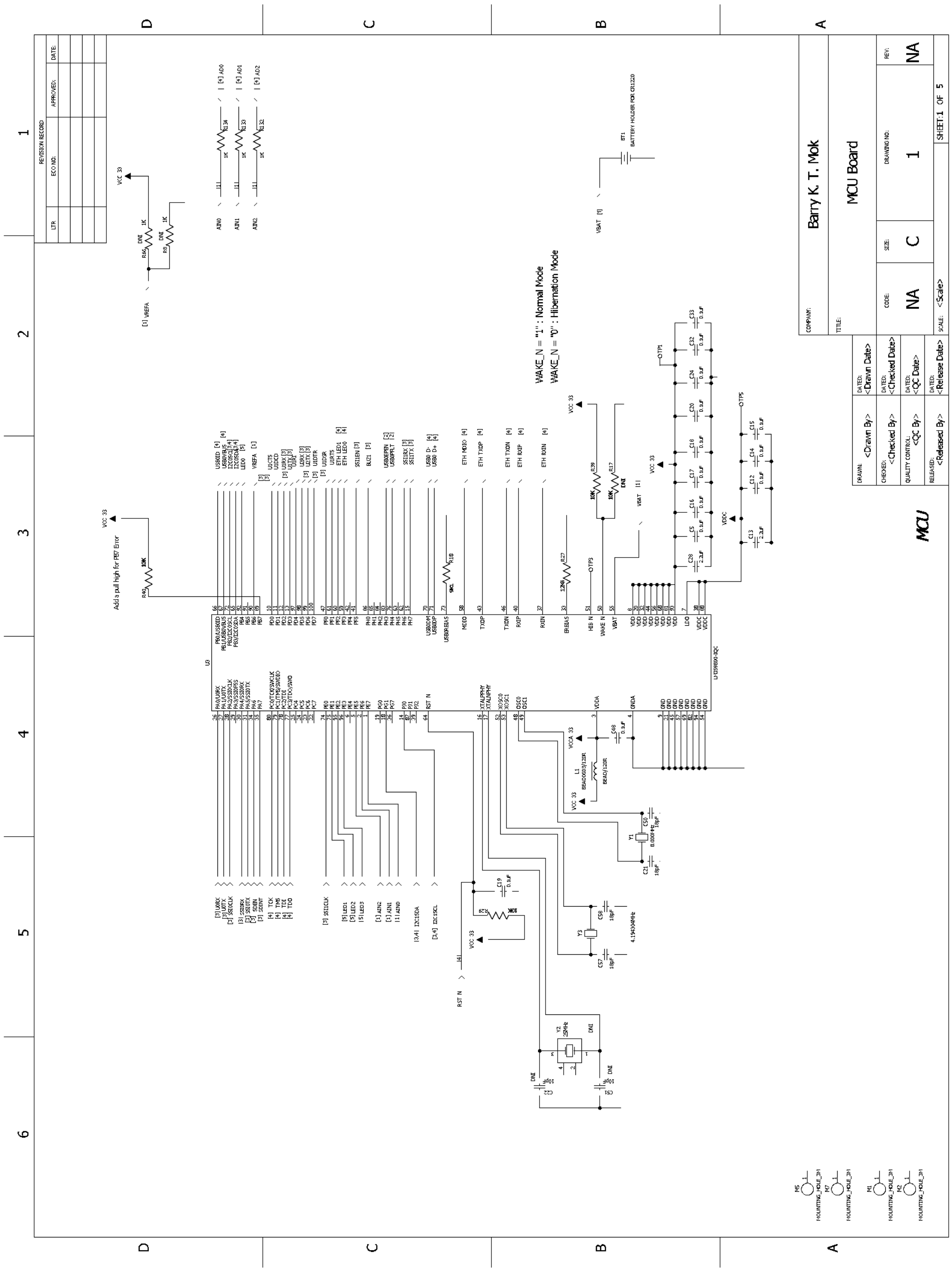

Figure 3: Full schematic diagram of the MCU-controlled data acquisition board.

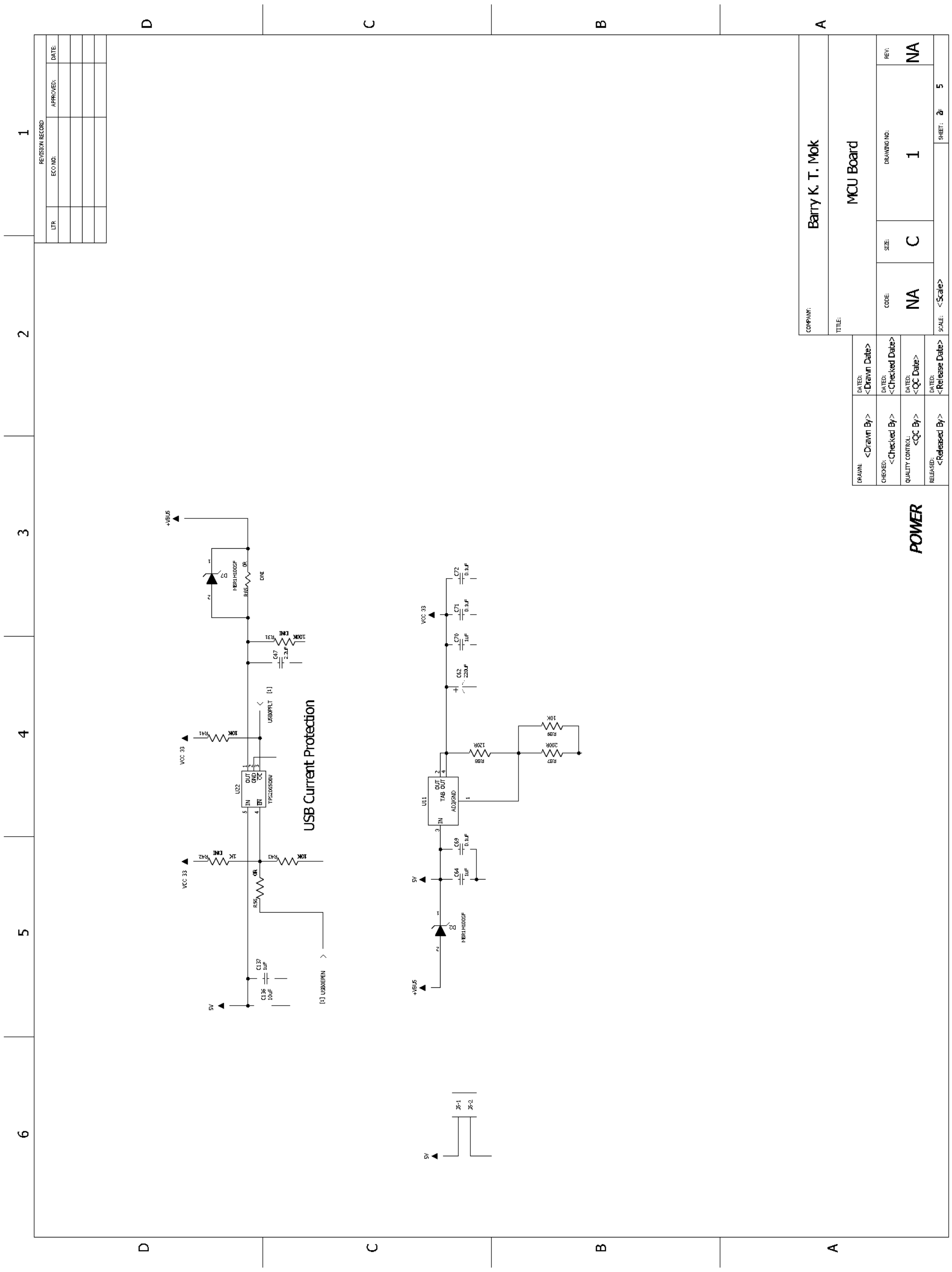

Figure 4: Full schematic diagram of the MCU-controlled data acquisition board.(Cont'd)

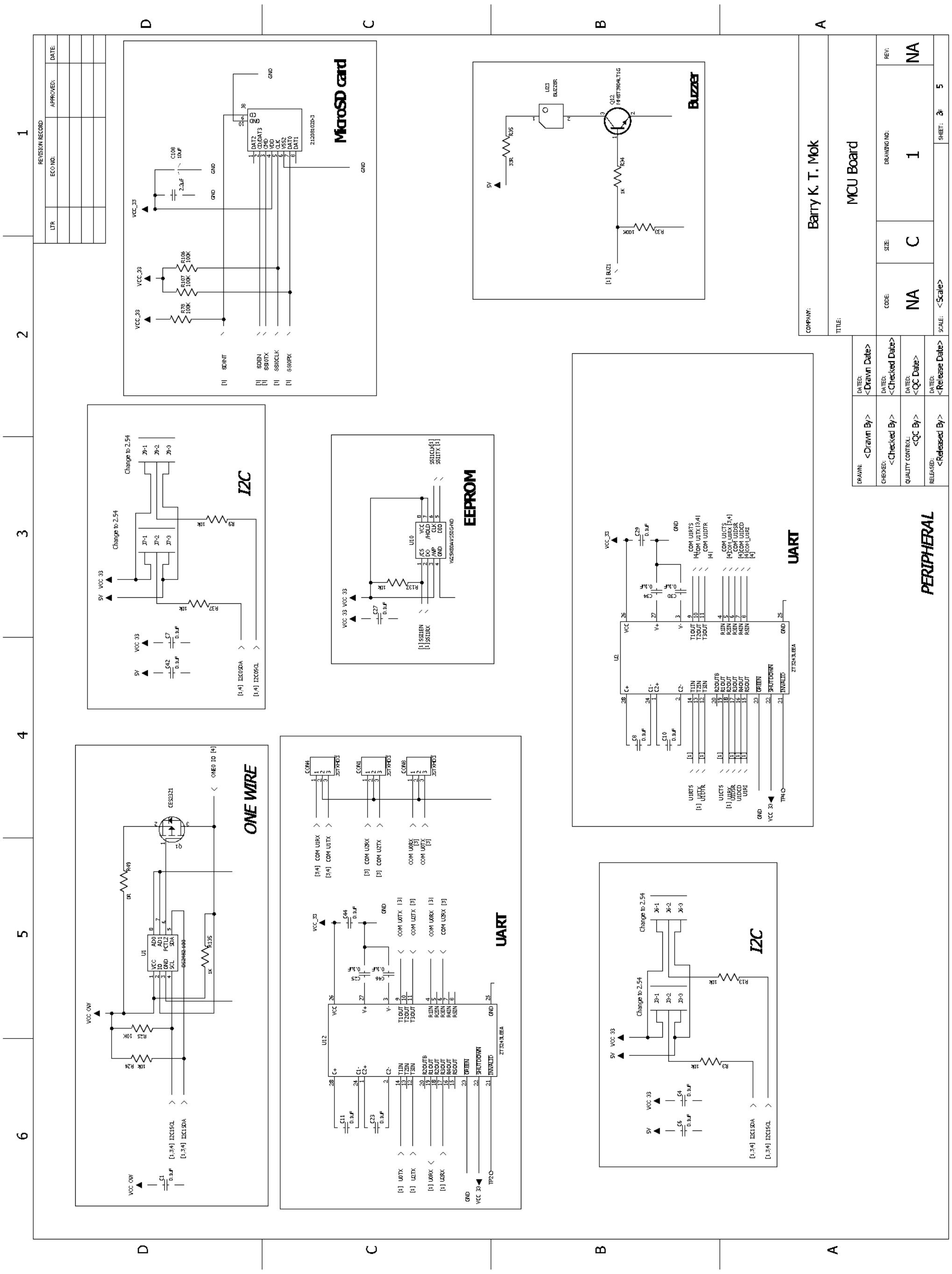

Figure 5: Full schematic diagram of the MCU-controlled data acquisition board.(Cont'd)

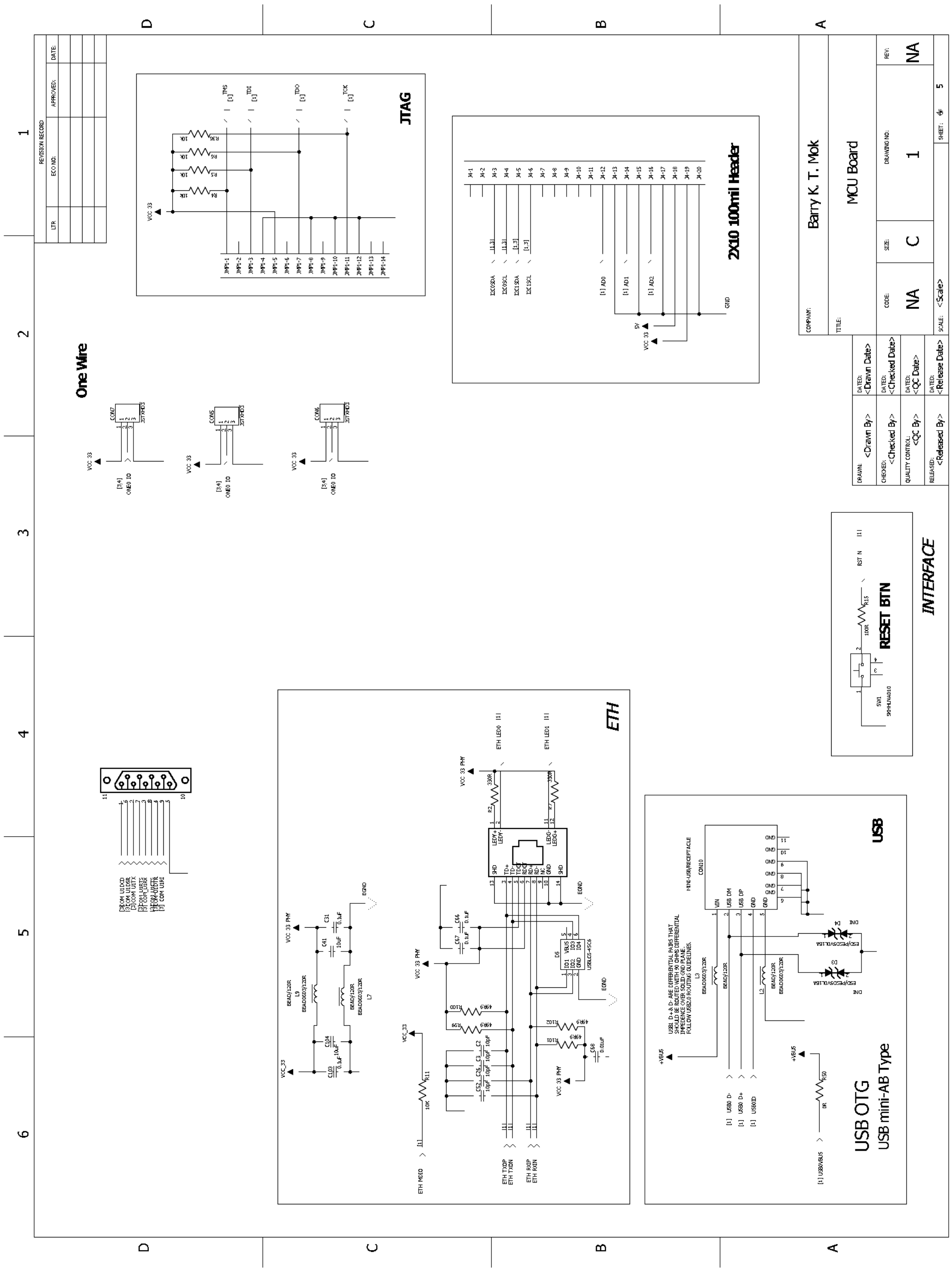

Figure 6: Full schematic diagram of the MCU-controlled data acquisition board.(Cont'd)

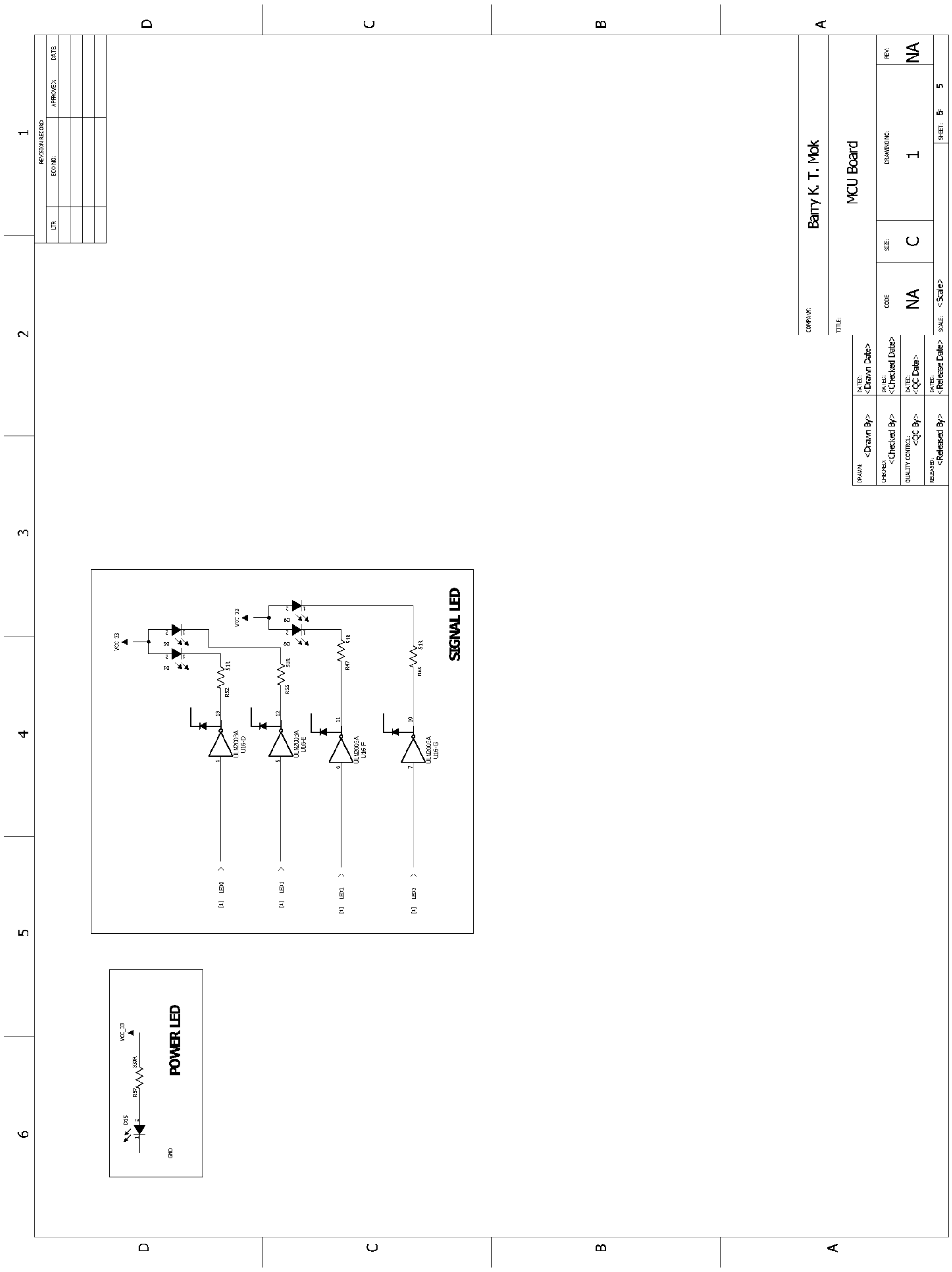

Figure 7: Full schematic diagram of the MCU-controlled data acquisition board.(Cont'd)

Table 1: Measurement Result of LED, LUXEON K2 LXK2-PW14-U00.

No.	v_{d}(V)	i_{d}(A)	T_{C}(°C)	No.	v_{d}(V)	i_{d}(A)	T_{C}(°C)	No.	v_{d}(V)	i_{d}(A)	T_{C}(°C)
1	3.011	0.089	22	46	3.492	0.852	22.5	91	3.187	0.233	24.5
2	3.093	0.138	22	47	3.503	0.899	22.5	92	3.23	0.28	24.5
3	3.148	0.185	22	48	3.511	0.947	22.5	93	3.261	0.327	24.5
4	3.198	0.232	22	49	3.527	0.996	22.5	94	3.292	0.375	24.5
5	3.238	0.28	22	50	3.539	1.043	23	95	3.32	0.422	24.5
6	3.273	0.327	22	51	3.55	1.091	23	96	3.347	0.471	24.5
7	3.304	0.374	22	52	3.558	1.139	23	97	3.367	0.518	24.5
8	3.327	0.422	22	53	3.57	1.186	23	98	3.386	0.566	24.5
9	3.355	0.469	22	54	3.582	1.233	23	99	3.402	0.613	24.5
10	3.374	0.518	22	55	3.586	1.282	23	100	3.417	0.661	24.5
11	3.398	0.565	22	56	3.597	1.328	23	101	3.437	0.708	24.5
12	3.417	0.613	22	57	3.609	1.377	23	102	3.453	0.757	24.5
13	3.433	0.661	22.5	58	2.893	0.044	23	103	3.464	0.805	24.5
14	3.449	0.708	22.5	59	3.011	0.091	23	104	3.484	0.852	25
15	3.464	0.757	22.5	60	3.089	0.138	23	105	3.5	0.9	25
16	3.48	0.804	22.5	61	3.148	0.186	23	106	3.511	0.947	25
17	3.492	0.852	22.5	62	3.195	0.233	23	107	3.523	0.996	25
18	3.507	0.9	22.5	63	3.234	0.28	23	108	3.535	1.043	25
19	3.519	0.947	22.5	64	3.265	0.327	23	109	3.546	1.091	25
20	3.527	0.996	22.5	65	3.292	0.375	23	110	3.554	1.139	25
21	3.543	1.043	22.5	66	3.324	0.424	23	111	3.558	1.186	25
22	3.55	1.091	22.5	67	3.351	0.471	23	112	3.57	1.235	25
23	3.562	1.139	22.5	68	3.37	0.518	23	113	3.582	1.282	25
24	3.57	1.186	22.5	69	3.39	0.565	23.5	114	3.593	1.33	25.5
25	3.582	1.235	23	70	3.413	0.613	23.5	115	3.601	1.378	25.5
26	3.593	1.282	23	71	3.425	0.66	23.5	116	2.886	0.044	25.5
27	3.601	1.33	23	72	3.441	0.708	23.5	117	3.003	0.091	25.5
28	3.609	1.377	23	73	3.457	0.757	23.5	118	3.081	0.138	25.5
29	2.897	0.043	22.5	74	3.472	0.805	23.5	119	3.14	0.186	25.5
30	3.015	0.089	22.5	75	3.484	0.852	23.5	120	3.187	0.233	25.5
31	3.089	0.138	22.5	76	3.5	0.899	23.5	121	3.226	0.28	25.5
32	3.148	0.185	22.5	77	3.511	0.947	23.5	122	3.257	0.327	25.5
33	3.195	0.232	22.5	78	3.523	0.996	23.5	123	3.284	0.374	25.5
34	3.238	0.28	22.5	79	3.535	1.043	23.5	124	3.316	0.422	25.5
35	3.273	0.327	22.5	80	3.546	1.091	23.5	125	3.339	0.471	25.5
36	3.3	0.375	22.5	81	3.558	1.138	24	126	3.363	0.518	25.5
37	3.327	0.422	22.5	82	3.566	1.186	24	127	3.382	0.565	25.5
38	3.351	0.471	22.5	83	3.574	1.235	24	128	3.398	0.613	25.5
39	3.374	0.518	22.5	84	3.586	1.282	24	129	3.421	0.66	25.5
40	3.394	0.566	22.5	85	3.597	1.328	24	130	3.437	0.708	25.5
41	3.41	0.613	22.5	86	3.605	1.377	24	131	3.449	0.757	25.5
42	3.429	0.661	22.5	87	2.89	0.044	24.5	132	3.464	0.805	25.5
43	3.445	0.708	22.5	88	3.007	0.091	24.5	133	3.48	0.853	26
44	3.46	0.757	22.5	89	3.085	0.138	24.5	134	3.492	0.899	26
45	3.476	0.804	22.5	90	3.144	0.186	24.5	135	3.503	0.947	26

Table 2: Measurement Result of LED, LUXEON K2 LXK2-PW14-U00(Cont'd).

No.	v_d(V)	i_d(A)	T_C(°C)	No.	v_d(V)	i_d(A)	T_C(°C)	No.	v_d(V)	i_d(A)	T_C(°C)
136	3.515	0.996	26	181	3.277	0.374	27.5	226	3.539	1.139	29.5
137	3.527	1.043	26	182	3.308	0.424	27.5	227	3.55	1.186	29.5
138	3.539	1.091	26	183	3.331	0.469	28	228	3.558	1.233	29.5
139	3.55	1.139	26	184	3.355	0.518	28	229	3.566	1.28	29.5
140	3.558	1.186	26	185	3.374	0.566	28	230	3.578	1.33	30
141	3.566	1.233	26	186	3.394	0.613	28	231	3.589	1.377	30
142	3.578	1.282	26	187	3.413	0.661	28	232	2.87	0.044	30.5
143	3.589	1.328	26.5	188	3.429	0.708	28	233	2.987	0.089	30.5
144	3.597	1.377	26.5	189	3.445	0.758	28	234	3.062	0.136	30.5
145	2.886	0.043	26.5	190	3.46	0.804	28	235	3.12	0.183	30.5
146	2.999	0.091	26.5	191	3.476	0.852	28	236	3.167	0.232	30.5
147	3.073	0.138	26.5	192	3.484	0.899	28	237	3.206	0.282	30.5
148	3.132	0.185	26.5	193	3.5	0.949	28	238	3.241	0.331	30.5
149	3.183	0.232	26.5	194	3.507	0.996	28	239	3.273	0.372	30.5
150	3.222	0.28	26.5	195	3.523	1.043	28	240	3.3	0.419	30.5
151	3.257	0.327	26.5	196	3.535	1.091	28	241	3.324	0.468	30.5
152	3.284	0.375	26.5	197	3.543	1.138	28.5	242	3.347	0.516	30.5
153	3.312	0.422	26.5	198	3.554	1.186	28.5	243	3.367	0.565	30.5
154	3.335	0.471	26.5	199	3.558	1.233	28.5	244	3.382	0.613	30.5
155	3.363	0.518	26.5	200	3.57	1.282	28.5	245	3.398	0.661	30.5
156	3.378	0.565	26.5	201	3.582	1.328	28.5	246	3.421	0.708	30.5
157	3.398	0.613	26.5	202	3.593	1.377	28.5	247	3.433	0.757	30.5
158	3.413	0.66	26.5	203	2.874	0.043	29	248	3.449	0.804	30.5
159	3.429	0.708	26.5	204	2.991	0.089	29	249	3.46	0.85	30.5
160	3.445	0.757	27	205	3.069	0.136	29	250	3.48	0.899	30.5
161	3.46	0.804	27	206	3.124	0.186	29	251	3.492	0.947	31
162	3.476	0.852	27	207	3.175	0.232	29	252	3.5	0.994	31
163	3.488	0.899	27	208	3.21	0.28	29	253	3.511	1.043	31
164	3.496	0.947	27	209	3.245	0.327	29	254	3.523	1.091	31
165	3.507	0.996	27	210	3.277	0.374	29	255	3.535	1.139	31
166	3.523	1.043	27	211	3.304	0.422	29	256	3.546	1.186	31
167	3.539	1.091	27	212	3.327	0.471	29	257	3.554	1.233	31
168	3.546	1.138	27	213	3.351	0.518	29	258	3.562	1.282	31
169	3.554	1.186	27	214	3.37	0.565	29	259	3.574	1.328	31
170	3.566	1.233	27.5	215	3.386	0.613	29	260	3.586	1.377	31
171	3.574	1.282	27.5	216	3.406	0.66	29	261	2.858	0.045	34
172	3.586	1.33	27.5	217	3.421	0.707	29	262	2.976	0.089	34
173	3.597	1.378	27.5	218	3.437	0.757	29	263	3.05	0.136	34
174	2.882	0.044	27.5	219	3.453	0.805	29	264	3.109	0.186	34
175	2.995	0.091	27.5	220	3.468	0.852	29.5	265	3.155	0.232	34
176	3.073	0.138	27.5	221	3.48	0.9	29.5	266	3.191	0.282	34
177	3.132	0.186	27.5	222	3.492	0.947	29.5	267	3.226	0.327	34
178	3.179	0.233	27.5	223	3.503	0.996	29.5	268	3.257	0.375	34
179	3.218	0.279	27.5	224	3.519	1.043	29.5	269	3.284	0.421	34
180	3.245	0.327	27.5	225	3.527	1.091	29.5	270	3.308	0.472	34

Table 3: Measurement Result of LED, LUXEON K2 LXK2-PW14-U00(Cont'd).

No.	v_d(V)	i_d(A)	T_C(°C)	No.	v_d(V)	i_d(A)	T_C(°C)	No.	v_d(V)	i_d(A)	T_C(°C)
271	3.331	0.518	34	316	3.543	1.284	39.5	361	3.367	0.663	39.5
272	3.355	0.566	34	317	3.546	1.328	39.5	362	3.382	0.71	39.5
273	3.37	0.616	34	318	3.558	1.377	39.5	363	3.398	0.755	39.5
274	3.39	0.658	34	319	2.839	0.044	40	364	3.413	0.804	39.5
275	3.406	0.707	34	320	2.952	0.091	40	365	3.425	0.852	39.5
276	3.421	0.757	34	321	3.026	0.138	40	366	3.441	0.899	39.5
277	3.433	0.804	34	322	3.085	0.185	40	367	3.453	0.947	40
278	3.449	0.852	34.5	323	3.132	0.232	40	368	3.464	0.996	40
279	3.464	0.899	34.5	324	3.171	0.28	40	369	3.48	1.044	40
280	3.476	0.947	34.5	325	3.206	0.327	40	370	3.492	1.091	40
281	3.488	0.997	34.5	326	3.238	0.374	40	371	3.503	1.139	40
282	3.503	1.043	34.5	327	3.261	0.421	40	372	3.511	1.188	40
283	3.511	1.091	34.5	328	3.288	0.471	40	373	3.523	1.233	40
284	3.519	1.138	34.5	329	3.312	0.518	40	374	3.535	1.28	40
285	3.535	1.186	34.5	330	3.327	0.566	40	375	3.543	1.33	40.5
286	3.546	1.232	34.5	331	3.347	0.613	40	376	3.554	1.377	40.5
287	3.554	1.282	34.5	332	3.367	0.663	40	377	2.839	0.044	40
288	3.566	1.33	34.5	333	3.382	0.707	40	378	2.952	0.089	40
289	3.574	1.377	34.5	334	3.398	0.757	40	379	3.022	0.138	40
290	2.843	0.041	39	335	3.413	0.805	40	380	3.081	0.183	40
291	2.956	0.091	39	336	3.429	0.85	40	381	3.128	0.232	40
292	3.034	0.138	39	337	3.441	0.9	40	382	3.171	0.28	40
293	3.089	0.185	39	338	3.453	0.947	40.5	383	3.206	0.326	40
294	3.136	0.232	39	339	3.464	0.997	40.5	384	3.238	0.375	40
295	3.175	0.28	39	340	3.48	1.044	40.5	385	3.261	0.422	40
296	3.206	0.327	39	341	3.488	1.089	40.5	386	3.284	0.472	40
297	3.238	0.375	39	342	3.503	1.139	40.5	387	3.308	0.518	40
298	3.265	0.422	39	343	3.511	1.185	40.5	388	3.327	0.565	40
299	3.288	0.469	39	344	3.523	1.232	40.5	389	3.347	0.611	40
300	3.312	0.518	39	345	3.527	1.282	40.5	390	3.367	0.66	40
301	3.335	0.566	39	346	3.543	1.328	40.5	391	3.382	0.708	40
302	3.351	0.611	39	347	3.554	1.377	40.5	392	3.398	0.757	40
303	3.37	0.66	39	348	2.839	0.044	39.5	393	3.413	0.804	40
304	3.386	0.708	39	349	2.952	0.091	39.5	394	3.429	0.852	40.5
305	3.398	0.757	39	350	3.03	0.139	39.5	395	3.441	0.899	40.5
306	3.417	0.804	39	351	3.085	0.185	39.5	396	3.453	0.949	40.5
307	3.433	0.852	39	352	3.132	0.232	39.5	397	3.464	0.994	40.5
308	3.445	0.9	39	353	3.175	0.279	39.5	398	3.476	1.043	40.5
309	3.457	0.947	39	354	3.206	0.327	39.5	399	3.492	1.091	40.5
310	3.468	0.994	39	355	3.234	0.375	39.5	400	3.503	1.141	40.5
311	3.48	1.043	39.5	356	3.261	0.422	39.5	401	3.511	1.185	40.5
312	3.496	1.091	39.5	357	3.288	0.472	39.5	402	3.523	1.233	40.5
313	3.507	1.139	39.5	358	3.312	0.518	39.5	403	3.527	1.282	40.5
314	3.515	1.186	39.5	359	3.331	0.565	39.5	404	3.539	1.33	41
315	3.523	1.233	39.5	360	3.351	0.614	39.5	405	3.554	1.377	41

Table 4: Measurement Result of LED, LUXEON K2 LXK2-PW14-U00(Cont'd).

No.	v_{d}(V)	i_{d}(A)	T_{C}(°C)	No.	v_{d}(V)	i_{d}(A)	T_{C}(°C)	No.	v_{d}(V)	i_{d}(A)	T_{C}(°C)
406	2.835	0.044	40.5	451	3.41	0.804	41.5	496	3.073	0.183	42.5
407	2.948	0.091	40.5	452	3.421	0.853	41.5	497	3.12	0.23	42.5
408	3.026	0.139	40.5	453	3.433	0.9	41.5	498	3.159	0.28	42.5
409	3.085	0.185	40.5	454	3.449	0.949	42	499	3.195	0.328	42.5
410	3.128	0.232	40.5	455	3.46	0.996	42	500	3.226	0.377	42.5
411	3.171	0.28	40.5	456	3.472	1.041	42	501	3.249	0.421	42.5
412	3.195	0.327	40.5	457	3.484	1.091	42	502	3.277	0.469	43
413	3.23	0.374	40.5	458	3.496	1.138	42	503	3.3	0.518	43
414	3.257	0.422	40.5	459	3.507	1.185	42	504	3.312	0.565	43
415	3.284	0.471	40.5	460	3.515	1.233	42	505	3.335	0.613	43
416	3.304	0.516	40.5	461	3.523	1.282	42	506	3.355	0.66	43
417	3.324	0.566	41	462	3.539	1.328	42	507	3.374	0.708	43
418	3.347	0.613	41	463	3.546	1.377	42	508	3.386	0.757	43
419	3.363	0.66	41	464	2.831	0.044	42	509	3.402	0.802	43
420	3.378	0.708	41	465	2.944	0.089	42	510	3.417	0.852	43
421	3.39	0.755	41	466	3.019	0.138	42	511	3.433	0.9	43
422	3.413	0.804	41	467	3.077	0.185	42	512	3.441	0.947	43
423	3.425	0.852	41	468	3.124	0.232	42	513	3.453	0.994	43
424	3.437	0.9	41	469	3.163	0.279	42	514	3.468	1.043	43
425	3.449	0.947	41	470	3.195	0.328	42	515	3.48	1.091	43
426	3.46	0.994	41	471	3.226	0.374	42	516	3.492	1.139	43
427	3.476	1.044	41	472	3.249	0.422	42	517	3.503	1.186	43
428	3.484	1.091	41	473	3.281	0.469	42	518	3.511	1.233	43
429	3.5	1.141	41	474	3.3	0.518	42	519	3.519	1.283	43
430	3.507	1.186	41	475	3.32	0.563	42	520	3.535	1.328	43.5
431	3.519	1.233	41.5	476	3.339	0.613	42	521	3.546	1.378	43.5
432	3.531	1.282	41.5	477	3.359	0.66	42	522	2.827	0.043	43.5
433	3.539	1.328	41.5	478	3.374	0.71	42	523	2.94	0.092	43.5
434	3.55	1.377	41.5	479	3.39	0.758	42	524	3.015	0.139	43.5
435	2.835	0.043	41.5	480	3.406	0.804	42	525	3.073	0.183	43.5
436	2.948	0.091	41.5	481	3.417	0.853	42.5	526	3.12	0.232	43.5
437	3.022	0.136	41.5	482	3.433	0.9	42.5	527	3.159	0.28	43.5
438	3.077	0.185	41.5	483	3.449	0.949	42.5	528	3.187	0.326	43.5
439	3.124	0.236	41.5	484	3.457	0.994	42.5	529	3.222	0.375	43.5
440	3.167	0.28	41.5	485	3.468	1.043	42.5	530	3.249	0.422	43.5
441	3.198	0.326	41.5	486	3.48	1.089	42.5	531	3.273	0.468	43.5
442	3.23	0.375	41.5	487	3.492	1.138	42.5	532	3.296	0.516	43.5
443	3.257	0.422	41.5	488	3.503	1.186	42.5	533	3.316	0.567	43.5
444	3.277	0.469	41.5	489	3.515	1.233	42.5	534	3.335	0.614	43.5
445	3.304	0.518	41.5	490	3.527	1.282	42.5	535	3.355	0.66	43.5
446	3.324	0.566	41.5	491	3.535	1.328	43	536	3.37	0.705	43.5
447	3.343	0.614	41.5	492	3.546	1.377	43	537	3.382	0.755	43.5
448	3.359	0.663	41.5	493	2.831	0.045	42.5	538	3.398	0.805	43.5
449	3.374	0.708	41.5	494	2.94	0.089	42.5	539	3.413	0.852	43.5
450	3.394	0.757	41.5	495	3.019	0.138	42.5	540	3.429	0.899	43.5

Table 5: Measurement Result of LED, LUXEON K2 LXK2-PW14-U00(Cont'd).

No.	v_d(V)	i_d(A)	T_C(°C)	No.	v_d(V)	i_d(A)	T_C(°C)	No.	v_d(V)	i_d(A)	T_C(°C)
541	3.441	0.947	44	586	3.187	0.328	45	631	3.472	1.091	46
542	3.453	0.996	44	587	3.218	0.372	45	632	3.48	1.138	46
543	3.464	1.044	44	588	3.245	0.422	45	633	3.492	1.186	46
544	3.476	1.088	44	589	3.269	0.471	45	634	3.507	1.232	46.5
545	3.488	1.138	44	590	3.292	0.518	45	635	3.515	1.283	46.5
546	3.503	1.186	44	591	3.312	0.565	45	636	3.527	1.33	46.5
547	3.511	1.233	44	592	3.331	0.611	45	637	3.539	1.375	46.5
548	3.523	1.28	44	593	3.347	0.663	45	638	2.819	0.043	46
549	3.531	1.33	44	594	3.367	0.708	45	639	2.933	0.089	46
550	3.543	1.378	44	595	3.382	0.755	45	640	3.007	0.139	46
551	2.827	0.044	44	596	3.398	0.805	45	641	3.065	0.183	46
552	2.936	0.091	44	597	3.41	0.853	45	642	3.112	0.233	46
553	3.015	0.138	44	598	3.425	0.899	45	643	3.148	0.28	46
554	3.069	0.185	44	599	3.437	0.95	45.5	644	3.179	0.327	46
555	3.116	0.232	44	600	3.445	0.996	45.5	645	3.21	0.374	46
556	3.159	0.28	44	601	3.46	1.043	45.5	646	3.238	0.422	46
557	3.191	0.327	44	602	3.472	1.089	45.5	647	3.269	0.471	46
558	3.222	0.375	44	603	3.484	1.139	45.5	648	3.288	0.519	46
559	3.249	0.422	44	604	3.492	1.186	45.5	649	3.308	0.565	46
560	3.273	0.469	44	605	3.507	1.235	45.5	650	3.327	0.613	46
561	3.296	0.516	44	606	3.519	1.282	45.5	651	3.343	0.663	46
562	3.316	0.565	44.5	607	3.527	1.33	46	652	3.363	0.707	46
563	3.335	0.614	44.5	608	3.539	1.378	46	653	3.374	0.758	46.5
564	3.355	0.661	44.5	609	2.823	0.044	45.5	654	3.39	0.805	46.5
565	3.37	0.707	44.5	610	2.933	0.094	45.5	655	3.406	0.85	46.5
566	3.382	0.755	44.5	611	3.003	0.136	45.5	656	3.421	0.9	46.5
567	3.398	0.804	44.5	612	3.065	0.186	45.5	657	3.433	0.947	46.5
568	3.417	0.85	44.5	613	3.112	0.235	45.5	658	3.445	0.996	46.5
569	3.429	0.9	44.5	614	3.152	0.28	45.5	659	3.457	1.043	46.5
570	3.437	0.947	44.5	615	3.187	0.328	45.5	660	3.468	1.091	46.5
571	3.449	0.994	44.5	616	3.214	0.375	45.5	661	3.476	1.139	46.5
572	3.464	1.043	44.5	617	3.241	0.424	45.5	662	3.492	1.185	46.5
573	3.476	1.091	44.5	618	3.265	0.468	45.5	663	3.503	1.233	47
574	3.488	1.139	44.5	619	3.292	0.518	45.5	664	3.511	1.283	47
575	3.5	1.186	44.5	620	3.312	0.565	45.5	665	3.523	1.328	47
576	3.511	1.235	45	621	3.327	0.611	45.5	666	3.535	1.375	47
577	3.519	1.283	45	622	3.347	0.66	46	667	2.815	0.043	47
578	3.531	1.33	45	623	3.363	0.707	46	668	2.929	0.092	47
579	3.543	1.378	45	624	3.378	0.757	46	669	3.003	0.139	47
580	2.823	0.044	45	625	3.394	0.805	46	670	3.062	0.185	47
581	2.936	0.092	45	626	3.41	0.85	46	671	3.109	0.23	47
582	3.011	0.139	45	627	3.421	0.899	46	672	3.148	0.28	47
583	3.069	0.186	45	628	3.429	0.947	46	673	3.183	0.326	47
584	3.112	0.233	45	629	3.445	0.994	46	674	3.21	0.375	47
585	3.155	0.28	45	630	3.46	1.043	46	675	3.238	0.421	47

Table 6: Measurement Result of LED, LUXEON K2 LXK2-PW14-U00(Cont'd).

No.	v_{d}(V)	i_{d}(A)	T_{C}(°C)	No.	v_{d}(V)	i_{d}(A)	T_{C}(°C)	No.	v_{d}(V)	i_{d}(A)	T_{C}(°C)
676	3.261	0.471	47	721	3.496	1.233	48.5	766	3.292	0.567	49
677	3.281	0.519	47	722	3.507	1.282	48.5	767	3.316	0.613	49
678	3.304	0.565	47	723	3.519	1.33	48.5	768	3.335	0.661	49
679	3.324	0.616	47	724	3.527	1.378	48.5	769	3.351	0.708	49
680	3.343	0.66	47	725	2.811	0.041	48.5	770	3.367	0.757	49
681	3.359	0.708	47	726	2.925	0.089	48.5	771	3.382	0.804	49
682	3.374	0.757	47	727	2.995	0.138	48.5	772	3.394	0.853	49.5
683	3.39	0.805	47	728	3.058	0.185	48.5	773	3.406	0.903	49.5
684	3.406	0.852	47	729	3.101	0.233	48.5	774	3.421	0.946	49.5
685	3.421	0.9	47	730	3.144	0.28	48.5	775	3.433	0.994	49.5
686	3.429	0.949	47	731	3.175	0.33	48.5	776	3.445	1.043	49.5
687	3.441	0.996	47	732	3.206	0.374	48.5	777	3.457	1.089	49.5
688	3.457	1.043	47.5	733	3.234	0.424	48.5	778	3.468	1.138	49.5
689	3.464	1.091	47.5	734	3.257	0.469	48.5	779	3.48	1.186	49.5
690	3.48	1.138	47.5	735	3.281	0.518	48.5	780	3.488	1.233	49.5
691	3.488	1.186	47.5	736	3.304	0.565	48.5	781	3.5	1.282	49.5
692	3.5	1.233	47.5	737	3.316	0.613	48.5	782	3.507	1.328	49.5
693	3.507	1.282	47.5	738	3.335	0.658	48.5	783	3.523	1.377	49.5
694	3.515	1.328	47.5	739	3.351	0.707	48.5	784	2.811	0.044	49.5
695	3.531	1.377	47.5	740	3.37	0.757	48.5	785	2.921	0.089	49.5
696	2.811	0.043	47.5	741	3.386	0.805	48.5	786	2.999	0.138	49.5
697	2.929	0.091	47.5	742	3.398	0.852	49	787	3.054	0.185	49.5
698	3.003	0.139	47.5	743	3.413	0.9	49	788	3.101	0.23	49.5
699	3.058	0.183	47.5	744	3.425	0.949	49	789	3.136	0.282	49.5
700	3.105	0.232	47.5	745	3.437	0.994	49	790	3.171	0.328	49.5
701	3.144	0.282	47.5	746	3.445	1.043	49	791	3.202	0.371	49.5
702	3.175	0.326	47.5	747	3.46	1.092	49	792	3.226	0.425	49.5
703	3.206	0.377	47.5	748	3.472	1.138	49	793	3.249	0.471	50
704	3.238	0.422	47.5	749	3.484	1.185	49	794	3.273	0.519	50
705	3.261	0.472	47.5	750	3.5	1.235	49	795	3.296	0.565	50
706	3.281	0.518	47.5	751	3.503	1.28	49	796	3.312	0.613	50
707	3.304	0.565	47.5	752	3.511	1.328	49	797	3.327	0.658	50
708	3.32	0.613	47.5	753	3.523	1.377	49	798	3.347	0.707	50
709	3.339	0.66	47.5	754	2.413	0.001	49	799	3.367	0.757	50
710	3.355	0.707	47.5	755	2.815	0.044	49	800	3.378	0.804	50
711	3.374	0.755	48	756	2.925	0.089	49	801	3.394	0.85	50
712	3.382	0.804	48	757	2.999	0.138	49	802	3.406	0.899	50
713	3.398	0.85	48	758	3.054	0.185	49	803	3.417	0.947	50
714	3.413	0.9	48	759	3.101	0.233	49	804	3.429	0.996	50
715	3.429	0.949	48	760	3.14	0.279	49	805	3.437	1.044	50
716	3.437	0.993	48	761	3.171	0.327	49	806	3.453	1.091	50
717	3.453	1.043	48	762	3.198	0.375	49	807	3.464	1.138	50
718	3.464	1.089	48	763	3.23	0.424	49	808	3.476	1.186	50
719	3.476	1.138	48	764	3.253	0.468	49	809	3.488	1.236	50.5
720	3.484	1.185	48	765	3.277	0.519	49	810	3.496	1.282	50.5

Table 7: Measurement Result of LED, LUXEON K2 LXK2-PW14-U00(Cont'd).

No.	v_d(V)	i_d(A)	T_C(°C)	No.	v_d(V)	i_d(A)	T_C(°C)	No.	v_d(V)	i_d(A)	T_C(°C)
811	3.507	1.33	50.5	831	3.394	0.9	52	851	3.241	0.469	53
812	3.519	1.375	50.5	832	3.41	0.946	52	852	3.261	0.519	53
813	2.804	0.043	51.5	833	3.425	0.994	52	853	3.288	0.565	53
814	2.917	0.092	51.5	834	3.433	1.041	52	854	3.304	0.613	53
815	2.991	0.138	51.5	835	3.449	1.091	52	855	3.32	0.661	53
816	3.05	0.185	51.5	836	3.46	1.139	52	856	3.335	0.708	53
817	3.093	0.235	51.5	837	3.468	1.186	52	857	3.355	0.757	53
818	3.132	0.28	51.5	838	3.48	1.233	52	858	3.367	0.804	53
819	3.163	0.327	51.5	839	3.492	1.282	52	859	3.374	0.853	53
820	3.191	0.375	51.5	840	3.5	1.328	52	860	3.39	0.899	53
821	3.218	0.424	51.5	841	3.511	1.377	52	861	3.402	0.946	53
822	3.245	0.471	51.5	842	2.8	0.043	52.5	862	3.417	0.994	53
823	3.265	0.518	51.5	843	2.913	0.089	52.5	863	3.429	1.041	53
824	3.288	0.565	51.5	844	2.987	0.136	52.5	864	3.441	1.089	53
825	3.308	0.611	51.5	845	3.042	0.185	52.5	865	3.449	1.139	53.5
826	3.324	0.661	51.5	846	3.089	0.232	52.5	866	3.46	1.186	53.5
827	3.339	0.71	51.5	847	3.128	0.28	53	867	3.476	1.233	53.5
828	3.351	0.757	51.5	848	3.163	0.327	53	868	3.484	1.28	53.5
829	3.37	0.804	51.5	849	3.191	0.375	53	869	3.492	1.328	53.5
830	3.386	0.852	52	850	3.218	0.422	53	870	3.503	1.377	53.5

Appendix B

This appendix gives a summary of all possible combinations of DC-DC two-switch ladder-structured power converters from the first order to the fourth order formulated by using the proposed power converter synthesis method. The mode of converters represents one of the possible combinations. For instance, the first-order voltage-to-voltage mode-1 converter represents a voltage buck converter. This appendix also contains the schematic diagrams.

Table 8: All possible combinations of two-switch ladder-structured power converters (from first to fourth order)

Mode	**First Order V-to-I**	Mode	**First Order I-to-V**
1	S S L	1	S S C
Mode	**Second Order V-to-V**	Mode	**Second Order I-to-I**
1	S S L C	1	S S C L
2	L S S C	2	S S C L
3	S L S C	3	S S C L
Mode	**Third Order V-to-I**	Mode	**Third Order I-to-V**
1	S S L C L	1	S S C L C
2	L S S C L	2	C S S L C
3	L C S S L	3	C L S S C
4	S L S C L	4	S C S L C
5	L S C S L	5	C S L S C
6	S L C S L	6	S C L S C
Mode	**Fourth Order V-to-V**	Mode	**Fourth Order I-to-I**
1	S S L C L C	1	S S C L C L
2	L S S C L C	2	C S S L C L
3	L C S S L C	3	C L S S c L
4	L C L S S C	4	C L C S S L
5	S L S C L C	5	S C S L C L
6	L S C S L C	6	C S L S C L
7	L C S L S C	7	C L S C S L
8	S L C S L C	8	S C L S C L
9	L S C L S C	9	C S L C S L
10	S L C L S C	10	S C L C S L

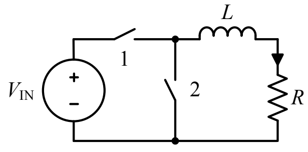

Figure 8: First-order voltage-to-current converter.

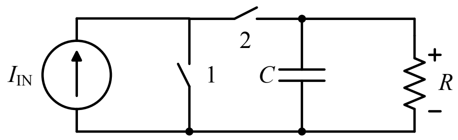

Figure 9: First-order current-to-voltage converter.

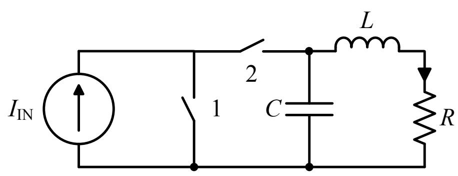

(a) Mode-1 (current-buck)

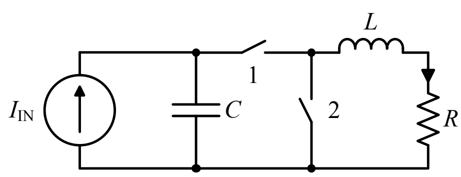

(b) Mode-2 (current-boost)

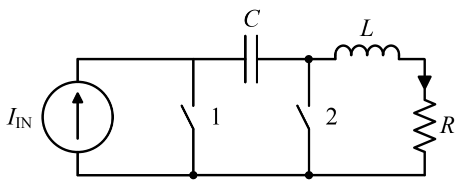

(c) Mode-3 (current-buck-boost)

Figure 10: Second-order current-to-current converters

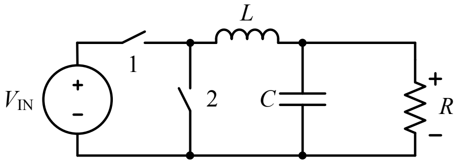

(a) Mode-1 (voltage-buck)

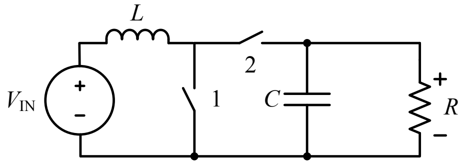

(b) Mode-2 (voltage-boost)

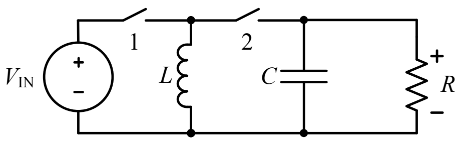

(c) Mode-3 (voltage-buck-boost)

Figure 11: Second-order voltage-to-voltage converters

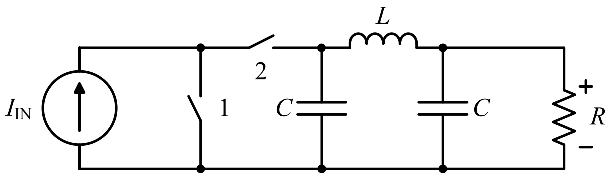

(a) Mode-1

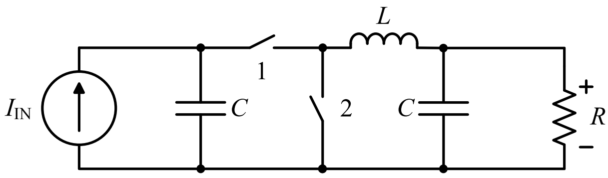

(b) Mode-2

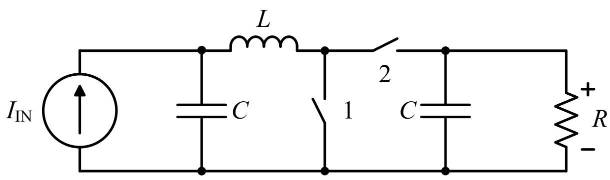

(c) Mode-3

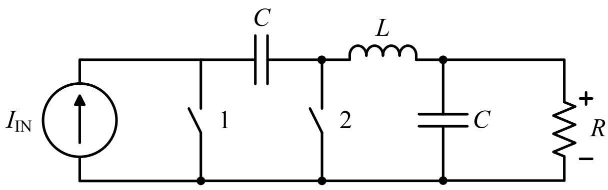

(d) Mode-4

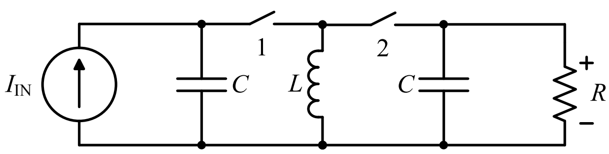

(e) Mode-5

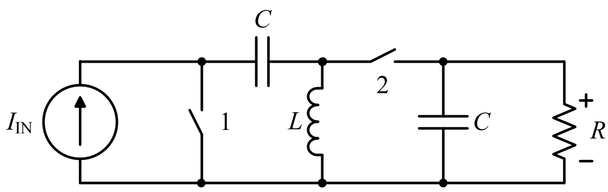

(f) Mode-6

Figure 12: Third-order current-to-voltage converters

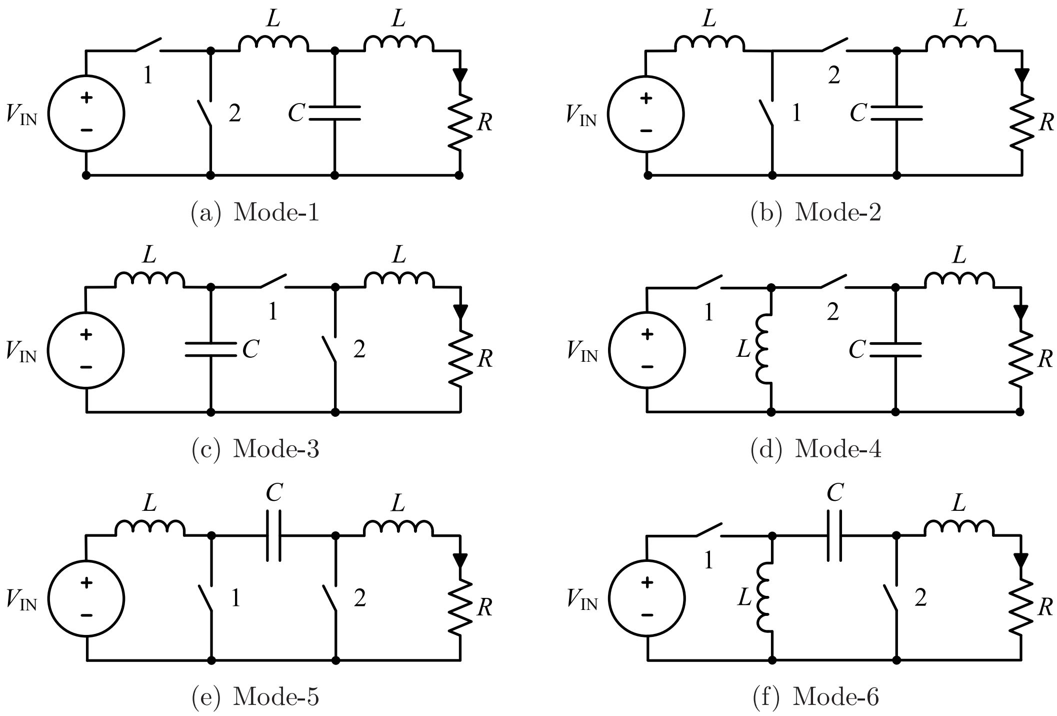

(a) Mode-1 (b) Mode-2 (c) Mode-3 (d) Mode-4 (e) Mode-5 (f) Mode-6

Figure 13: Third-order current-to-voltage converters

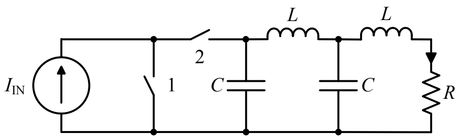

(a) Mode-1

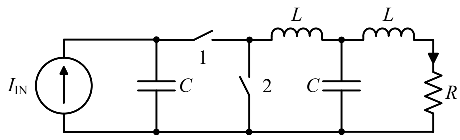

(b) Mode-2

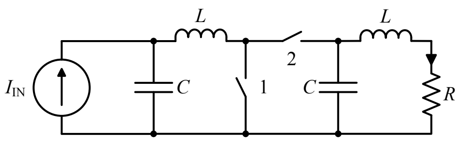

(c) Mode-3

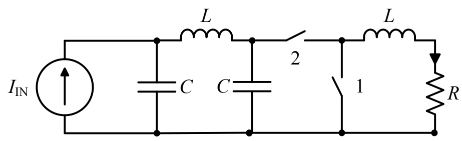

(d) Mode-4

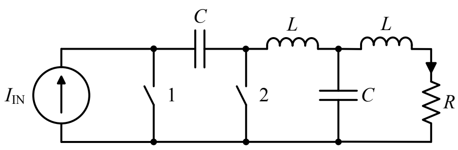

(e) Mode-5

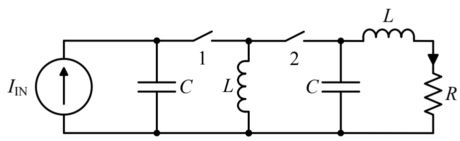

(f) Mode-6

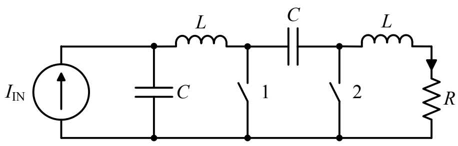

(g) Mode-7

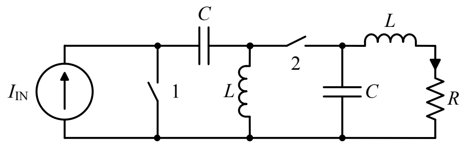

(h) Mode-8

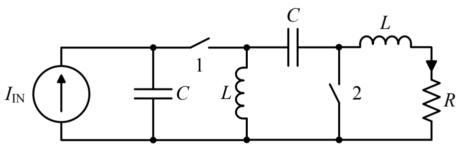

(i) Mode-9

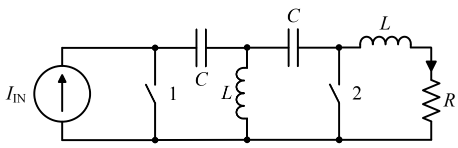

(j) Mode-10

Figure 14: Forth-order current-to-current converters

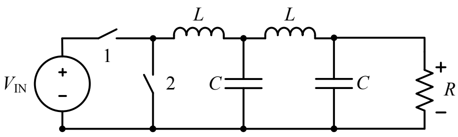

(a) Mode-1 (voltage-buck with output CLC network)

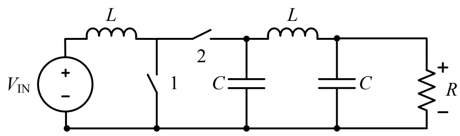

(b) Mode-2 (voltage-boost with output CLC network)

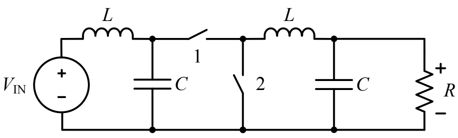

(c) Mode-3 (voltage-buck with input LC network)

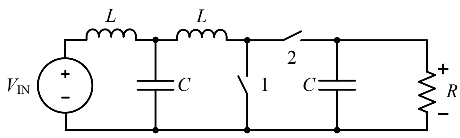

(d) Mode-4 (voltage-boost with output CLC network)

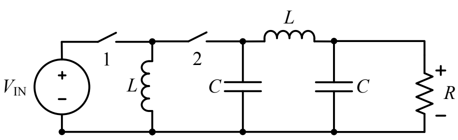

(e) Mode-5 (voltage-buck-boost with output CLC network)

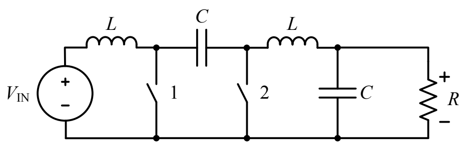

(f) Mode-6 (Ćuk)

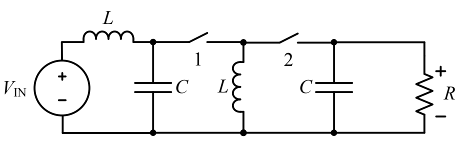

(g) Mode-7 (voltage-buck-boost with input LC network)

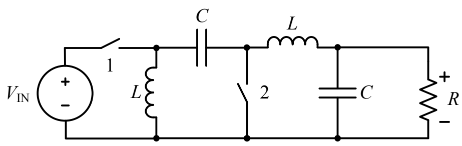

(h) Mode-8 (Zeta)

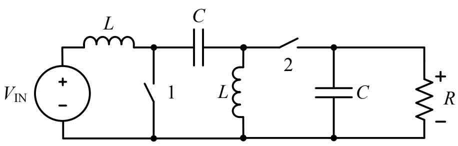

(i) Mode-9 (SEPIC)

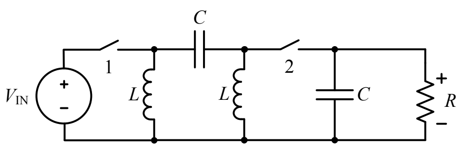

(j) Mode-10 (New converter)

Figure 15: Forth-order voltage-to-voltage converters

Bibliography

[1] I. Azevedo, M. Morgan, and F. Morgan, "The transition to solid-state lighting," *Proceedings of the IEEE*, vol. 97, no. 3, pp. 481 –510, march 2009. 1, 5

[2] C. J. Humphreys, "The transition to solid-state lighting," *Materials Research Society (MRS Bulletin)*, vol. 33, pp. 459–470, april 2008. 1

[3] M. Shur and R. Zukauskas, "Solid-state lighting: Toward superior illumination," *Proceedings of the IEEE*, vol. 93, no. 10, pp. 1691 –1703, oct. 2005. 1

[4] E. E. H. R. Berman and V. D. Roberts, "Starting behavior of rapid start fluorescent lamps with internal starting aids," *J. IES*, vol. 5, 1976. 1

[5] M. G. Craford, "High power leds for solid state lighting:status, trends, and challenges," *Journal of Light and Visual Environment*, vol. 32, pp. 58–62, 2008. 1

[6] M. Krames, O. Shchekin, R. Mueller-Mach, G. Mueller, L. Zhou, G. Harbers, and M. Craford, "Status and future of high-power light-emitting diodes for

solid-state lighting," *Display Technology, Journal of*, vol. 3, no. 2, pp. 160 –175, june 2007. 2

[7] L. Trevisanello, M. Meneghini, G. Mura, M. Vanzi, M. Pavesi, G. Meneghesso, and E. Zanoni, "Accelerated life test of high brightness light emitting diodes," *Device and Materials Reliability, IEEE Transactions on*, vol. 8, no. 2, pp. 304 –311, june 2008. 2

[8] M.-T. Lin, C.-C. Chang, R.-H. Horng, D.-S. Huang, and C.-M. Lai, "Heat dissipation performance for the application of light emitting diode," in *Design, Test, Integration Packaging of MEMS/MOEMS, 2009. MEMS/MOEMS '09. Symposium on*, april 2009, pp. 145 –149. 2

[9] X. Luo, W. Xiong, T. Cheng, and S. Liu, "Design and optimization of horizontally-located plate fin heat sink for high power led street lamps," in *Electronic Components and Technology Conference, 2009. ECTC 2009. 59th*, may 2009, pp. 854 –859. 2

[10] S.-Y. Tseng, J.-S. Kuo, S.-W. Wang, and C.-T. Hsieh, "Buck-boost combined with active clamp flyback converter for pv power system," in *Power Electronics Specialists Conference, 2007. PESC 2007. IEEE*, june 2007, pp. 138 –144. 2

[11] J. Garcia, J. Ramos, D. Lamar, M. Dalla-Costa, and J. Cardesin, "Evaluation of a synchronous flyback driving parallelized high efficiency leds," in *Industrial Electronics, 2007. ISIE 2007. IEEE International Symposium on*, june 2007, pp. 3036 –3040.

[12] H. Chang and Y.-S. Lai, "Novel ac driver and protection circuits with dimming control for light emitting diodes," in *Industry Applications Conference, 2007. 42nd IAS Annual Meeting. Conference Record of the 2007 IEEE*, sept. 2007, pp. 696 –700. 2

[13] W.-K. Lun, K. Loo, S.-C. Tan, Y. Lai, and C. Tse, "Bilevel current driving technique for leds," *Power Electronics, IEEE Transactions on*, vol. 24, no. 12, pp. 2920 –2932, dec. 2009. 2, 13, 43

[14] K. Loo, W.-K. Lun, S.-C. Tan, Y. Lai, and C. Tse, "On driving techniques for leds: Toward a generalized methodology," *Power Electronics, IEEE Transactions on*, vol. 24, no. 12, pp. 2967 –2976, dec. 2009. 2, 13, 43

[15] W.-H. Chang, H.-S. Nien, and C.-H. Chen, "A digital boost converter to drive white leds," in *Applied Power Electronics Conference and Exposition, 2008. APEC 2008. Twenty-Third Annual IEEE*, 24-28 2008, pp. 558 –564. 4

[16] M. Xie and J. Zhang, "A dc-dc current source power supply with novel load current signal extraction," in *Applied Power Electronics Conference and Exposition, 2008. APEC 2008. Twenty-Third Annual IEEE*, 24-28 2008, pp. 1651 –1655. 4

[17] J. de Britto, A. Demian, L. de Freitas, V. Farias, E. Coelho, and J. Vieira, "A proposal of led lamp driver for universal input using cuk converter," in *Power Electronics Specialists Conference, 2008. PESC 2008. IEEE*, 15-19 2008, pp. 2640 –2644. 4

[18] J. de Britto, L. de Freitas, V. Farias, E. Coelho, and J. Vieira, "Led lamp driver using a converter with wide range conversion microcontroller-based,"

in *Industrial Electronics, 2008. IECON 2008. 34th Annual Conference of IEEE*, 10-13 2008, pp. 1988 –1993. 4

[19] M. Rico-Secades, J. Garcia, J. Cardesin, and A. Calleja, "Using tapped-inductor converters as led drivers," in *Industry Applications Conference, 2006. 41st IAS Annual Meeting. Conference Record of the 2006 IEEE*, vol. 4, 8-12 2006, pp. 1794 –1800. 4

[20] H. Pang and M. Pong, "A stability issue with current mode control flyback converter driving leds," in *Power Electronics and Motion Control Conference, 2009. IPEMC '09. IEEE 6th International*, 17-20 2009, pp. 1402 –1406. 5

[21] T.-L. Chern, L.-H. Liu, P.-L. Pan, and Y.-J. Lee, "Single-stage flyback converter for constant current output led driver with power factor correction," in *Industrial Electronics and Applications, 2009. ICIEA 2009. 4th IEEE Conference on*, 25-27 2009, pp. 2891 –2896. 5

[22] L. Gu, X. Ruan, M. Xu, and K. Yao, "Means of eliminating electrolytic capacitor in ac/dc power supplies for led lightings," *Power Electronics, IEEE Transactions on*, vol. 24, no. 5, pp. 1399 –1408, may 2009. 5, 12

[23] K. Hwu, Y. Yau, and L.-L. Lee, "Powering led using high-efficiency sr flyback converter," in *Applied Power Electronics Conference and Exposition, 2009. APEC 2009. Twenty-Fourth Annual IEEE*, 15-19 2009, pp. 563 –569. 5

[24] K. Yao, M. Xu, X. Ruan, and L. Gu, "Boost-flyback single-stage pfc converter with large dc bus voltage ripple," in *Applied Power Electronics Con-*

ference and Exposition, 2009. APEC 2009. Twenty-Fourth Annual IEEE, 15-19 2009, pp. 1867 –1871. 6

[25] Z. Bo, Y. Xu, X. Ming, C. Qiaoliang, and W. Zhaoan, “Design of boost-flyback single-stage pfc converter for led power supply without electrolytic capacitor for energy-storage,” in *Power Electronics and Motion Control Conference, 2009. IPEMC ’09. IEEE 6th International*, 17-20 2009, pp. 1668 –1671. 6

[26] Z. Ye, F. Greenfeld, and Z. Liang, “Design considerations of a high power factor sepic converter for high brightness white led lighting applications,” in *Power Electronics Specialists Conference, 2008. PESC 2008. IEEE*, 15-19 2008, pp. 2657 –2663. 6

[27] ——, “Single-stage offline sepic converter with power factor correction to drive high brightness leds,” in *Applied Power Electronics Conference and Exposition, 2009. APEC 2009. Twenty-Fourth Annual IEEE*, 15-19 2009, pp. 546 –553. 6

[28] X. Qu, S. Wong, C. Tse, and X. Ruan, “Isolated pfc pre-regulator for led lamps,” in *Industrial Electronics, 2008. IECON 2008. 34th Annual Conference of IEEE*, 10-13 2008, pp. 1980 –1987. 6

[29] Y. Qin, H. Chung, D. Lin, and S. Hui, “Current source ballast for high power lighting emitting diodes without electrolytic capacitor,” in *Industrial Electronics, 2008. IECON 2008. 34th Annual Conference of IEEE*, 10-13 2008, pp. 1968 –1973. 6

[30] K. Zhou, J. G. Zhang, S. Yuvarajan, and D. F. Weng, "Quasi-active power factor correction circuit for hb led driver," *Power Electronics, IEEE Transactions on*, vol. 23, no. 3, pp. 1410 –1415, may 2008. 6

[31] E. Mineiro Sa, F. Antunes, and A. Perin, "Low cost self-oscillating zvs-cv driver for power leds," in *Power Electronics Specialists Conference, 2008. PESC 2008. IEEE*, 15-19 2008, pp. 4196 –4201. 5, 6

[32] S. Spitzer, N. Schumaker, L. Koszi, and J. North, "Multijunction ac or dc integrated gap light emitting diode array," *Electron Devices, IEEE Transactions on*, vol. 22, no. 9, pp. 701 – 706, sep 1975. 7

[33] G. Onushkin, Y.-J. Lee, J.-J. Yang, H.-K. Kim, J.-K. Son, G.-H. Park, and Y. Park, "Efficient alternating current operated white light-emitting diode chip," *Photonics Technology Letters, IEEE*, vol. 21, no. 1, pp. 33 –35, jan.1, 2009. 7

[34] J. Patterson and R. Zane, "Series input modular architecture for driving multiple leds," in *Power Electronics Specialists Conference, 2008. PESC 2008. IEEE*, 15-19 2008, pp. 2650 –2656. 8

[35] Q. Hu and R. Zane, "Led drive circuit with series input connected converter cells operating in continuous conduction mode," in *Applied Power Electronics Conference and Exposition, 2009. APEC 2009. Twenty-Fourth Annual IEEE*, 15-19 2009, pp. 1511 –1517. 8

[36] C.-H. Lin, T.-Y. Hung, C.-M. Wang, and K.-J. Pai, "A balancing strategy and implementation of current equalizer for high power led backlighting,"

in *Power Electronics and Drive Systems, 2007. PEDS '07. 7th International Conference on*, nov. 2007, pp. 1613 –1617. 9

[37] Y. Hu and M. Jovanovic, "A novel led driver with adaptive drive voltage," in *Applied Power Electronics Conference and Exposition, 2008. APEC 2008. Twenty-Third Annual IEEE*, 24-28 2008, pp. 565 –571. 9

[38] W. Thomas and J. Pforr, "A novel low-cost current-sharing method for automotive led-lighting systems," in *Power Electronics and Applications, 2009. EPE '09. 13th European Conference on*, 8-10 2009, pp. 1 –10. 10

[39] S. Baddela and D. Zinger, "Parallel connected leds operated at high to improve current sharing," in *Industry Applications Conference, 2004. 39th IAS Annual Meeting. Conference Record of the 2004 IEEE*, vol. 3, 3-7 2004, pp. 1677 – 1681 vol.3. 10

[40] M. Nishikawa, Y. Ishizuka, H. Matsuo, and K. Shigematsu, "An led drive circuit with constant-output-current control and constant-luminance control," in *Telecommunications Energy Conference, 2006. INTELEC '06. 28th Annual International*, sept. 2006, pp. 1 –6. 10

[41] C.-H. Wang, T.-P. Sun, H.-L. Shieh, C.-D. Chang, and S.-F. Tang, "A novel automatic power control system for a light emitting diode driving system," in *Industrial Electronics and Applications, 2009. ICIEA 2009. 4th IEEE Conference on*, 25-27 2009, pp. 2232 –2235. 10

[42] J. Garcia, M. Dalla-Costa, J. Cardesin, J. Alonso, and M. Rico-Secades, "Dimming of high-brightness leds by means of luminous flux thermal esti-

mation," *Power Electronics, IEEE Transactions on*, vol. 24, no. 4, pp. 1107 –1114, april 2009. 10

[43] H. van der Broeck, G. Sauerlander, and M. Wendt, "Power driver topologies and control schemes for leds," in *Applied Power Electronics Conference, APEC 2007 - Twenty Second Annual IEEE*, feb. 2007, pp. 1319 –1325. 11

[44] C.-F. Lu, C.-H. Liao, C.-Y. Chen, C. Hsieh, Y.-W. Kiang, and C. C. Yang, "Reduction in the efficiency droop effect of a light-emitting diode through surface plasmon coupling," *Applied Physics Letters*, vol. 96, no. 26, pp. 261 104 –261 104–3, jun 2010. 12

[45] C.-F. Lu, C.-H. Liao, C.-Y. Chen, C. Hsieh, and C. C. Yang, "Reduction of the efficiency droop effect of a light-emitting diode through surface plasmon coupling," in *Lasers and Electro-Optics (CLEO) and Quantum Electronics and Laser Science Conference (QELS), 2010 Conference on*, 16-21 2010, pp. 1 –2. 12

[46] H. Zhao, G. Liu, R. Arif, and N. Tansu, "Effect of current injection efficiency on efficiency-droop in ingan quantum well light-emitting diodes," in *Semiconductor Device Research Symposium, 2009. ISDRS '09. International*, 9-11 2009, pp. 1 –2. 12

[47] P. Narra and D. Zinger, "An effective led dimming approach," in *Industry Applications Conference, 2004. 39th IAS Annual Meeting. Conference Record of the 2004 IEEE*, vol. 3, 3-7 2004, pp. 1671 – 1676 vol.3. 13, 41

[48] National-Semiconductor, "LM3406 evaluation board," *National Semiconductor Application Notes*, 2008. 13

[49] S. Ng, K. Loo, S. Ip, Y. Lai, C. Tse, and K. Mok, "Sequential variable bi-level driving approach suitable for use in high color precision led display panels," *Industrial Electronics, IEEE Transactions on*, vol. PP, no. 99, p. 1, 2011. 13

[50] K. Loo, Y. Lai, S. Tan, and C. Tse, "On the color stability of phosphor-converted white leds under dc, pwm, and bilevel drive," *Power Electronics, IEEE Transactions on*, vol. 27, no. 2, pp. 974 –984, feb. 2012. 13

[51] K. Loo, Y. Lai, S.-C. Tan, and C. Tse, "Stationary and adaptive color-shift reduction methods based on the bilevel driving technique for phosphor-converted white leds," *Power Electronics, IEEE Transactions on*, vol. 26, no. 7, pp. 1943 –1953, july 2011. 13

[52] S. Muthu, F. Schuurmans, and M. Pashley, "Red, green, and blue led based white light generation: issues and control," in *Industry Applications Conference, 2002. 37th IAS Annual Meeting. Conference Record of the*, vol. 1, 2002, pp. 327 – 333 vol.1. 14

[53] ——, "Red, green, and blue leds for white light illumination," *Selected Topics in Quantum Electronics, IEEE Journal of*, vol. 8, no. 2, pp. 333 –338, mar/apr 2002. 14

[54] S. Muthu and J. Gaines, "Red, green and blue led-based white light source: implementation challenges and control design," in *Industry Applications Conference, 2003. 38th IAS Annual Meeting. Conference Record of the*, vol. 1, 12-16 2003, pp. 515 – 522 vol.1. 14

[55] X. Qu, S.-C. Wong, and C. Tse, "Temperature measurement technique for stabilizing the light output of rgb led lamps," *Instrumentation and Mea-*

surement, IEEE Transactions on, vol. 59, no. 3, pp. 661 –670, march 2010. 14

[56] R. L. A. Betty Lise Anderson, *Fundamentals of semiconductor devices*. McGraw-Hill, 2005. 19

[57] K. Werner, “Higher visibility for leds,” *Spectrum, IEEE*, vol. 31, no. 7, pp. 30 –34, july 1994. 19

[58] S. Nakamura, “A bright future for blue/green leds,” *Circuits and Devices Magazine, IEEE*, vol. 11, no. 3, pp. 19 –23, may 1995. 19

[59] S. Ghazanfar, L. Deming, A. Alla, L. Hairong, and M. Bhatti, “Stabilization and control of the wavelength of gan led,” in *Emerging Technologies, 2006. ICET ’06. International Conference on*, nov. 2006, pp. 358 –361. 19

[60] A. Bhattacharya, B. Lehman, C. DiMarzio, A. Shteynberg, and H. Rodriguez, “Effects of parametric uncertainty in designing a high-brightness led light system,” in *Applied Power Electronics Conference and Exposition, 2008. APEC 2008. Twenty-Third Annual IEEE*, feb. 2008, pp. 544 –550. 19

[61] Y. Acharya and P. Vyavahare, “Remodeling light emitting diode in low current region,” *Electron Devices, IEEE Transactions on*, vol. 45, no. 7, pp. 1426 –1430, jul 1998. 21

[62] Y. Xi and E. F. Schubert, “Junction temperature measurement in gan ultraviolet light-emitting diodes using diode forward voltage method,” *Applied Physics Letters*, vol. 85, no. 12, pp. 2163 –2165, sep 2004. 21

[63] C. Chen, C.-Y. Wu, and T.-F. Wu, "Led back-light driving system for lcd panels," in *Applied Power Electronics Conference and Exposition, 2006. APEC '06. Twenty-First Annual IEEE*, march 2006, p. 5 pp. 28

[64] C.-H. Lin, T.-Y. Hung, C.-M. Wang, and K.-J. Pai, "A balancing strategy and implementation of current equalizer for high power led backlighting," in *Power Electronics and Drive Systems, 2007. PEDS '07. 7th International Conference on*, nov. 2007, pp. 1613 –1617.

[65] M. Doshi and R. Zane, "Digital architecture for driving large led arrays with dynamic bus voltage regulation and phase shifted pwm," in *Applied Power Electronics Conference, APEC 2007 - Twenty Second Annual IEEE*, 25 2007-march 1 2007, pp. 287 –293. 39

[66] T.-F. Wu, C.-C. Chen, C.-Y. Wu, P.-C. Lu, and Y.-R. Chen, "Sequential color led backlight driving system for lcd panels with area control," in *Power Electronics Specialists Conference, 2007. PESC 2007. IEEE*, june 2007, pp. 2947 –2952.

[67] H.-J. Chiu and S.-J. Cheng, "Led backlight driving system for large-scale lcd panels," *Industrial Electronics, IEEE Transactions on*, vol. 54, no. 5, pp. 2751 –2760, oct. 2007. 28

[68] J.-S. Kim, Y.-K. Lee, J.-S. Lee, Y.-K. Shin, J.-H. Tark, K.-C. Ryu, and B.-D. Yang, "A fast-switching current-pulse driver for led backlight," in *Circuits and Systems, 2009. ISCAS 2009. IEEE International Symposium on*, may 2009, pp. 1775 –1778.

[69] X. Xu and X. Wu, "High dimming ratio led driver with fast transient boost converter," in *Power Electronics Specialists Conference, 2008. PESC 2008. IEEE*, june 2008, pp. 4192 –4195. 41

[70] P. Narra and D. Zinger, "An effective led dimming approach," in *Industry Applications Conference, 2004. 39th IAS Annual Meeting. Conference Record of the 2004 IEEE*, vol. 3, oct. 2004, pp. 1671 – 1676 vol.3. 39

[71] A. Wilkins, J. Veitch, and B. Lehman, "Led lighting flicker and potential health concerns: Ieee standard par1789 update," in *Energy Conversion Congress and Exposition (ECCE), 2010 IEEE*, sept. 2010, pp. 171 –178. 40

[72] B. Lehman, A. Wilkins, S. Berman, M. Poplawski, and N. Miller, "Proposing measures of flicker in the low frequencies for lighting applications," in *Energy Conversion Congress and Exposition (ECCE), 2011 IEEE*, sept. 2011, pp. 2865 –2872. 40

[73] W.-k. Lun, "On driving techniques for high-brightness light-emitting diodes," Ph.D. dissertation, Hong Kong Polytechnic University, 2010. 43, 44

[74] F. Li, T. Wei, R. Zheng, and H. Yan, "Algorithm to realize zero steady-state error for voltage controlled switching dc-dc converters," in *Mechatronics and Automation (ICMA), 2010 International Conference on*, aug. 2010, pp. 1522 –1526. 80

[75] H. S. Tam, "Loop gain simulation and measurement of pwm switching converters," M. Phil. Thesis, HKUST, 1999. 82

[76] C. F. Lee, "Design of Monolithic Current-Mode DC-DC Buck Converters with Internal Current Sensing," M. Phil. Thesis, HKUST, 1999. 82

[77] R. D. Middlebrook, "Measurement of loop gain feedback systems," *Int. J. Electronics*, vol. 38, no. 4, pp. 485–512, 1975. 82

[78] J. Falin, *Compensating and Measuring the control loop of a high-power LED driver*, Texas Instruments Incorporated, 2008, analog Applications Journal. 83

[79] A. J. Calleja, A. Torres, J. Garcia, M. R. Secades, J. Ribas, and J. A. Martinez, "Evaluation of power leds drivers with supercapacitors and digital control," in *Industry Applications Conference, 2007. 42nd IAS Annual Meeting. Conference Record of the 2007 IEEE*, sept. 2007, pp. 1129 –1134. 84

[80] D. Gacio, J. M. Alonso, A. J. Calleja, J. Garcia, and M. Rico-Secades, "A universal-input single-stage high-power-factor power supply for hb-leds based on integrated buck-flyback converter," in *Applied Power Electronics Conference and Exposition, 2009. APEC 2009. Twenty-Fourth Annual IEEE*, feb. 2009, pp. 570 –576. 84

[81] R. Tymerski and V. Vorperian, "Generation, classification and analysis of switched-mode dc-to-dc converters by the use of converter cells," in *Telecommunications Energy Conference, 1986. INTELEC '86. International*, 19-22 1986, pp. 181 –195. 91, 93

[82] ——, "Generation and classification of pwm dc-to-dc converters," *Aerospace and Electronic Systems, IEEE Transactions on*, vol. 24, no. 6, pp. 743 –754, Nov. 1988. 91, 93

[83] D. Maksimovic and S. Cuk, "General properties and synthesis of pwm dc-to-dc converters," in *Power Electronics Specialists Conference, 1989. PESC '89 Record., 20th Annual IEEE*, vol. 2, 26-29 1989, pp. 515 –525. 91

[84] S. Cuk and R. D. Middlebrook, "A new optimum topology switching dc-to-dc converter," in *IEEE Power Electronics Specialists Conference, 1977 Record*, vol. 1, Jun. 1977, pp. 160 –179. 94

[85] G. C. Temes and J. W. LaPatra, *Introduction to Circuit Synthesis and Design*. McGraw-Hill, 1977. 94

[86] X. R. J. Tse C. K., Lai Y. M. and C. M. H. L., "Application of duality principle to synthesis of single-stage power-factor-correction voltage regulators," *International journal of circuit theory and applications*, vol. 31, pp. 555 –570, Jun. 2003. 96, 98, 99

[87] D. M. Mitchell., *DC-DC switching regulator analysis*. New York, USA: McGraw-Hill, 1988. 96, 98

[88] D. Hopkins and J. Root, D.W., "Synthesis of a new class of converters that utilize energy recirculation," in *Power Electronics Specialists Conference, PESC '94 Record., 25th Annual IEEE*, vol. 2, 20-25 1994, pp. 1167 –1172. 98, 99

[89] C. K. Tse, *Linear Circuit Analysis*. Addison-Wesley, 1998. 98

[90] R. Paul and D. Maksimovic, “Analysis of pwm nonlinearity in non-inverting buck-boost power converters,” in *Power Electronics Specialists Conference, 2008. PESC 2008. IEEE*, 15-19 2008, pp. 3741 –3747. 100

[91] N. Semiconductor, *LM3406: 1.5 A Constant Current Buck Regulator for Driving High Power LED.* Data Sheet, 2010. 102

[92] S. Hui and Y. Qin, “A general photo-electro-thermal theory for light emitting diode (led) systems,” *Power Electronics, IEEE Transactions on*, vol. 24, no. 8, pp. 1967 –1976, aug. 2009. 110

[93] X. Tao and S. Hui, “Dynamic photoelectrothermal theory for light-emitting diode systems,” *Industrial Electronics, IEEE Transactions on*, vol. 59, no. 4, pp. 1751 –1759, april 2012. 110